



**Computer- and synthesis-based approaches
towards the discovery of novel BACE-1 inhibitors
as potential anti-Alzheimer's drugs**

Thesis submitted for the degree of
Philosophiae Doctor

Candidate:

GianPaolo Chiriano

Supervisors:

Prof. Paolo Carloni

Prof. Giuseppe Legname

Prof. Marinella Roberti

Prof. Andrea Cavalli

Prof. Maria Laura Bolognesi

October, 2011

To my family and Valentina

Table of Contents

Motivations of the thesis	6
Outlines of the thesis	9
Chapter 1. Alzheimer's disease (AD)	10
1.1. Introduction to AD	10
1.2. Genetics and epidemiology of AD	12
1.3. Molecular causes of AD	13
1.4. Current AD therapies	18
1.5. $A\beta$ -based therapeutic approaches	19
1.6. Alternative therapeutic approaches	24
Chapter 2. β -secretase APP cleaving enzyme (BACE-1)	27
2.1. Biology, function and structural features of BACE-1	27
2.2. BACE-1 inhibition	34
Chapter 3. Computational methods	43
3.1. Molecular docking	43
3.2. Molecular screening	53
Chapter 4. Novel classes of BACE-1 inhibitors as potential anti-Alzheimer's drugs	56
4.1. A small chemical library of 2-aminoimidazole derivatives as BACE-1 inhibitors: structure-based design, synthesis, and biological evaluation (Strategy 1)	57
4.1.1. <i>Introduction</i>	58
4.1.2. <i>Structure-based design</i>	59
4.1.3. <i>Chemistry</i>	61
4.1.4. <i>Results and discussion</i>	63
4.2. Sequential virtual screening approach to the identification of small organic molecules as potential BACE-1 inhibitors (Strategy 2)	70
4.2.1. <i>Introduction</i>	71
4.2.2. <i>Results and discussion</i>	72
4.3. Synthesis of monomeric derivatives to probe memoquin's bivalent interactions (Strategy 3)	77
4.3.1. <i>Introduction</i>	78
4.3.2. <i>Design</i>	79
4.3.3. <i>Results and discussion</i>	81
Chapter 5. Concluding remarks and future perspectives	86

Chapter 6. Experimental section	89
6.1. Computational studies	89
6.1.1. <i>Methods in Strategy 1</i>	89
6.1.2. <i>Methods in Strategy 2</i>	92
6.1.3. <i>Methods in Strategy 3</i>	97
6.2. Chemistry	98
6.2.1. <i>General chemical methods</i>	98
6.2.2. <i>General procedure for the microwave-assisted synthesis of 2-aminoimidazoles 21-31 and their characterization</i>	98
6.2.3. <i>General parallel procedure for the synthesis of 3-(bromophenyl)-propionic methyl esters 36-37 and their characterization</i>	105
6.2.4. <i>General parallel procedure for the synthesis of biphenyl propanoic acid methyl esters 42a-e and their characterization</i>	106
6.2.5. <i>General procedure for the synthesis of 3-biphenyl propyl alcohols 43a-e and their characterization</i>	108
6.2.6. <i>General procedure for the synthesis of 3-substituted propyl aldehydes 44a-f and their characterization</i>	109
6.2.7. <i>General procedure for the synthesis of 3-substituted-α-bromopropyl aldehydes 33a-f and their characterization</i>	111
6.3. Biology	114
6.3.1. <i>BACE-1 inhibition: enzymatic procedures</i>	114
6.3.2. <i>Inhibition of AChE and BuChE activities</i>	115
6.3.3. <i>Inhibition of AChE-induced Aβ-amyloid aggregation</i>	115
6.3.4. <i>Inhibition of Aβ₄₂ self-aggregation</i>	116
6.3.5. <i>BACE-1 inhibition: cellular assays procedures</i>	117
6.3.6. <i>CNS penetration: in vitro PAMPA-BBB test</i>	119
Chapter 7. Outlook	122
7.1. 2-Aminoimidazole derivatives as interfering probes in the replication process of prion protein	122
7.1.1. <i>Overview of Prion diseases (PrDs)</i>	122
7.1.2. <i>Introduction</i>	124
7.1.3. <i>Preliminary results</i>	126
Bibliography	129
List of publications related to the thesis	146

Motivations of the thesis

Alzheimer's disease (AD) is a progressive and fatal brain disorder, for which there is no cure. AD causes memory loss, steady deterioration of cognition, and dementia afflicting currently over 30 million people worldwide. The incidence of AD is thought to triple approximately by 2050 (World Alzheimer Report 2010) (<http://www.alz.org/>). In parallel with this increase, the speed of drug research has accelerated noticeably over the last decades. However, the number of therapeutic options on the market remains severely narrow. No disease-modifying therapy is available yet, despite the intensive efforts to develop innovative medicines.¹ At present, four drugs for AD have been approved by FDA. These drugs, however, are not able to alter or prevent disease progression. They are, instead, palliative in alleviating the symptoms of disease.¹

One of the major characteristic and pathological hallmarks of AD is represented by the senile plaques, whose main component is the amyloid- β peptide ($A\beta$). According to the amyloid hypothesis, the generation of $A\beta$ is a key event of AD. Indeed, soluble $A\beta$ is thought to undergo a conformational change into high β -sheet content, which renders it prone to aggregate into soluble oligomers $A\beta$ and, then, to form toxic extra-cellular (proto)-fibrils, which initiate the pathogenic cascade.^{2,3}

The self-assembly of soluble proteins and peptides into β -sheet-rich oligomeric structures and insoluble fibrils is a hallmark of a large number of human diseases known as amyloid diseases. In particular, as in AD, small oligomeric assemblies of misfolded proteins have been identified in other neurodegenerative disorders: α -synuclein (involved in Parkinson's disease), huntingtin with extended polyglutamine stretches (involved in Huntington disease) and the prion protein (PrP, involved in transmissible and inherited spongiform encephalopathies).⁴ Drugs able to interfere within the fibrillization process may prevent and/or cure these diseases. However, experimental difficulties in the characterization of the early oligomers involved in the amyloid formation process, given their transient nature, have seriously hampered the application of rational drug design approaches to the inhibition of amyloid formation.

The amyloidogenic pathway in AD, responsible for the generation of $A\beta$, has been experimentally defined, and inhibiting this process may affect the disease progression. $A\beta$ is produced by sequential proteolytic cleavage of a large trans-membrane protein, the amyloid precursor protein (APP), by two proteases, β - and γ -secretase (the details are discussed in the Chapter 1). Therefore, β - and γ -secretase enzymes have been studied in depth in the search for their inhibitors as potential anti-AD drugs. So far, a β -secretase inhibitor, CTS-21666 from CoMentis, advanced up to Phase II clinical trials. Instead, a γ -secretase inhibitor, semagestat from Eli-Lilly, failed in Phase III clinical

trials because of lack of efficacy and increased risk of skin cancer.⁵ Thus, β - than γ -secretase has appeared to be a better target for drug discovery purposes.⁶

The β -secretase APP cleaving enzyme (BACE-1) catalyzes the rate limiting step in the production of $A\beta$. BACE-1 is a member of the pepsin-like family of aspartyl proteases. It is a class I transmembrane protein consisting of an NH_2 -terminal protease domain structurally well-defined, a connecting strand, a transmembrane region, and a cytosolic domain.⁷ Moreover, localization, activity, and regulation of BACE-1 have been well investigated.⁸ Its mechanism has been studied in detail in our sector at SISSA.⁹

BACE-1 is recognized as one of the most promising targets in the treatment of AD.¹⁰ Since its inhibition has been validated as a suitable therapeutic strategy to reduce the production of $A\beta$, there was a boom in the development of several chemical classes of compounds as BACE-1 inhibitors that have been discovered by means of different approaches (see more details in Chapter 2), such as high-throughput screening (HTS), fragment-based, and structure-based strategies.¹¹ In particular, compared with traditional HTS, a significantly higher *hit* rate can be obtained by using a structure-based approach, which can fully exploit the large amount of structural information related to BACE-1 and, at the same time, allows the researchers to contain the costs related to the drug discovery and development process.

During my PhD project, I aimed at the discovery of novel BACE-1 inhibitors as potential anti-Alzheimer drugs in a joint collaborative effort between SISSA and the Department of Pharmaceutical Sciences from the University of Bologna. To reach this aim, I adopted two different strategies: a rational structure-based drug design by molecular docking and a random search for new chemical entities (NCEs) by virtual screening (see Figure 1).

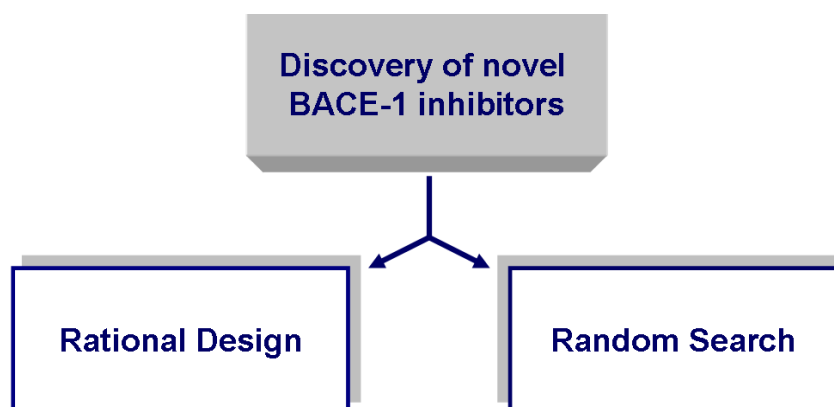


Figure 1. The two main strategies employed here as starting point for the discovery of novel BACE-1 inhibitors

In the first strategy, I applied a rational structure-based approach to identify a new series of 2-aminoimidazoles as BACE-1 inhibitors. Taking advantage of a microwave-assisted synthetic protocol, a small library of derivatives was obtained and biologically evaluated. Remarkably, two compounds showed low micromolar activities in both enzymatic (Prof. Andrisano's Lab - University of Bologna, Italy) and cellular assays (JSW Bio-company of Graz, Austria). Moreover, one of them exhibited the capability to cross the blood brain barrier in the parallel artificial membrane permeability assay (this work has been performed in the Prof. Martinez's Lab – CSIC of Madrid, Spain) (Chapter 4, Strategy 1).

In the second strategy, I performed a sequential application of two different *in silico* screening approaches combined with bioassays (performed in the Prof. Andrisano's Lab) towards the identification of low molecular weight organic molecules as potential BACE-1 inhibitors. Two *hits*, having novel structural features and endowed with micromolar inhibitory potency were selected, and the binding mode of the most potent compound was further characterized through docking simulations (Chapter 4, Strategy 2).

During my stay in Bologna, I have been also engaged in a project devoted to the identification of new multitarget-directed ligands (MTDLs) as an alternative way to develop effective anti-AD drugs. We generated a small library of new monomeric congeners, related to the anti-AD multitarget *lead* candidate “memoquin”, and determined their polypharmacological profile against three molecular targets involved in AD pathology, namely acetylcholinesterase (AChE), A β and BACE-1 (Prof. Andrisano's and JSW Labs). All these novel derivatives bind to AChE with similar low nanomolar affinities, and function as effective inhibitors of A β aggregation. The most potent monovalent ligand also inhibits BACE-1 *in vitro* and APP metabolism in primary chicken telencephalic neurons (Chapter 4, Strategy 3).

Finally, in light of reported experimental evidences¹²⁻¹⁴ which showed possible correlations between AD and prion disease (PrD), we preliminarily tested selected 2-aminoimidazoles (see the Chapter 7), as potential anti-prion compounds. The cellular assays were carried out at the Prion Biology Laboratory of SISSA, headed by Prof. G. Legname. Two of them resulted to inhibit at low micromolar concentrations the PrP^{Sc} replication process. These preliminary results confirmed that: i) the 2-aminoimidazoles are “privileged structures” in the CNS medicinal chemistry; ii) it is reasonable to speculate that we might have the same therapy for two distinct neurodegenerative disorders, such as AD and PrD.¹⁵

Outlines of the thesis

Chapter 1. Introduction to AD: genetics, epidemiology, molecular causes and therapeutic approaches.

Chapter 2. Illustration of the enzyme BACE-1, its key role in the amyloidogenesis, structural features, function and its inhibitors.

Chapter 3. A succinct survey of computational methods here used, namely molecular docking for the rational drug design, and molecular screening for a random search.

Chapter 4. Description of strategies adopted towards the discovery of novel classes of BACE-1 inhibitors as potential anti-AD drugs.

Chapter 5. Concluding remarks and future perspectives.

Chapter 6. Experimental section: computational studies; synthetic procedures, physical and spectroscopic characterization for intermediate and final compounds; description of experimental procedures adopted for biological evaluation of novel compounds reported and described in the Chapter 4.

Chapter 7. An outlook at work in progress.

Chapter 1

1. Alzheimer's disease (AD)

1.1. Introduction to AD

AD stands out among the neurodegenerative diseases as one of the major leading cause of death in the developed countries and the most common cause of acquired dementia in the elderly population. Generally, AD leads to impairment of cognitive and memory function, communication problems, personality changes, erratic behaviour, dependence and loss of control over bodily functions. The common early symptoms of AD include confusion, disturbances in short-term memory, problems with attention and spatial orientation, changes in personality, language difficulties and unexplained mood swings. Although these symptoms will likely vary in severity and chronology, overlap and fluctuate, the overall progress of the disease is fairly predictable. On average, people live for 8 to 10 years after diagnosis, but this terminal disease can last for as long as 20 years. AD does not affect every person the same way. Approximately by 2050, the incidence of AD is expected to triple (World Alzheimer Report 2010). AD has a dramatic consequence on quality of life for the sufferers and their families, and combination of direct and indirect costs in the treatment and care of Alzheimer's patients is tremendously increasing (<http://www.alz.org/>). In parallel with this increase, the speed of drug research has accelerated noticeably in the last decades. However, the number of therapeutic options on the market remains severely narrow. Currently, the registered drugs for AD are not able to alter or prevent disease progression.¹ They are, instead, on the market approved for the treatment of disease symptoms. Several years after the discovery of AD, the scientific consensus is quite firm that although the pathogenesis of AD is not yet fully understood, it is a multi-factorial disease caused by genetic, environmental, and endogenous factors, as with the other neurodegenerative disorders. These factors include excessive protein misfolding and aggregation, often related to the ubiquitin-proteasomal system (UPS), oxidative stress and free radical formation, impaired bioenergetics and mitochondrial abnormalities, and neuroinflammatory processes. These insights, together with further ongoing discoveries about AD pathogenesis, have provided the rationale for therapies directly targeting AD molecular causes. New drug candidates with disease

modifying potential are now in the pipeline and have reached testing in clinical trials (<http://www.neuroinvestment.com/>).

1.2. Genetics and epidemiology of AD

Mutations in three genes, amyloid precursor protein (*APP*), presenilin 1 (*PS1*, also known as *PSEN1*) and *PS2* (also known as *PSEN2*) respectively,¹⁶ and duplication of the *APP* gene¹⁷ all lead to early-onset autosomal dominant AD. From a therapeutic perspective, targeting the mechanisms of familial early-onset AD makes the implicit assumption that this disease is fundamentally similar to the common sporadic late-onset form. The genetics of the more common late-onset AD is an active area of investigation. The $\epsilon 4$ allele of the apolipoprotein E (*APOE*) gene has been identified as the major risk factor for late-onset AD.¹⁸ Exactly how the mutated genes or different isoforms are related to the increase of disease risk is not clear, and, at least in the case of the isoform *APOE4*, a consensus mechanism of pathogenesis has not emerged yet after the discovery of its role in AD. No specific environmental toxin has been found to be consistently associated with AD, and there have been no randomized clinical trials as yet to support any specific dietary intervention. Epidemiological evidences point to depression, traumatic head injury and cardiovascular and cerebrovascular factors (i. e. cigarette smoking, midlife high blood pressure, obesity and diabetes) as increasing disease risk, while anti-inflammatory medications seem to reduce risk. Some studies even suggest a beneficial role of psychosocial factors (for example, higher education, physical exercise and mental activity). Such studies may point to a role of previously unconsidered pathways in the aetiology of the disease, but the mechanistic interpretation of retrospective epidemiological studies is challenging.

1.3. Molecular causes of AD

Since Alois Alzheimer's seminal report of November 1906,¹⁹ several scientists have considered the defining and main pathological hallmarks of the disease to be extracellular $A\beta$ deposits in senile plaques and intracellular neurofibrillary tangles (NFT) (Figure 1.1), consisting mainly of paired helical filaments of abnormally hyper-phosphorylated τ protein. As the disease progresses, neuronal death appears. In particular, cholinergic neurons and synapses of the basal forebrain are selectively lost, accounting for the development of cognitive impairments. These findings constituted the premises for the so-called "cholinergic hypothesis", which proposed cholinergic enhancement as an approach for improving cognitive function in AD.²⁰

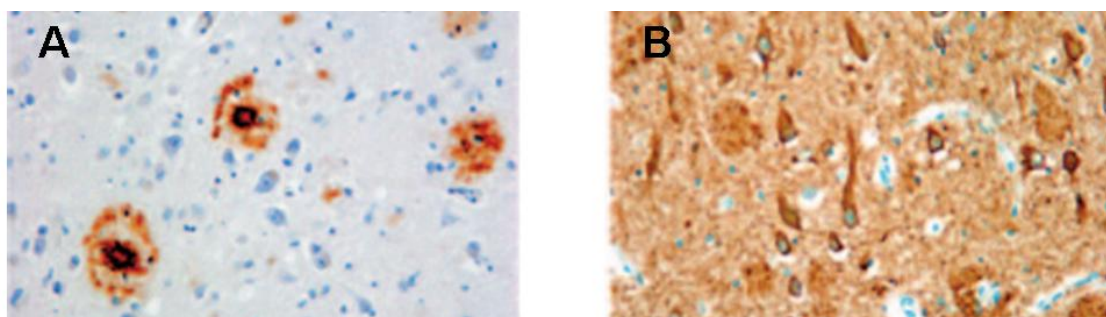


Figure 1.1. The two main morphological lesions of AD: senile plaques (A) and neurofibrillary tangles (B), consisting of aggregates of $A\beta$ and hyper-phosphorylated τ protein respectively.

This approach has so far produced the majority of drugs approved for treating AD. Nowadays, compelling evidence suggests that the generation of $A\beta$ is a key event in the pathogenesis of AD and that τ aggregation may be an important secondary event linked to neurodegeneration.²¹

According to the "amyloid cascade hypothesis",^{2,3,22} the generation of $A\beta$ would happen from the sequential post-translational proteolysis of a large trans-membrane protein, the amyloid precursor protein (APP), and it would aggregate or deposit (or deposit and aggregate) in extracellular insoluble plaques. β -secretase generates the NH_2 -terminus of $A\beta$, cleaving APP to produce a soluble version of APP (β -APPs) and a 99-residue $COOH$ -terminal fragment (C_{99}) that remains membrane bound (Figure 1.2). Alternatively, α -secretase cuts within the $A\beta$ region to produce α -APPs and an 83-residue $COOH$ -terminal fragment (C_{83}). Both C_{99} and C_{83} are substrates for γ -secretase, which performs an unusual proteolysis in the middle of the trans-membrane domain to produce the amyloidogenic peptide $A\beta$ from C_{99} and the not amyloidogenic one called p3 from C_{83} (Figure 1.2). Proteolysis by γ -secretase is heterogeneous: most of the full-length $A\beta$ species produced is a 40-residue peptide ($A\beta_{40}$), whereas a small proportion is a 42-residue $COOH$ -terminal variant ($A\beta_{42}$).

The longer and more hydrophobic $A\beta_{42}$ is much more prone to fibril formation than is $A\beta_{40}$, and even though $A\beta_{42}$ is a minor form of $A\beta$, it is the major $A\beta$ species found in cerebral plaques. In addition to $A\beta_{40}$ and $A\beta_{42}$, one more isoform of $A\beta$ exist, the 38-residue peptide ($A\beta_{38}$), whose levels in AD patients resulted particularly increased in the cerebrospinal fluid (CSF).²³

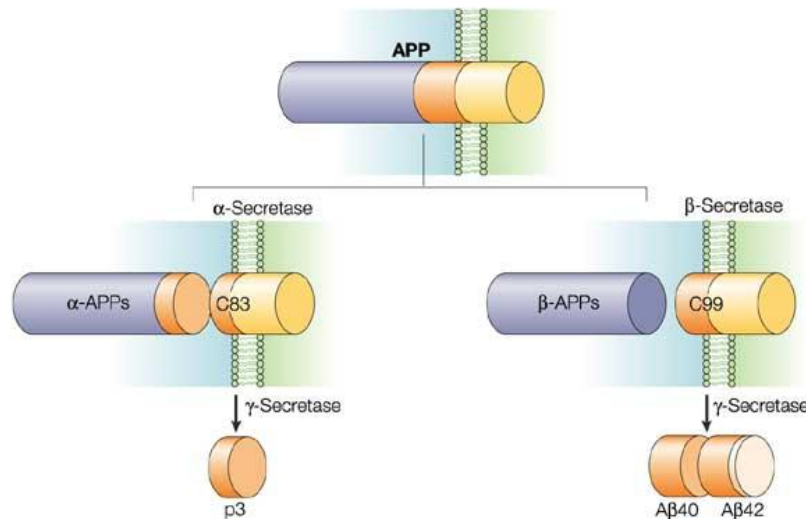


Figure 1.2. The protein sequences are not drawn to scale. The transmembrane protein APP (membrane indicated in green) can be processed along two main pathways, the α -secretase pathway and the amyloid-forming β -secretase pathway. In the α -secretase pathway, α -secretase cleaves in the middle of the amyloid- β region (orange) to release a large soluble APP-fragment, α -APPs (blue). The carboxy (C)-terminal C_{83} peptide is metabolized to p3 by γ -secretase. In the amyloid-forming β -secretase pathway, β -secretase releases a large soluble fragment, β -APPs (blue). The C-terminal C_{99} peptide is then cleaved by γ -secretase at several positions, leading to the formation of amyloid- β 40 ($A\beta_{40}$) and the pathogenic amyloid- β 42 ($A\beta_{42}$). γ -secretase cleavage also releases the APP intracellular domain (AICD), which could have a role in transcriptional regulation. The effects of β - and γ -secretase inhibitors can be distinguished in secondary assays: both inhibitor classes block the formation of pathogenic $A\beta_{42}$, but β -secretase inhibitors also block the formation of β -APPs and C_{99} , whereas γ -secretase inhibitors also block the formation of p3 and the APP C-terminal fragment (yellow), leading to accumulation of C_{99} and C_{83} .

Experimental evidences consolidated the “amyloid hypothesis” (Figures 1.3 and 1.4) showing that the amount of fibrillogenic $A\beta$ is increased by the vast majority of mutations causing familial AD and that $A\beta$ impairs neuronal functions in a variety of experimental models.²⁴ Soluble $A\beta$ is thought to undergo a conformational change to high β -sheet content, which renders it prone to aggregate into soluble oligomers and larger insoluble fibrils in plaques. (Figure 1.3) In this process, the fibrillogenic $A\beta_{42}$ isoform triggers the misfolding of other $A\beta$ species. Currently, the nature of the neurotoxic $A\beta$ species is very difficult to define because monomers, soluble oligomers, insoluble oligomers, and insoluble amyloid fibrils are expected to accumulate and exist in dynamic equilibrium in the brain. Initially, only $A\beta$ deposited in plaques was assumed to be neurotoxic, but

more recent findings suggest that soluble oligomers ($A\beta$ -derived diffusible ligands or ADDLs) might be the central players.

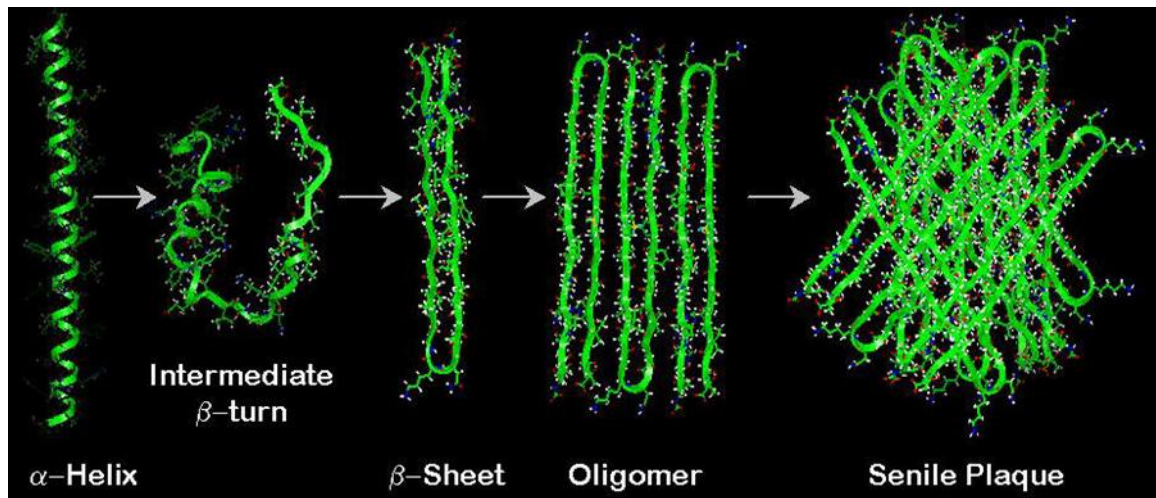


Figure 1.3. Aggregation process of $A\beta$ peptide and subsequent formation of senile plaques

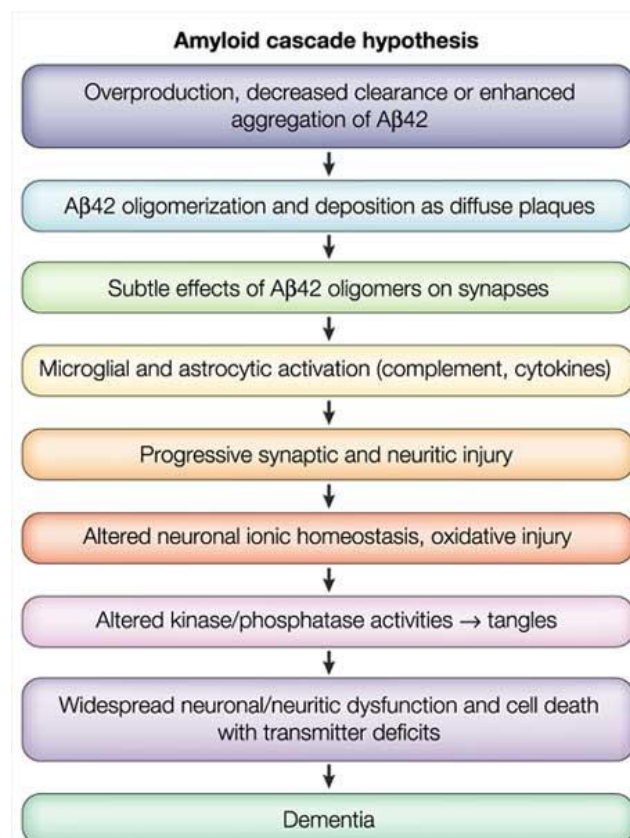


Figure 1.4. The sequence of pathogenic events that are thought to lead to Alzheimer's disease (AD) is shown. The cascade is initiated by the generation of $A\beta_{42}$. In familial early onset AD, $A\beta_{42}$ is overproduced owing to pathogenic mutations. In sporadic AD, various factors can contribute to an increased load of $A\beta_{42}$ oligomers and aggregates. $A\beta$ oligomers might directly injure the synapses and neurites of brain neurons, in addition to activating microglia and

astrocytes. Tau pathology, which contributes substantially to the disease process through hyper-phosphorylated τ and tangles, is triggered by $A\beta_{42}$.

Afterward, $A\beta$ may exert its neurotoxic effects in a variety of ways (Figure 1.4), including disruption of mitochondrial function via binding of the $A\beta$ -binding alcohol dehydrogenase protein,²⁵ induction of apoptotic genes through inhibition of Wnt²⁶ and insulin signaling,²⁷ formation of ion channels,²⁸ stimulation of the stress-activated protein kinases (SAPK) pathway²⁹ or activation of microglia cells leading to the expression of pro-inflammatory genes, an increase in reactive oxygen species (ROS), and eventual neuronal toxicity and death.³⁰ More recently, it has become clear that, in addition to forming extracellular aggregates, $A\beta$ (or its precursor APP) has complicated intracellular effects involving a variety of subcellular organelles, including mitochondria. Mitochondrial APP has been shown to accumulate in the protein import channels of mitochondria of human AD brains, and this accumulation inhibits the entry of cytochrome *c* oxidase subunits proteins,³¹ with decreased activity of respiratory chain enzymes, increased free radical generation, and impaired reducing capacity. These data provide a potential explanation for the well-established observation that mitochondrial function and energy metabolism are impaired early in AD.³²

NFTs are composed mainly of paired helical filaments (PHF) that contain an abnormal hyper-phosphorylated form of the microtubule-associated protein τ . Phosphorylation within the microtubule binding domain of τ protein results in its reduced ability to stabilize microtubules assembly, leading to the disruption of neuronal transport and eventually to accelerated synaptic loss and cell death. Dephosphorylation of τ protein isolated from NFT restores its ability to bind with neuronal microtubules, indicating that the mechanisms regulating phosphorylation/dephosphorylation kinetics are perturbed in AD. The nature of protein kinases, phosphatases, and τ sites involved in this lesion has recently been elucidated, suggesting that activation of phosphoserine/phosphothreonyl protein phosphatase-2A (PP-2A) or inhibition of both glycogen synthase kinase-3 β (GSK-3 β) and cyclin-dependent protein kinase 5 (cdk5) might be required to inhibit AD neurofibrillary degeneration.³³

Several other hypotheses have been proposed to explain the pathogenesis of AD, including oxidative stress, metal ion dyshomeostasis, and inflammation.³⁴ In the context of such a complex disease, it is not trivial to state that these hypotheses are not mutually exclusive. Rather, they complement each other, intersecting at a high level of complexity. Oxidative damage is present within the brain of AD patients and is observed within every class of biological macromolecules, including nucleic acids, proteins, lipids, and carbohydrates.³⁵ Oxidative injuries may develop secondary to excessive oxidative stress resulting from $A\beta$ -induced free radicals, mitochondrial

abnormalities, inadequate energy supply, inflammation, or altered antioxidant defences. Oxidative stress is thought to have a causative role in the pathogenesis of AD.³⁶ Support for this hypothesis has also been provided by the current notion that, while AD is probably associated with multifaceted aetiologies and pathogenic phenomena, all these mechanisms seem to share oxidative stress as a unifying factor. Strictly related to the oxidative damage hypothesis, there is general acceptance that redox active metals can contribute to excess production of damaging ROS through Fenton's chemistry.³⁷ Besides creating oxidative stress, copper, together with other metal ions, influences the protein aggregation processes that are critical in most neurodegenerative diseases. For example, APP and A β are able to bind and reduce copper, which forms a high-affinity complex with A β , promoting its aggregation, and A β neurotoxicity depends on catalytically generated H₂O₂ by A β -copper complexes in vitro. Moreover, copper, together with zinc and iron, is accumulated in the amyloid deposits of AD brains, which are partially disassembled by metal chelators.

Finally, neuroinflammation of CNS cells has been recognized as an invariable feature of all neurodegenerative disorders. In AD, among CNS cells, microglia have received special interest. Microglia are activated by A β to produce cytokines, chemokines, and neurotoxins that are potentially toxic and therefore may contribute to neuronal degeneration. However, recent findings suggest that microglia may play a neuroprotective role in AD. This highlights the potential risk of using the inhibition of monocyte/macrophage recruitment as a therapeutic strategy and argues for caution in the pursuit of this approach.³⁸ Despite this, modulation of inflammation is one of the most dynamic areas in the search for new therapeutic targets for AD and related neurodegenerative disorders.³⁹

1.4. Current AD therapies

Among the previously mentioned hypotheses, the cholinergic one is the oldest. It has also had the strongest influence on the development of clinical treatment strategies. In fact, in 1993, it led to the introduction of the acetylcholinesterase inhibitor (AChEI) tacrine (**1**), the first drug to be approved for the treatment of AD, not longer used because of its hepatotoxicity. Later, three other AChEIs, donepezil (**2**), galantamine (**3**), and rivastigmine (**4**) reached the market, becoming the standard for AD therapy, only later complemented by memantine (**5**), a non-competitive NMDA antagonist (Figure 1.5). Not with standing the diffused clinical practice, the debate on whether or not AChEIs are effective medications continues. Although beneficial in improving cognitive, behavioural, and functional impairments, they seem unable to address the molecular mechanisms that underlie the pathogenic processes. Current AD drug development programs focus primarily on agents with anti-amyloid disease-modifying properties. Many different pharmacological approaches to reducing amyloid pathology and tauopathy are being studied.

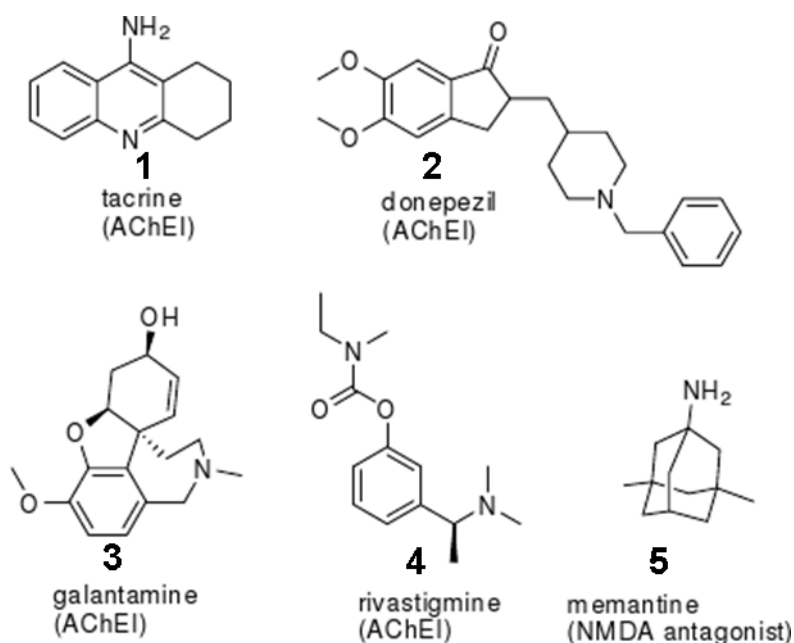


Figure 1.5. Chemical structures of the five drugs available for AD treatment (mechanisms of action are indicated in parentheses).

1.5. A β -based therapeutic approaches

Genetic and pathological evidence strongly supports the amyloid cascade hypothesis of AD, which states that A β , a proteolytic derivative of the large trans-membrane protein APP, and in particular the least soluble 42 amino-acid long A β_{42} isoform, have an early and vital role in all forms of AD. Key experimental evidences support a crucial role of A β in the pathogenesis of AD: i) amyloid deposits provide early pathological evidence of AD and neuritic plaques are a key diagnostic criterion; ii) in peripheral amyloidoses (unrelated to A β and AD), amyloid burden drives tissue dysfunction, thereby suggesting that brain amyloid is pathogenic as well; iii) A β oligomers show acute synaptic toxicity effects, whereas plaque-derived A β fibrils have pro-inflammatory effects and cause neuronal toxicity; iv) the most important genetic risk factor, *APOE4*, is associated with increased amyloid burden; v) most importantly, all mutations that cause familial early-onset AD increase A β_{42} production or the ratio of A β_{42} compared to the less aggregation-prone A β_{40} isoform. All these mutations directly enhance amyloidogenic APP processing: *APP* mutations by changing the substrate properties of APP and *PSEN* mutations by changing the properties of the γ -secretase complex. Based on this evidence, several A β -targeted therapeutic strategies are being pursued, including: (I) modulation of A β production; (II) inhibition of A β aggregation; (III) enhancement of A β degradation; (IV) immunotherapy targeted at A β .

(I) Modulation of A β production

The post-translational APP processing pathway outlines immediately three radical strategies to reduce A β generation: α -secretase stimulation, β - and γ -secretase inhibition.

(i) α -secretase stimulation

α -secretase pathway stimulation might lead to a reduction of the APP substrates available for A β formation, activating non-amyloidogenic α APPs. Moreover, α -secretase is stimulated also by AChEIs via selective muscarinic activation inducing the translation of APP mRNA with the final goal of restricting amyloid fibre assembly. Three members of the ADAM family (“a disintegrin and metalloproteinase”) ADAM-10, ADAM-17 and ADAM-9 have been proposed as α -secretases. To date, it is accepted that each of these enzymes acts as a physiologically relevant α -secretase. Genetic studies revealed that ADAM-10 is a key protein involved in neurogenesis and axonal extension.^{40,41} This underlines the positive, neuroprotective role of ADAM-10 and, thus, of α -secretase like cleavage activity in the metabolic processing of APP. In addition to ADAMs, other membrane-associated metalloproteinases could contribute to the shedding of APP. Stimulation of α -secretase

activities can be achieved via several signalling cascades including phospholipase C, phosphatidylinositol 3-kinase and serine/threonine-specific kinases such as protein kinases C, and mitogen activated protein kinases. Direct activation of protein kinase C and stimulation of distinct G protein-coupled receptors are known to increase α -secretase processing of APP.⁴² Agonists for M1 muscarinic receptors and serotonin 5-HT receptors are currently in clinical trials to test their efficiency in the treatment of AD.^{43,44}

(ii) β -secretase inhibition

β -secretase, also called BACE-1 is a membrane bound aspartic protease specifically abundant in brain, which forms, together with its homologue BACE-2, a new branch of the pepsin family.⁴⁵ The enzyme catalyzes the cleavage of APP to produce *N*-terminus of $A\beta$ peptides. The data suggesting BACE-1 is the enzyme relevant to AD-related APP processing are strong, and have recently been reviewed along with other aspect of BACE-1 biology.⁴⁶ BACE-1 inhibition holds promise for the production of safe anti-amyloid therapy, as transgenic mice lacking the *BACE* gene produce little or no $A\beta$, and do not display any robust negative phenotype.^{47,48} For these reasons, BACE-1 appears to be an excellent drug target, even if the absence of toxicity in mice does not prove absence of human toxicity. Although the biology of BACE-1 inhibition seems to be a promising line in inquiry, development of compounds able to inhibit this enzyme is proving to be challenging.¹⁰ Research aimed at the discovery of BACE-1 inhibitors has been strengthened by the large amount of available information, particularly, on the proteasic domain which has structurally well-defined opening new opportunities for a rational drug design.

(iii) γ -secretase inhibition and modulation

γ -secretase is responsible for the final cut of the APP to produce the $A\beta$ peptide implicated in the pathogenesis of AD. Thus, this protease has resulted a drug target for the development of anti-AD therapeutics. γ -secretase is a complex of four different integral membrane proteins, with the multi-pass presenilin being the catalytic component of a novel intramembrane-cleaving aspartyl protease. Several inhibitors of the γ -secretase complex have been identified, including peptidomimetics that block the active site, helical peptides that interact with the initial substrate docking site, and drug-like compounds. To date, one peptidomimetic γ -secretase inhibitor (DAPT) has advanced into late-phase clinical trials for the treatment of AD, but serious concerns remain. γ -secretase cleaves other substrates besides APP, the most notorious being the Notch receptor that is required for many cell differentiation events. Because proteolysis of Notch by γ -secretase is essential for Notch signalling, interference with this process by γ -secretase inhibitors can cause severe toxicities. γ -secretase

inhibitors may cause abnormalities in the gastrointestinal tract, thymus and spleen in rodents. Thus, the potential of γ -secretase as therapeutic target likely depends on the ability to selectively inhibit $A\beta$ production without hindering Notch proteolysis. Unfortunately, recently, semagacestat, a γ -secretase inhibitor, failed in Phase III clinical trials for AD showing no evidence of beneficial effects and the increase in the risk of skin cancer.⁵ The discovery of compounds capable of such allosteric modulation of the protease activity has revived γ -secretase as an attractive target. Structural modifications of these γ -secretase modulators have allowed to discover and advance novel compounds in clinical trials, renewing interest in γ -secretase as therapeutic target. Small molecules, that shift $A\beta_{42}$ to shorter $A\beta$ species, were discovered while investigating the mechanism for the reduced prevalence of AD among users of non-steroidal anti-inflammatory drugs (NSAIDs).⁴⁹ Subsequent studies have shown that some NSAIDs are able to modulate $A\beta$ synthesis by binding γ -secretase and, despite this mechanism, without interfering with Notch metabolism. As a result of this, some of these NSAIDs have recently advanced up to the clinical trials (<http://www.neuroinvestment.com/>). However, recently, *R*-flurbiprofen developed by Myriad (the enantiomer of the NSAID flurbiprofen that has almost no COX activity) culminated in the largest 18-month Phase III clinical trial in AD completed so far.

(II) Inhibition of $A\beta$ -aggregation

Small amounts of the various $A\beta$ isoforms are constitutively generated by neurons. Monomeric $A\beta$ molecules, in particular $A\beta_{42}$, can form oligomeric aggregates that are thought to initiate the pathogenic cascade. Initially, it was assumed that only $A\beta$ that had aggregated into the large fibrils that constitute the mature neuritic amyloid plaques would exert toxic properties. However, in recent years small soluble oligomeric assemblies of $A\beta$ have attracted a lot of attention, as it was demonstrated that they can directly induce synaptic dysfunction. The exact nature of the pathogenic oligomeric species remains unclear and a consensus pathogenic oligomer assembly mechanism has not yet emerged.⁵⁰ Nevertheless, in principle, developing brain penetrable small-molecule drugs that interfere with $A\beta$ - $A\beta$ peptide interactions seems an alternative approach. If the peptide interactions are the same in oligomers and in larger fibrils, then such molecules could inhibit both the formation of toxic oligomers and of neuritic plaques. If the peptide-peptide interactions were different in both aggregates, then one could theoretically identify molecules that interfere with just one or the other process. In this case, the assay set-up would be a key experiment to find molecules that block only formation of oligomers or molecules that block only formation of large fibrils. In the 1990s, several different assay formats for the identification of nucleation and deposition inhibitors that would block the formation of large fibrils were described. However, very few aggregation inhibitors have

moved into clinical testing. One can only speculate whether it was simply not feasible to generate potent drug-like molecules that block $A\beta$ - $A\beta$ peptide interactions in a specific manner or whether decision-makers felt uncomfortable committing to this unvalidated mechanism of action for a drug. Tramiprosate from Neurochem, able to bind to $A\beta$ monomers and maintain it in a non-fibrillar form,⁵¹ progressed into large Phase III trials, but without beneficial effects. Drawing mechanistic conclusions from this trial is difficult, because it is not known whether the drug blocked $A\beta$ aggregation in the brain. $A\beta_{42}$ reduction in cerebrospinal fluid had been reported in a previous Phase II trial of the drug,⁵² but whether this represents a desirable pharmacodynamic effect of an aggregation inhibitor is not clear. A different class of molecule, cyclohexanehexol isomers, has been suggested to stabilize $A\beta$ into non-toxic conformers and inhibit $A\beta$ fibrils assembly *in vitro*, translating into the amelioration of several AD-related phenotypes in *APP* transgenic mice.⁵³ Currently, Elan is testing one of these isomers, eIND005, in Phase II trials for AD. Another approach to interfere with toxic $A\beta$ species is based on the notion that trace metals, in particular zinc and copper, contribute to amyloid pathology.⁵⁴ This has led to the investigation of orally available brain-penetrant ‘metal–protein attenuating compounds’. The first of these compounds, clioquinol, has been reported to drastically reduce amyloid pathology in *APP* transgenic mice.⁵⁵ Prana is advancing a second-generation compound, PBT2, in Phase II trials.⁵⁶

(III) Enhancement of $A\beta$ -degradation

The strategy aimed at stimulating $A\beta$ degradation represents an additional approach to decrease levels of $A\beta$ oligomers. In particular, in the last years, several key enzymes involved in $A\beta$ degradation have been identified, most notably the proteases neprilysin, insulin-degrading enzyme and plasmin.⁵⁷ From a drug development perspective, specific activation of enzymes is much more challenging than inhibition. Indeed, researchers from Wyeth, in contrast to the difficulty to directly activate a protease, have aimed at blocking the inhibitor of a protease necessary for activating an $A\beta$ -degrading enzyme. On the basis of experimental evidences showing that plasmin cleaves $A\beta$ *in vitro* and that tissue plasminogen

activator (required to generate plasmin from plasminogen) is inhibited *in vivo* by plasminogen activator inhibitor 1 (PAI-1), orally available PAI-1 inhibitors lowering plasma and brain $A\beta$ levels in transgenic mice have been generated.⁵⁸ In addition, an other strategy is based on targeting proteins involved in the transport from CNS to periphery (or viceversa) where $A\beta$ can be degraded. In fact, other two potential targets, the receptor for advanced glycation end products (RAGE, also called AGeR), which mediates the influx of $A\beta$ from peripheral sites into the brain, and the low-density lipoprotein receptor-related protein 1 (LRP-1), which mediates efflux of $A\beta$

from the brain, have been proposed to dominate $A\beta$ transport at the BBB. Moreover, $A\beta$ -RAGE interactions have been proposed to activate nuclear factor- κ B signalling pathways, which may promote apoptosis and inflammatory responses.⁵⁹ If this model is correct, a RAGE inhibitor could lower amyloid load in the brain and also block the other detrimental effects of $A\beta$ -RAGE signalling. In according to these findings, Pfizer is currently testing an orally bio-available RAGE inhibitor in Phase II trials for mild to moderate AD.

(IV) Anti- $A\beta$ immunotherapy

Anti- $A\beta$ immunotherapy for AD has received considerable attention over the past few years, and more than ten immunotherapeutic agents have entered clinical trials. Currently, three of these are in Phase III trials: Elan's bapineuzumab (humanized 3D6), Lilly's solanezumab (humanized 266) and Baxter's intravenous immunoglobulin G (IvIG), a preparation of human serum immunoglobulin that contains naturally occurring antibodies directed against $A\beta$.⁶⁰

Generally, four models of antibody-mediated amyloid clearance, which are not mutually exclusive, have been proposed: i) small amounts of amyloid-specific antibodies reach amyloid deposits in the brain and trigger a phagocytic response by microglia;⁶¹⁻⁶⁵ ii) amyloid-specific antibodies reach amyloid deposits in the brain and resolve them directly through interaction of the antibody with the amyloid deposit;⁶⁶ iii) amyloid-specific antibodies act as a peripheral sink for soluble $A\beta$ species, leading ultimately to the resolution of brain deposits by pulling soluble $A\beta$ into the periphery, where it is rapidly cleared; iv) amyloid-specific antibodies rapidly bind to oligomeric $A\beta$ species, blocking their toxic effects without immediate impact on amyloid load.

As immunotherapy is at the crossroads of immunology and the nervous system, a deeper understanding of the $A\beta$ peptide clearance mechanism may lead to an optimized therapeutic approach to the treatment of AD. Antibodies generated with the first-generation vaccine might not have the desired therapeutic properties to target the "correct" mechanism, however, new immunological approaches are now under consideration.

1.6. Alternative therapeutic approaches

Hyper-phosphorylated tau (τ) protein and τ -based therapeutics

Together with the senile plaques, the intra-cellular NFT, which consist of paired helical filaments of hyper-phosphorylated and conformationally altered τ protein, are the main pathological hallmarks of AD. τ and tangle pathology are also present in a number of other disorders such as Pick's disease, progressive supranuclear palsy, corticobasal degeneration and motor neuron diseases. However, there is a strong correlation between cognitive dysfunction and tangle load and localization in AD.⁶⁷ τ binds and stabilizes microtubules, while its hyper-phosphorylated in AD brain disrupt microtubule structure. The presence of NFT in AD and their correlation with cognitive status suggest an important role in dementia. Phosphorylation within the microtubule binding domain of τ results in its reduced ability to stabilize microtubules assembly, leading to the disruption of neuronal transport and eventually to faster synaptic loss and cell death. De-phosphorylation of τ isolated from NFT restores its ability to bind with neuronal microtubules, indicating that the mechanisms regulating phosphorylation or de-phosphorylation kinetics are perturbed in AD.

Inhibition of τ aggregation and blockade of its hyper-phosphorylation are the main strategies which have been exploited. Inhibition of aggregation is conceptually more appealing, because there seems to be general consensus that τ aggregates are detrimental.⁶⁸ However, as for $A\beta$ peptide, from a drug development perspective anti-aggregation approaches pose a lot of challenges. Indeed, finding drug-like molecules that specifically disrupt protein-protein interactions over large interaction surfaces is theoretically very difficult, even though τ -specific hexapeptide motifs critically contribute to the overall aggregation process.⁶⁸ In the case of anti-AD drugs, from a pharmacokinetic perspective the BBB penetration would represent additional hurdle for such molecules. Nonetheless, academic researchers are pursuing anti- τ aggregation strategies: screens have been run, hits have been identified and medicinal chemistry efforts have been initiated.⁶⁸ Strategies aimed at reducing τ hyper-phosphorylation, which appear to be more straightforward, are more widely pursued. Several drug target candidates have been proposed, including cyclin-dependent kinase 5 activator 1 (CDK5R1), MAP/microtubule affinity-regulating kinase 1 (MARK-1) and glycogen synthase kinase 3 (GSK-3), even if it is not clear yet whether a single culprit kinase even exists. In particular some of these kinases have been investigated in preclinical studies by various companies, but, at present, no updates on clinical trials were presented. However the clinically most advanced τ -directed therapy is methylthionium chloride (methylene blue), which has been reported to dissolve τ filaments isolated from AD brains *in vitro* and to prevent τ aggregation in cell-based models. Based on these findings, TauRx Therapeutics initiated a Phase II

placebo-controlled clinical trial in subjects with mild to moderate AD. Significant AD assessment scale-cognitive score differences relative to placebo were observed in the middle-dose group, but not in the low- and high-dose groups after 24 and 50 weeks of treatment, what the authors interpreted as evidence of arrested disease progression.

Anti-inflammatory approaches

Inflammation in CNS has been recognized as an invariable feature of all neurodegenerative disorders. However, there is currently no consensus about whether and how the inflammatory process in AD should be targeted therapeutically. Activated microglia are strongly associated with senile plaques and, in particular, many inflammatory mediators including prostaglandins, pentraxins, complement components, cytokines, chemokines, proteases and protease inhibitors are up-regulated in AD brains. This has led to the hypothesis that anti-inflammatory therapy could be beneficial, as also highlighted by lower incidence of AD in patients with arthritis, most of whom use NSAIDs. Statistical studies have shown a roughly 50% reduction in AD risk in long-term users of NSAIDs and warranted their testing in clinical trials for AD. However, COX2-selective compounds celecoxib and rofecoxib, and of the mixed COX1/COX2 inhibitor naproxen, did not show any therapeutic benefit in clinical trials. In according to this, firstly, the data are consistent with the idea that NSAIDs and anti-inflammatory approaches in general work only in primary prevention of AD, not in treatment.⁶⁹ Secondly, the trials may not have addressed the right molecular targets. In fact, it has been suggested that one should focus on COX1, because, in contrast to COX2, it is highly up-regulated in microglia. It was argued that doses in the naproxen trial were too low and that future trials should use full therapeutic doses of COX1-targeted NSAIDs despite the gastrointestinal side effects.⁶⁹ In addition, NSAIDs have molecular targets in addition to COX, which may not have been optimally engaged in the previous trials. For example, specific activation of peroxisome proliferator-activated receptor- γ (PPAR γ) elicits anti-amyloidogenic, anti-inflammatory and insulin-sensitizing effects.⁷⁰ However, the recent failure of rosiglitazone in large Phase III trials⁷⁰ does not support further evaluation of this target in AD treatment. It has also been proposed that the epidemiologically promising NSAIDs, in contrast to the NSAIDs tested in large trials, show direct γ -secretase modulating activity (unrelated to their COX effects) and that this explains the failure of the NSAID trials and points to a direction for future development.⁴⁹ Although inflammation plays a role AD pathology, an increasing number of preclinical studies suggest that some aspects of the immune response may actually be beneficial.⁷¹ In AD, microglia probably phagocytose and clear $A\beta$, and ongoing clinical immuno therapy studies promise to improve microglial phagocytosis of $A\beta$, thus reducing amyloid pathology. Clearly, distinguishing and

modulating beneficial and detrimental parts of the immune response in AD will be an exciting and challenging field for many years to come.

APOE-related treatment approaches

APOE is a major carrier of apolipoprotein and cholesterol in the brain. There are three major human isoforms, APOE2, APOE3 and APOE4, encoded by polymorphic alleles $\epsilon 2$, $\epsilon 3$ and $\epsilon 4$, respectively.⁷² Over all the possible genetic causes of AD, $\epsilon 4$ is the one involved in most cases.⁷³ However, because of the complex biological effects of APOE and its different isoforms, the development of APOE-related treatments is slow. The fact that $\epsilon 4$ is also a risk factor for a number of other conditions raises the question of whether an AD-specific molecular pathway even exists. The key question is whether $\epsilon 4$ is a risk factor because it has gained toxic properties with respect to $\epsilon 3$ or because it has lost beneficial $\epsilon 3$ function. Some investigators are pursuing different approaches to reduce toxic effects of APOE4. For example, by inhibiting a neuronal protease that, according to their model, generates a toxic APOE4 fragment or by developing ‘structural correctors’, small molecules that would bind to APOE4 and block the intramolecular domain interaction that is characteristic of this isoform, thus converting it into an APOE3-like structure.⁷⁴ Others promote the idea that APOE4 has partially lost the beneficial function of APOE3, at least with respect to its involvement in the amyloid pathway.⁷⁵ Analyses of $A\beta$ deposition in which *APOE*-knockout or human $\epsilon 2$ -, $\epsilon 3$ - or $\epsilon 4$ -knock-in mice were cross-bred with *APP* transgenic mice showed that APOE3 caused less $A\beta$ deposition than APOE4, and that APOE4 caused less $A\beta$ deposition than the knockout mice.⁷⁵ These results suggest that enhancing *APOE* expression could be a therapeutic strategy that could benefit anyone who carries at least one *APOE3* allele.⁷⁶ Progression of APOE-directed treatment approaches into clinical trials has not been reported yet.

Chapter 2

2. β -secretase APP cleaving enzyme (BACE-1)

2.1. Biology, function and structural features of BACE-1

Nowadays, the β -secretase APP cleaving enzyme, more commonly known in literature as BACE-1, is universally recognized as the protease which initiates the cleavage of APP at the β site and, as such, catalyses the rate limiting step in the production of $A\beta$. In the last years, this biological hypothesis was in depth studied and widely accepted by scientific community. Initially, the unknown enzyme cleaving APP at the beginning of $A\beta$, prior to aminoacid 1, was called β -secretase. In 1992, the discovery of the Swedish APP (APP_{SWE}) double mutation, located at -2 and -1 (Lys670 \rightarrow Asn; Met671 \rightarrow Leu) of the site, where BACE-1 acts,⁷⁷ and a cause of rare autosomal dominant forms of AD drew attention to the possibility that this mutation could cause AD by being more favourable to BACE-1 cleavage. This was substantiated in studies showing that APP_{SWE} significantly enhanced the proteolytic activity of BACE-1 causing a ~ 10 fold increase in $A\beta$ production.⁷⁸

Several research groups applied an intensive search for identifying an aspartic protease fitting all the requirements for BACE-1, which was identified in 1999 and 2000.^{45,79-82} This protease was initially named memapsin-2, and Asp-2, though it is now more commonly known as BACE-1. After the discovery of BACE-1, a homologue was described and identified.⁸³ The gene identified was named memapsin-1 and is also referred to as Asp-1, ALP-56, CDA-13, DRAP (Down's region aspartic protease), but now more commonly identified as BACE-2. Both BACE-1 and BACE-2 can process APP at the β -site, but BACE-2 has a preference to cleave the APP between aminoacids 19 and 20 of the $A\beta$ sequence, thus precluding $A\beta$ formation. A number of studies provide strong evidence that BACE-1 is the major responsible for $A\beta$ generation in the brain. Thus, BACE-1 cleaves at the β and also the β' site (between aminoacid 10 and 11 of $A\beta$) of APP and has a higher preference to cleave APP_{SWE} .^{45,79-81}

BACE-1 mRNA has highest expression levels in the mammalian brain,⁸⁴ and is found in organelles of the secretory pathway⁴⁵ displaying optimal activity at pH = 4.5,⁸⁵ which is consistent with its detection in acidic organelles of the endosomes and trans-Golgi network (TGN) where $A\beta$ is

predominantly generated.^{78,86,87} The most interesting discovery was to assess that targeted deletion of BACE-1 in *APP* transgenic mice completely abolishes the production and deposition of $A\beta$.^{48,88,89} BACE-1 and BACE-2 are the newest described members of the A1 aspartic protease family, commonly known as the pepsin family. Human aspartic proteases of this family also include pepsin, cathepsin-E, cathepsin-D, renin, pepsinogen-C and napsin. The BACE proteins represent a novel subgroup of this family, being the first reported aspartic proteases to contain a trans-membrane domain and carboxyl terminal extension,⁸⁴ and also possessing unique disulphide bridge distribution.^{7,90} The eight known functional human A1 aspartic proteases vary in genomic structure. The main features of A1 aspartic proteases are their bilobar structure, with an essential catalytic aspartic dyad located at the interface of the homologous N- and C-terminal lobes, with maximal enzyme activity occurring in an acidic environment. These Asp residues activate water molecules to mediate nucleophilic attack on the substrate peptide bond (see the general proteolysis mechanism for the aspartic proteases in Figure 2.1),⁹ and mutation of the catalytic active site aspartic residues abolishes enzyme activity.

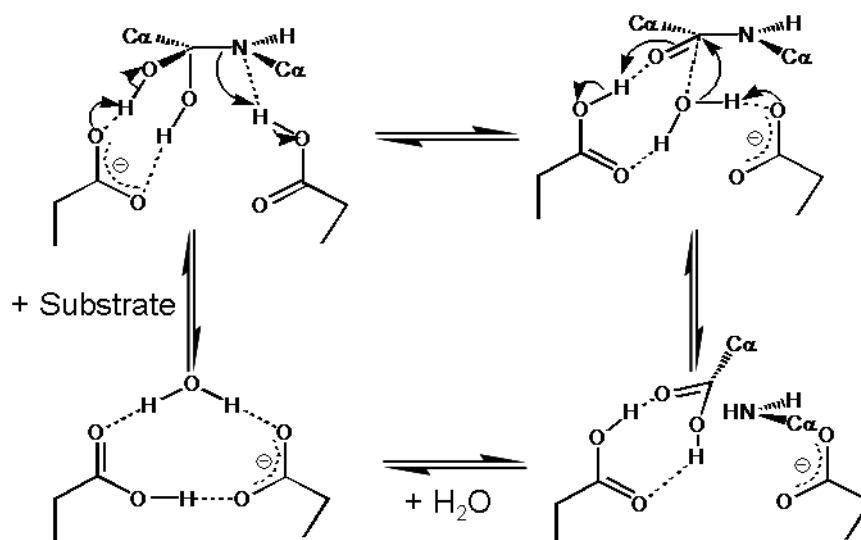


Figure 2.1. General reaction mechanism of aspartic proteases (APs). A general reaction mechanism for the chemical catalytic steps of APs. Starting from the lower-left angle and following the reaction clockwise: aspartic dyad in the free form, binding of the substrate, and nucleophilic attack of water; formation of the tetrahedral *gem*-diol intermediate; protonation of the nitrogen atom and formation of the products; release of the products and regeneration of the catalyst.

For BACE-1 the catalytic dyad is represented by two aspartic acids, Asp32 and Asp228. A1 aspartic proteases are usually synthesised as inactive pre-pro-enzymes (zymogens), where pro-domain removal is necessary for enzymatic activity.⁹¹ In contrast to this, BACE-1 possesses enzymatic activity. It is synthesised with a pro-sequence that is rapidly removed during transit through the Golgi⁹² by the action of a furin-like convertase.⁹³ BACE-1 is highly glycosylated,⁹⁴ and its

carbohydrate chains may favour interaction with its substrate or with glycoproteins that help regulate its activity. All A1-aspartic proteases have six conserved Cys residues which form three disulphide bridges. BACE-1 disulphide bridges maintain correct folding and orientation of BACE, but are not vital to its enzymatic activity.^{7,90} In addition, the unique trans-membrane regions of BACE-1 and BACE-2 confer an evolutionary specialisation, allowing their sequestration to membranes of specific organelles and the plasma membrane. This serves to expose their catalytic lobes to the luminal regions of vesicles such as endosomes or Golgi where the low pH environment sustains their optimal protease activity, while their C-termini are exposed to the cytoplasm, enabling post-translational modification and protein-protein interaction. Although very short, the cytoplasmic domain of BACE-1 plays an important role in orienting BACE-1 cellular trafficking and compartmentalization. BACE-1 resides in the trans-Golgi network (TGN) and in the endosomes, the main cellular sites of APP processing and A β production.⁹⁵ As shown in Figure 2.2, after synthesis, BACE-1 resides in the endoplasmic reticulum (1) and is transported to the TGN (2). From this compartment, BACE-1 is transported to the plasma membrane (PM) (3) where a small proportion can undergo ectodomain compartment shedding (4). The majority of BACE-1 is internalized into endocytic compartments (EC) (5) where the acidic environment provides the optimal condition for the proteolysis of APP. From the endocytic compartments BACE-1 can be recycled to directly back to the cell surface (6a), transit to lysosomes for degradation (6b) or retrogradely to the TGN (6c) from where it can be trafficked back to the PM (7). It is also possible that BACE-1 can be transported directly from the TGN to endocytic compartments (8).

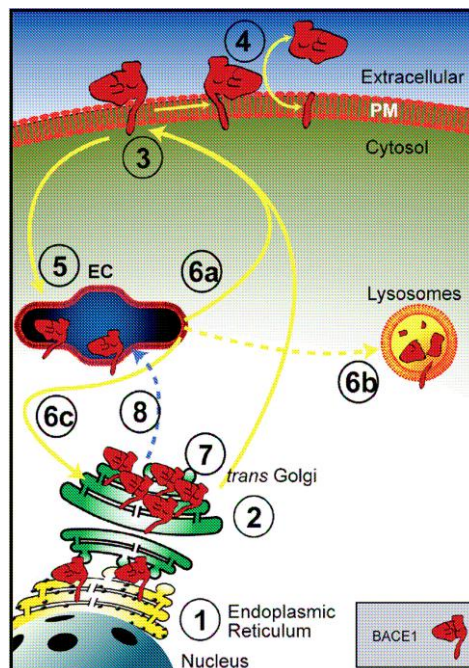


Figure 2.2. Intracellular trafficking of the enzyme BACE-1 (see text for the discussion).

Insight into the three-dimensional structure of BACE-1 is vital to understanding how the enzyme works catalytically,⁹ and in developing inhibitors which block BACE-1 activity as a therapy for AD. X-Ray crystallography of BACE-1 has determined numerous structures of BACE-1 complexes, and residues and regions that are important for substrate specificity and proteolysis.⁹⁶⁻⁹⁹ To date, there are over 100 known structures of BACE-1 in complex with inhibitor, seven without inhibitor and one of BACE-2 in the protein data bank (<http://www.pdb.org/pdb/home/home.do>). The number of crystal structures of BACE-1 is evidence to the variety of compounds being tested as AD-modifying drug candidates. The X-ray structure of BACE-1 protease domain was first determined to 1.9 Å resolution, with BACE-1 bound to an eight residue transition state analogue inhibitor OM99-2 (Figure 2.3).¹⁰⁰

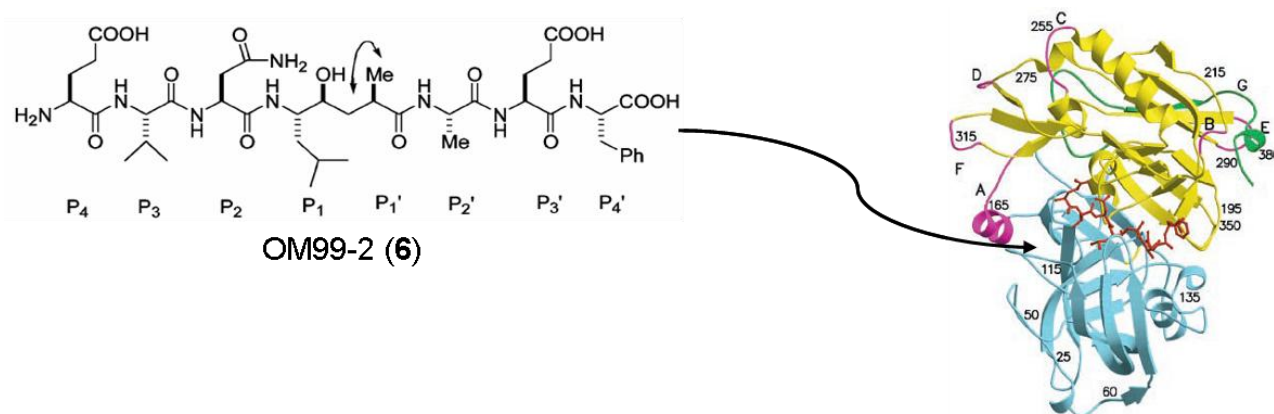


Figure 2.3. On the left, the chemical structure of BACE-1 inhibitor OM99-2 (**6**) with the constituent aminoacids and their subsite designations (the hydroxyethylene transition-state isostere is between P1 and P1'). On the right, a new cartoon model of the crystal structure of BACE-1 complexed to inhibitor OM99-2 (**6**) (PDB id: 1FKN).¹⁰⁰ The N-lobe and C-lobe are blue and yellow, respectively, except the insertion loops, designated A to G in the C-lobe are magenta and the COOH-terminal extension is green. The inhibitor bound between the lobes is shown in red.

OM99-2 (**6**) is a P4-P4' peptide (P4-P3-P2-P1*-P1'-P2'-P3'-P4') based on the aminoacid composition of APP_{SWE} (Glu-Val-Asn-Leu*Ala-Ala-Glu-Phe) but incorporating a non-cleavable hydroxyethylene isostere (*) at P1 and P1', blocking normal proteolytic BACE-1 cleavage between the P1 and P1' scissile bond (Figure 2.3). Further enzyme subsites were identified for BACE-1 with enzyme bound to other eight residues⁹⁸ and longer transition state inhibitors,⁹⁹ and the crystal structure of free BACE-1 has been studied.^{96,97} These crystal structure studies show BACE-1 has strong conservation when compared with A1 aspartic proteases, for which pepsin is prototypic, and also more recently with BACE-2.¹⁰¹ Ribbon diagrams of the 3D structure described for BACE-1, BACE-2 and pepsin, describing their major structural features, are reported in Figure 2.4. Regions

of commonality include: the conformation and location of the catalytic Asp dyad in the middle of the active site cleft at the interface between N- and C terminal lobes, and the shielding of the active site by a flexible antiparallel hairpin-loop, known as a flap.^{100,101} Overall accommodation of the eight peptide substrate (P1-P4) residues occurs at enzyme subsites (S1-S4) and P1'-P4' at enzyme subsites S1'-S4' in a similar way to other aspartic proteases. Thus, hydrogen bonds between the active site aspartates and 10 hydrogen bonds from different parts of the active site and flap bond to the substrate/inhibitor backbone in the active site cleft, with a high degree of conservation. There are key differences between the BACE-1 crystal structure and other aspartic proteases that may be exploited in design of novel and selective BACE-1 inhibitors. The most obvious difference is the larger molecular surface of BACE-1, due to the presence of five insertions (four loops and one helix) all in the C-terminal lobe, in addition to the presence of a 35 residue C-terminal extension, the latter being highly ordered in structure and possibly forming a stem with the trans-membrane domain.¹⁰⁰ In addition, although the general organisation of the active site subsites is similar to other aspartic proteases, their specificity and conformation display key differences.^{97,98,100} Moreover, the active site of BACE-1 is larger, having additional subsites (S5-S7), and although it works well with the eight substrate residues as is normal for other aspartic proteases, it can also accommodate a greater number of substrate residues.¹⁰² The larger opening of the active site occurs due to structural differences near subsites, and the absence of a constricting pepsin helix loop across from the active site.^{97,98,100} The S1 and S3 subsites consist mostly of hydrophobic residues and their conformations are very different to pepsin. S4 and S2 are much more hydrophilic than these subsites in other aspartic proteases, where S2 in BACE-1 and BACE-2 contains Arg (Arg235, Arg249, respectively), absent in other aspartic proteases and linked to more effective cleavage of APP_{SWE} compared to normal APP.^{100,101} Subsites S5-S7 localise in the vicinity of the insertion helix, a region also absent in other A1 aspartyl proteases, and is believed to contribute to substrate recognition and transition state binding.⁹⁹ The flexible flaps which cover the active sites of all A1 aspartic protease contribute to hydrolytic specificity and substrate access, believed to open to allow substrate/inhibitor access, close when substrate/inhibitor is bound, and open to release hydrolytic products. However, the details of this mechanism are unclear. The BACE-1 flap position can differ by 4.5 Å – 7 Å at the tip when comparing free unbound enzyme (*apo* form) with enzyme bound to transition state inhibitor.^{97,103} A conserved aspartic protease Tyr71 residue in the tip of the flap forms hydrogen bonds with substrates/inhibitors at the P1 and P2' positions of BACE-1, thereby mechanistically sealing the flap shut.⁹⁷ The open position is narrow and stabilised by intra-flap hydrogen bonds and a hydrogen bond with Tyr71 (Figure 2.4). A parallel side chain region in BACE-1 (and also in BACE-2), known as the third strand (see Figure 2.4), forms hydrogen bonds

with residues in the flap and active site residues, thereby influencing and stabilising the open or closed state of the enzyme.⁹⁷ Another region of flexibility shared between BACE-1 and BACE-2, most likely important in recognition and processing of APP substrate, is known as the 10s loop,¹⁰¹ which forms part of the hydrophobic S3 binding pocket (Figure 2.4). This region can also display flexible conformations in BACE-1 when comparing Apo and inhibitor complexed structures,^{96,97,100} and displays subtle differences in aminoacid composition between BACE-1 and BACE-2 (Figure 2.4) and may be involved in their substrate discrimination.¹⁰¹

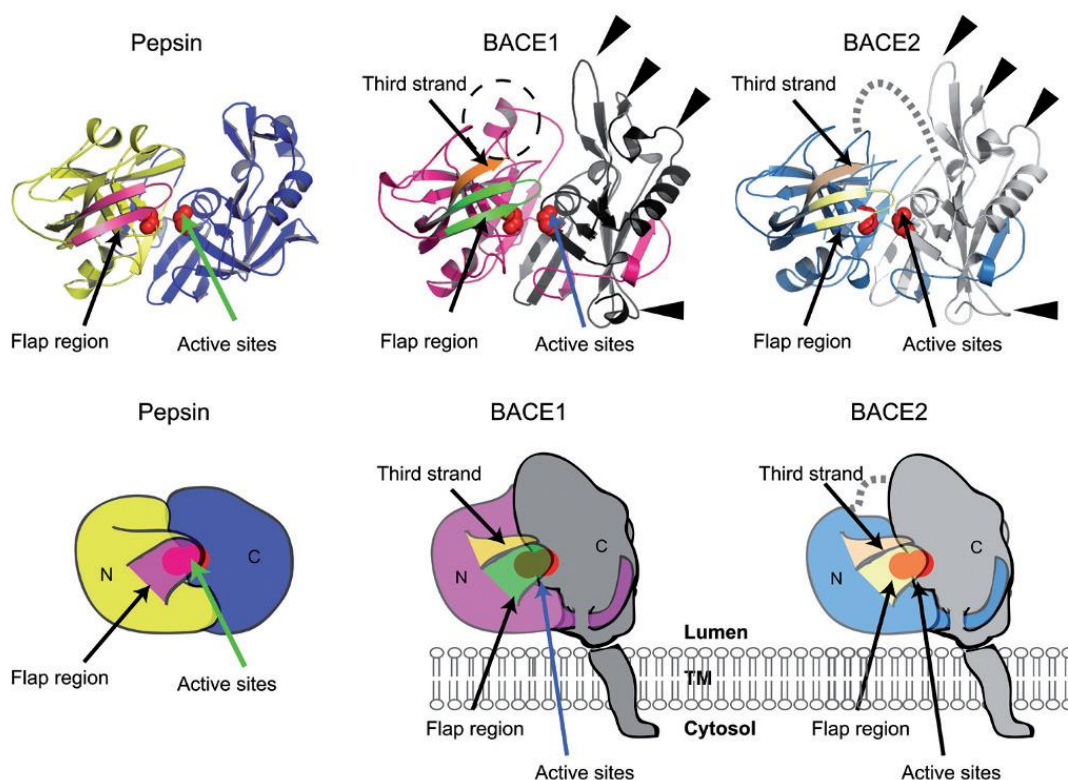


Figure 2.4. Structural features of BACE-1 compared to pepsin and BACE-2. Structures for pepsin (PDB id: 1PSN),¹⁰⁴ BACE-1 (PDB id: 1SGZ)⁹⁷ and BACE-2 (PDB id: 2EWY)¹⁰¹ were obtained from the protein data bank. The shown cartoon illustrations underneath the ribbon structures represent the surface structures of each protein and a possible orientation of BACE-1 and BACE-2 to the membrane. The N-terminal lobes of pepsin, BACE-1 and BACE-2 are coloured gold, magenta and blue respectively, and the C-terminal catalytic lobes are coloured dark blue, dark grey and silver respectively. The flap regions of pepsin, BACE-1 and BACE-2 are shown in their respective colours of purple, green and wheat. The third-strands in BACE-1 and BACE-2 are shown adjacent to the flaps and coloured orange and beige respectively. The active site aspartates of each enzyme are coloured in red space fill. The BACE-1 and BACE-2 insertion loops are indicated with arrow heads and the BACE-1 insertion helix is highlighted with a hatched circle. The dashed line in BACE-2 represents a disordered region in the BACE-2 crystal structure.

Examination of the interaction of the P4-P4' peptide inhibitor based on the mutant aminoacid composition of APP_{SWE} (Glu-Val-Asn-Leu*Ala-Ala-Glu- Phe) with active site of BACE-1 gives information about why this substrate displays a 60-fold increase in affinity of APP_{SWE} over that of

normal wild-type APP to cause AD.¹⁰⁰ Firstly, mutant P1-Leu is closely packed against P3-Val and both have considerable hydrophobic contacts with BACE-1, especially true for P1-Leu, part of which encompasses its interaction the Tyr71 at the flap tip. This hydrophobic interaction would likely be much more unfavourable with P1-Met in the normal APP substrate. Furthermore, the side-chain of mutant P2-Asn is H-bonded to P4-Glu and interacts strongly with Arg296 within the S2 subsite, both interactions would be much less favourable with the positively charged P2-Lys in normal APP. Together, the information gained on the unique structural features of BACE-1 through investigating crystal structure is lending to the rational design of inhibitor drugs,¹⁰⁵ incorporating such information on unique subsite inhibitor interaction and flap control. Definitely, crystal structures of BACE-1 inhibitors complexes have revealed key features regarding the possible protein-ligand interactions, and information related to the nature of binding sites has been of critical importance in the design and development of inhibitors as potential anti-AD drug candidates.

2.2. BACE-1 inhibition

Since BACE-1 has emerged as a promising target for the treatment of AD, its inhibition represents a possible therapeutic strategy to drastically reduce $A\beta$ levels.

Together with the experimental evidence showing that BACE-1 is the rate limiting enzyme in the production of $A\beta$ peptide, a further proof supporting BACE-1 as a superior AD drug target is the finding that BACE-1 knock-out mice do not produce $A\beta$.^{48,88,89} In particular, BACE-1 null mice are fertile and exhibit relatively mild phenotypes such as hypo-myelination^{106,107} and schizophrenia-like behaviours,¹⁰⁸ in contrast to mice with deficiencies in components of the γ -secretase complex. Indeed,¹⁰⁹ mice deficient in presenilin-1,¹¹⁰ nicastrin,¹¹¹ or APH-1¹¹² all exhibit serious developmental defects and die at early embryonic stages because γ -secretase is required to process Notch, a signalling molecule that controls cell fate in embryonic and adult myelopoiesis.¹¹³⁻¹¹⁵ Therefore, compared with γ -secretase, BACE-1 is viewed as a better drug target whose inhibition should cause less serious biological dysfunction.

Moreover, though BACE-1 and BACE-2 share 59% homology and adopt a similar structural organization, the cross inhibition of BACE-2 by BACE-1 inhibitors is less of a concern. In fact, it has been shown that mice with a deficiency in BACE-2 are fertile and healthy.¹¹⁶ However, mice both BACE-1 and BACE-2 knock-out mice displayed an increased mortality risk.

In light of these experimental evidences, in the last decade several drug discovery strategies have been actively exploited in the search for BACE-1 inhibitors as potential anti-AD drug candidates: i) substrate-based method and structure-based design, high-throughput screening and fragment-based lead generation.

Substrate-based method and structure-based design

Substrate-based methods have often been used as the starting point for developing aspartyl protease inhibitors. The first substrate-based BACE-1 inhibitor, P10–P4' StatVal, was developed by Elan Pharmaceuticals in order to purify BACE-1 from human brain homogenates.⁷⁹ This peptidic inhibitor is a P1 (S)-statine substituted substrate analogue with an *in vitro* half-maximal inhibitory concentration (IC_{50}) of ~ 30 nM. Shortly after the molecular cloning of BACE-1, Tang and Ghosh reported the crystal structure of BACE-1 in complex with the octapeptidic, hydroxyethylene (HE) isotere-based transition-state analogue inhibitor OM99-2 (**6**), which, as previously mentioned (see the previous section), was designed on the basis of aminoacidic sequence of APP_{SWE} (Lys670 -> Asn; Met671 -> Leu).¹⁰⁰

In spite of its excellent inhibitory potency *in vitro* ($K_i = 1.6$ nM), the bulky peptidic structure of OM99-2 (see Figure 2.3 in the previous section) precluded its application *in vivo*. Nevertheless, the crystallographic BACE-1/OM99-2 complex provided important molecular insights into the ligand binding interactions in the enzyme active site and significantly advanced the design and development for novel BACE-1 inhibitors.

In parallel, a new octapeptidic BACE-1 inhibitor KMI-008 (**7**) (cellular $IC_{50} = 413$ nM) was developed by Kiso's group employing a hydroxymethylcarbonyl (HMC) isostere as a transition-state mimic.¹¹⁷ Further chemical modifications of KMI-008 (**7**) yielded new more potent pentapeptidic BACE-1 inhibitors KMI-420 (**8**) (*in vitro* $IC_{50} = 8.2$ nM) and KMI-429 (**9**) (*in vitro* $IC_{50} = 3.9$ nM) (see the chemical structures are reported in Figure 2.5).¹¹⁸ In particular, KMI-429 (**9**) appears to significantly reduce brain $A\beta$ secretion when directly injected into the hippocampus of both wild-type mice ($> 30\%$ \downarrow soluble $A\beta$) and APP transgenic mice Tg2576 ($> 60\%$ \downarrow soluble $A\beta$).¹¹⁹ The model Tg2576 is particularly used to evaluate the capability of compounds (i.e. BACE-1 and γ -secretase) potentially able to reduce the secretion of $A\beta$. Indeed, it displays the following features: over-expression of APP_{SWE} and, related to this, increased production of $A\beta_{40}$, presence of $A\beta$ aggregates and lack of NFT.¹²⁰

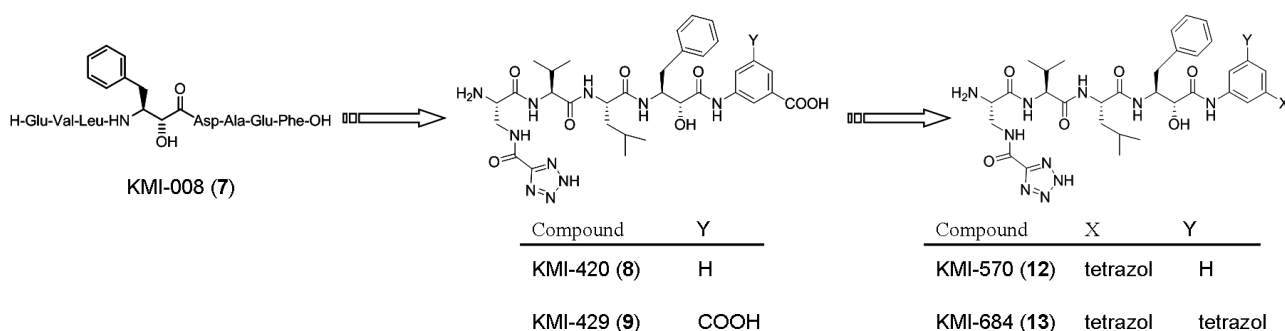


Figure 2.5. Substrate-based BACE-1 inhibitors developed by Kiso's group

At the same time, more substrate-based peptidomimetic inhibitors were also developed by big pharmaceutical companies and other academic research groups.^{121,122} Unfortunately, as expected, despite their nanomolar affinity *in vitro* for the enzyme, these peptidomimetic BACE-1 inhibitors do not present a valuable pharmacokinetic profile (i.e., large size, poor brain permeability, short half-life *in vivo*, and low oral availability) making them unsuitable anti-AD drug candidates.¹²³ On the other hand, based on the large amount of structural information and guided by a structure-based approach, these first-generation inhibitors have laid the foundation for the rational design of later generations of smaller, non-peptidic BACE-1 inhibitors that have significantly improved drug properties.¹²³

The BACE-1 inhibitors, **10** and **11** (see Figure 2.6), developed via chemical modifications of OM99-2 (**6**), are typical examples of BACE-1 inhibitors having less-peptidic features. Both of them exhibited stronger potency (cellular IC_{50} equal to 39 nM and 1 nM, respectively) and impressive *in vivo* efficacy (reduction of plasma $A\beta$ level by 30% and 65%, respectively) when intraperitoneally (i.p.) injected into Tg2576 mice.^{124,125}

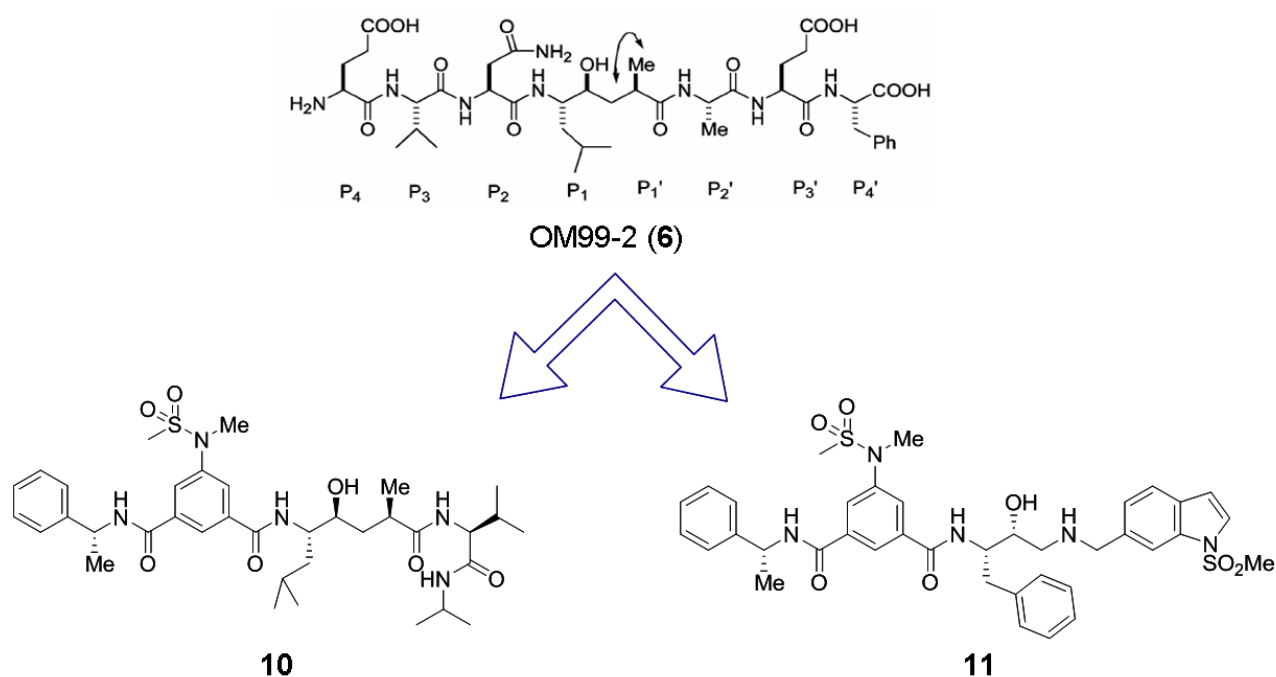


Figure 2.6. Chemical structures of substrate-based BACE-1 inhibitors obtained by modifications on the reference inhibitor OM99-2 (**6**).

In addition to this, further modifications of KMI-420 (**8**) and KMI-429 (**9**) produced tetrazole ring-containing compounds KMI-570 (**12**) (*in vitro* IC_{50} = 4.8 nM) and KMI-684 (**13**) (*in vitro* IC_{50} = 1.2 nM), Both of them also display improved brain permeability (see Figure 2.5).¹²⁶

In 2007 researchers from GSK reported the first orally available BACE-1 inhibitor GSK188909 (**14**), a small non-peptidic compound originated from substrate-based design (Figure 2.7). GSK188909 (**14**) displayed a cellular IC_{50} of 5 nM and showed excellent selectivity over other aspartic proteases. When orally administered in TASTPM mice, a *in vivo* model which expresses both mutant APP_{SWE} and PS1 mutant (Met146 → Val), GSK188909 (**14**) effectively reduced brain $A\beta$ levels.¹²⁷ Subsequently, Schering-Plough also reported an orally effective 4-phenoxyprolidine-based BACE-1 inhibitor, **15**, (Figure 2.7), with good pharmacokinetics and selectivity (K_i = 0.7 nM, cellular IC_{50} = 21 nM).¹²⁸

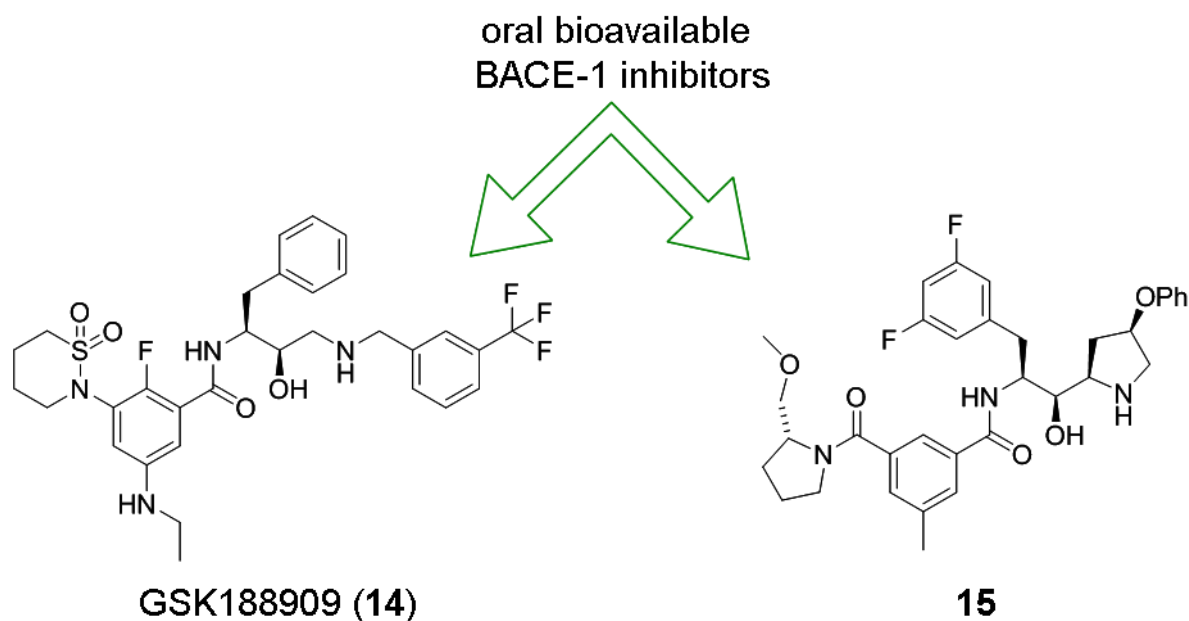


Figure 2.7. Chemical structures of first oral bioavailable BACE-1 inhibitors.

In the scenario of BACE-1 inhibitors, the most promising news have arrived from CoMentis, which has developed the only BACE-1 inhibitor CTS-21166 (cellular $IC_{50} = 1.2\text{--}3.6\text{ nM}$), that has resulted satisfactory enough to recently advance up the Phase II clinical trial thus far. In particular, in 2008, CoMentis revealed this small compound as a transition-state analog inhibitor (its structure is currently not available) with excellent properties in brain penetration, selectivity, metabolic stability, and oral availability. In particular, when i.p. injected (4 mg/kg over six weeks) into an aggressive APP transgenic mouse (expressing both the Swedish and London mutations), CTS-21166 reduced brain $A\beta$ levels by over 35% and plaque load by 40%. The data from human Phase I studies suggested that this compound appeared safe at dose as high as 225 mg, and when intravenously (i.v.) injected into AD patients, it caused a dose-dependant reduction of plasma $A\beta$ levels for an extended period of time (<http://www.alzforum.org/new/detail.asp?id=1790>). More thorough clinical evaluation of CTS-21166 is underway by CoMentis in a partnership with Astellas Pharma in Japan. Following this trend, several companies such as Merck, Eli Lilly, and Takeda are also considering Phase I human testing with their own BACE-1 inhibitors (<http://www.alzforum.org/new/detail.asp?id=1790>). Interesting clinical data will likely be available for these inhibitors in the near future.

High-throughput screening (HTS) and fragment-based lead generation methods

Though many BACE-1 inhibitors were successfully designed as substrate-based analogues mimicking the transition state, most of non-peptidic BACE-1 inhibitors were developed using HTS

or a fragment-based lead generation method. In particular, HTS has been conducted by many big pharmaceutical companies to identify *hit* compounds from different chemical libraries. In 2001, Takeda presented the first series of non-peptidic BACE-1 inhibitors with an *in vitro* IC₅₀ of 0.35–2.93 μM using this approach.¹²⁹ Subsequently, Wyeth reported their *hit* compound WY-25105 (**16**) (*in vitro* IC₅₀ = 3.7 μM, cellular IC₅₀ = 20 μM) containing an acylguanidine moiety that can form key interactions with the aspartic catalytic dyad (Asp32 and Asp228).¹³⁰ Structure optimization of this compound has led to the development of a more potent BACE-1 inhibitor **17** (Figure 2.8) with an *in vitro* IC₅₀ of 0.11 μM, also showing an 85-fold selectivity over the cathepsin D.¹³⁰ Using the similar approach, Johnson & Johnson developed the BACE-1 inhibitor **18** (Figure 2.8) having a stronger affinity for BACE-1 (K_i = 11 nM)¹³¹ and, nevertheless, exhibiting excellent brain permeability and oral availability. Indeed, when orally administered at 30 mg/kg to rats, **18** was able to lower plasma Aβ₄₀ levels by 40–70% 3 h post-dosing. In spite of all of these successes, none of these HTS-based inhibitors has entered a clinical trial.

Recently, fragment-based drug discovery (FBDD) has emerged as a novel alternative to the traditional HTS method in identifying potent BACE-1 inhibitory drugs. In contrast to HTS, which uses libraries of relatively high molecular weight compounds, the FBDD approach takes advantage of libraries comprising more diverse and smaller-sized compounds (fragments) to identify *hits* that can be efficiently developed into potent *leads* with drug-like properties. After the *hits* identification, chemical modifications may hamper to obtain *lead* compounds and to further optimize these *leads* into suitable drug candidates.

Together with these methods, a variety of biophysical techniques (NMR, X-ray crystallography, fluorescence resonance energy transfer (FRET) or surface plasmon resonance (SPR), etc.), computational tools and biochemical assays can be coupled in fragment screening. In particular, by a fragment screening approach assisted with NMR and followed by X-ray crystallography and FRET assays, AstraZeneca reported a FBDD-based BACE-1 inhibitor **19** (Figure 2.8) with a cellular IC₅₀ ≈ 0.47 μM.^{132,133} Astex, in a partnership with AstraZeneca, discovered several BACE-1 inhibitors by employing a X-ray crystallography based fragment screening.¹³⁴

This approach provides detailed structural information on the binding mode of fragments to the active pocket of BACE-1 highlighting the chemical optimizations which can be performed on these inhibitors. Huang et al. reported non-peptidic BACE-1 inhibitors using fragment screenings by a computer-assisted docking simulation method.^{135,136} Moreover, researchers from Evotec identified a series of BACE-1 inhibitors by a novel fluorescence-polarization-assay-based fragment screening method coupled with X-ray crystallography.¹³⁷ The integration of various techniques in the

fragment screening has made FBDD an increasingly popular method for designing potent small-molecule BACE-1 inhibitors.

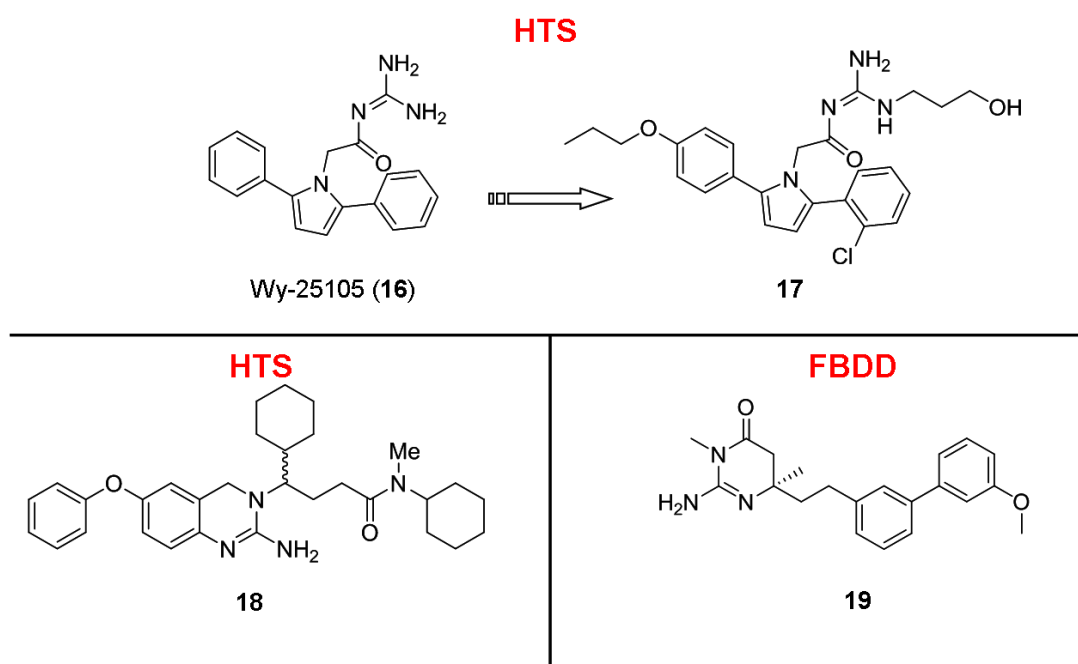


Figure 2.8. Chemical structures of non-substrate-based BACE-1 inhibitors.

It should be emphasized that each of the previously mentioned strategies of drug discovery has its pros and cons. While substrate-based BACE-1 inhibitors usually show high potency and selectivity, their poor oral availability and permeability across the blood-brain barrier frequently make them unsuitable drug candidates. By contrast, the HTS method has the advantage of generating *hits* with high diversity, smaller size, and more drug-like properties (*i.e.*, oral availability and brain penetration). However, the *hit* rate of HTS tends to be extremely low and the *hits* generally have lower potency and selectivity than substrate-based inhibitors. Compared with the traditional HTS method, however, fragment-based screening and structure-based approach enjoy much higher *hit* rates, and like HTS, can identify leads with favourable drug properties. On the other hand, fragment *leads* are too small to exhibit satisfactory potency and selectivity, thus requires considerable subsequent chemical modifications. Overall, a combinatorial approach associated with computational structure-based studies that carefully integrates the strengths of different design strategies may find its successful application in the future design of more applicable BACE-1 inhibitory drugs.

Alternative therapeutic approaches targeting BACE-1

Few therapeutic approaches outside of BACE-1 inhibitors have so far been reported. Chang et al.¹³⁸ explored the idea that neutralizing antibodies against BACE-1, generated from the immunization with the protease itself, may be enlisted to reduce $A\beta$ production. Immunization of BACE-1 produces polyclonal anti-BACE-1 antibodies in peripheral system such as plasma. Certain percentage of antibodies penetrates BBB and binds to BACE-1 on surface of brain cells. Rapid endocytosis on neuron membrane carries surface molecules to endosome with an optimal pH ~ 4.5 for BACE-1 activity. Because enzymatic site of BACE-1 is masked by antibodies, BACE-1 hydrolysis on APP is prevented. Therefore, production of $A\beta$ is reduced improving the cognitive performance of AD mice. The antibodies in this approach serve as inhibitors for BACE1 activity and thus do not require the participation of immune cells for $A\beta$ reduction. This may indeed lower the risk of autoimmune response as observed in $A\beta$ immunization. A conceptually related approach is immunization using peptides derived from the BACE-1 cleavage site in APP. A study with AD mice using this approach has shown promise.¹³⁹

Other strong evidences to deal with are the intracellular trafficking of BACE-1 allowing to perform its function of APP hydrolysis and consider endosome as the main location of enzyme activity. Considering this issue might explain the poor results obtained with some inhibitors in cellular assays.¹⁴⁰ In fact, although ubiquitously expressed, BACE-1 mRNA has the highest expression levels in the mammalian brain, and is found in acidic organelles of the endosomes and trans-Golgi network. This is consistent with the discovery that BACE-1 cleavage of APP occurs predominantly in endosomes, and that endocytosis of APP and BACE-1 is essential for $A\beta$ production.¹⁴⁰ BACE-1 activity and access to substrates is regulated by the composition of lipid raft domains in the membrane bilayer. Endosomes have high lipid raft and cholesterol content, critical in regulating APP endocytosis with increased amyloidogenic processing. In order to overcome this crucial issue, an innovative approach was recently reported, consisting of targeting inhibition to the subcellular compartment where the enzyme is active. A membrane anchored BACE-1 transition state inhibitor **20** was synthesized by coupling via a polyglycol linker the inhibitor to a sterol moiety (see Figure 2.9).^{140,141}

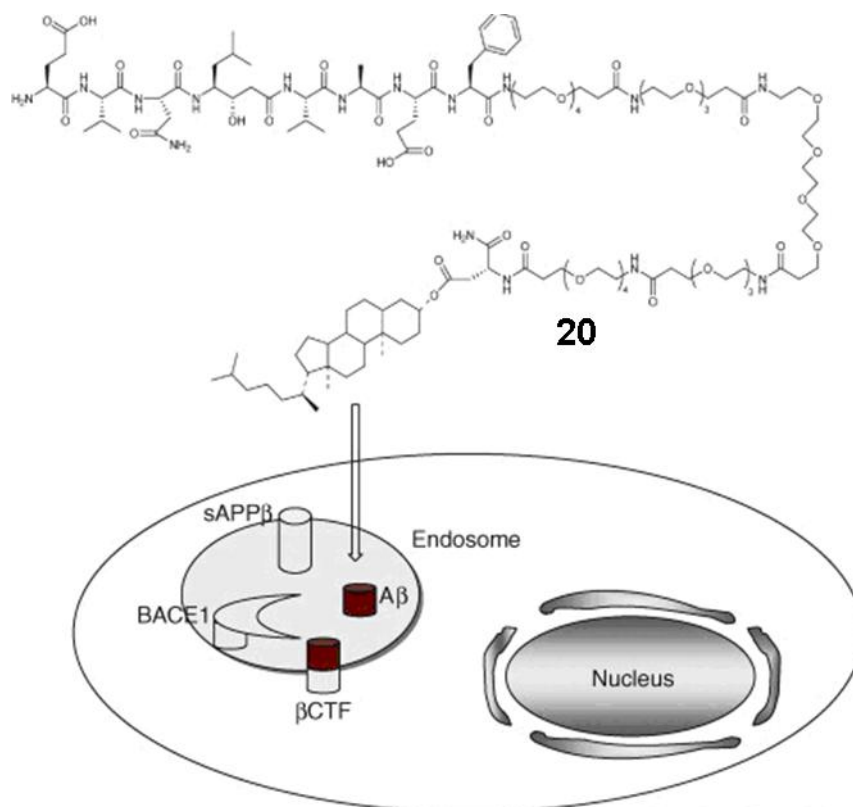


Figure 2.9. Illustration of sterol-linked BACE-1 inhibitor **20** targeting endosome.

This inhibitor efficiently targeted BACE-1 in endosomes via endocytosis, significantly enhancing the inhibitor efficacy, both in cell culture and in fly and mouse models of AD. Although it is too early to say whether this approach will lead to a functional drug therapy, the authors postulate that this membrane-tethering strategy might also be useful for designing inhibitors against other disease-associated membrane proteins.

Potential mechanism-based toxicity from BACE-1 inhibition

Actually, whether BACE-1 null mice did not display severe physiological dysfunctions it is plausible to expect that toxicity related to BACE-1 inhibition will not cause so warning side effects. However, it has become increasingly clear that APP is not the sole substrate for BACE-1, which also cleaves membrane-bound substrates. One of these substrates is neuregulin-1 (Nrg-1),^{106,107} an essential neurotrophic factor that, through the ErbB family of receptor-tyrosine kinases, regulates various neurological processes, such as synaptic functions, neuronal migration, myelination, and neurotransmitter functions, among many others.¹⁴²⁻¹⁴⁴ In BACE-1 null mice, abolished cleavage of Nrg1 disrupted BACE1-dependant Nrg1/ErbB signaling, causing hypo-myelination (thinner myelin) of both peripheral nerves^{106,107} and central nerves¹⁰⁶ as well as schizophrenia-like phenotypes in these mice.¹⁰⁸ Furthermore, it has shown that BACE-1 null mice exhibit impaired remyelination in adult mice.¹⁴⁵ Another important BACE-1 substrate is the voltage-gated sodium

channel $\beta 2$ (Nav $\beta 2$) subunit.^{146,147} Voltage-gated sodium channel proteins are composed of a pore-forming α subunit and auxiliary β subunits.¹⁴⁸ In particular, BACE-1 null mice display epileptic seizures which might derive from elevated neuronal surface expression of sodium channel proteins and the resulted increased neuronal excitability.¹⁴⁹ It is highly plausible that the abolished cleavage of Nav $\beta 2$ by BACE-1 leads to these observed alterations, because the disruption of this cleavage in BACE-1 null mice will potentially affect both the expression and cellular trafficking of sodium channel proteins. The absence of BACE-1 will reduce the shedding of Nav $\beta 2$ intracellular domain that can regulate gene expression of the sodium channel α subunit;¹⁴⁶ disruption of BACE-1 dependant cleavage of Nav $\beta 2$ will also increase the level of full-length Nav $\beta 2$ protein, able to bind to the α subunit and, then, to mediate its trafficking to the membrane surface.¹⁵⁰ Moreover, aged BACE-1 null mice were found to undergo to hippocampal neurodegeneration that is probably due to the sustained asynchronous neuronal stimulation in these mice.¹⁴⁹

All together these important findings strongly suggest that BACE-1 performs diverse physiological functions through processing of different substrates. Therefore, careful titration of drug dosage may still be a needed precaution to avoid the potential mechanism-based toxicity incurred by BACE-1 directed AD therapy.¹⁵¹

Chapter 3

3. Computational methods

3.1. Molecular docking

Introduction

Molecular docking is a computational tool and represents a crucial component of many drug discovery projects, from *hit* identification to *lead* optimization. In particular, it is employed in approaches such as structure-based design and virtual screening techniques, widely used in many discovery efforts: respectively, prediction of binding modes and selection from virtual large databases of putative ligands into the binding site of biological target. The docking methodology was pioneered during the early 1980s and remains a current and highly active area of research, thanks also to its short time and low computational cost.

In particular, it is a multi-step process in which each step introduces one or more additional degrees of complexity. Initially, the process begins with the application of algorithms that sample the several degrees of conformational freedom of small molecules “posing” them in the binding site. The algorithms are complemented by scoring functions that are designed to describe the biological activity through the evaluation of interactions between the ligand and the potential target as well as the entropic cost of the ligand conformation.

Some of these scoring functions adopted for molecular docking try to estimate the free energy of binding of the ligand-target complex. Unfortunately, this estimation is not always reliable because of the high error associated to it. However, the molecular docking represents a useful technique in the computer-aided drug design and discovery context towards delicate issues such as the identification of molecular features that are responsible for specific biological recognition and/or the prediction of chemical modifications to improve potency of ligands.

Molecular docking is a computational procedure that predicts binding mode of a ligand in its target protein. This is achieved by minimizing a scoring function, which describes the interactions between ligand and target with respect to the atomic positions of the two moieties.

In this work, GOLD¹⁵² and AutoDock^{153,154} programs were used to predict ligand-protein interactions. Both these programs adopt genetic algorithms to generate the single poses of ligands into the binding site of protein target, which are evaluated by their appropriate scoring functions.

Algorithms in molecular docking

Several algorithms are used in molecular docking programs to obtain the pose of ligand in the binding site of protein. In general, the docking problem is the search for the minimum of a function that depends on a large number of degrees of freedom, namely the position and the geometrical arrangement of ligand (its conformation) and of its target.

The searching algorithms adopted in molecular docking can be divided in three types of searches: systematic, stochastic and deterministic; some algorithms combine more than one of these approaches.

Systematic algorithms explore a grid of values for each degree of freedom considered, in a combinatorial way. As the number of degrees of freedom increases, the number of evaluations needed increases rapidly and termination criteria are inserted to prevent the algorithm from sampling space that is known to lead to the wrong solution. Stochastic search algorithms make random changes on the degrees of freedom of the system. To improve convergence, multiple independent runs are performed. In deterministic searches, the initial state determines the move that can be made to generate the next state, which generally has the same or a lower energy than the initial state.

Genetic algorithms (GAs)

The Genetic Algorithms (GAs) belong the class of stochastic algorithms and are based on the language of natural genetics and evolutionary biology. GAs are computer programs that mimic the process of evolution by manipulating a collection of n data structures called chromosomes. Indeed, using genetic operations they search for possible conformations of ligands.^{152,155}

The quality of results depends on the starting genes, the number of evolutionary events and the scoring function adopted to select the most favourable conformers. Firstly, the GA generates an initial population as set of chromosomes (conformations of ligands randomly chosen and determined into the binding pocket). The chromosomes are defined by one or more strings of genes (variables), that can assume binary, integer or real values corresponding to: i) ligand translation (x, y, z coordinates of the center of mass); ii) ligand orientation (rotation angles); iii) ligand conformation (torsion angle for each rotatable bond). The population undergoes to a fitness evaluation of ligand-protein complex: each chromosome is associated to a score based on a function

which approximately estimates the binding free energy/fitness. Starting from an initial population of chromosomes (parents), randomly generated and subsequently evaluated on the basis of specific scoring function, the GA repeatedly applies the three genetic operators, such as *reproduction*, *crossover* and *mutation*, to obtain a new population of chromosomes (children) that replace the least-fit members of the population.

- *reproduction* represents the selection process of the fittest members scored of a population that will survive in the next generation;
- *crossover* combines chromosomes by performing a one or two-point crossing on the parent strings resulting in the children ones (as higher the number of crossover points is, more information is exchanged between the parent strings);
- *mutation* randomly modifies one or more gene(s) to give the offspring chromosomes.

Thus, in contrast with the only *reproduction* operator, crossover and mutation allow the exploration of the conformational space through the introduction of children chromosomes to be submitted to a new cycle of genetic operations. The whole cycle is repeated until some generations are defined and/or until some conditions (i. e. RMSD, ΔG) are satisfied.

GOLD uses an island-based genetic algorithm search strategy¹⁵⁵ and includes rotational flexibility for selected receptor hydrogen along with full ligand flexibility. AutoDock uses a genetic algorithm as a global optimizer combined with energy minimization as a local search method.^{153,154} The ligand is flexible, while the receptor is rigid.

Genetic algorithm in GOLD

GOLD employs a so-called island-based genetic algorithm. This means that not only one large population of chromosomes (described in the previous section) is manipulated, but also several sub-populations (i.e. islands) are considered and individual chromosomes can migrate among them. This feature improves the efficiency of search (a diagram showing how the GA in GOLD works is given in Figure 3.1). In addition, information concerning H-bonds between the ligand and the protein target is also encoded in the chromosome. The H-bonds are matched with a least squares fitting protocol to maximize the number of this kind of inter-molecular interactions. A population of potential solutions (in this case, possible docking poses of ligand) is set up at random. Each member of the population is encoded as a chromosome which contains information on: i) the mapping of ligand H-bonded atoms onto complementary protein ones; ii) mapping of hydrophobic points on the ligand onto protein ones; conformation around flexible ligand bonds and protein OH-groups. Each chromosome is assigned a fitness score based on its predicted binding affinity and the

chromosomes within the population are ranked according to fitness. The population of chromosomes is iteratively optimized.¹⁵⁶

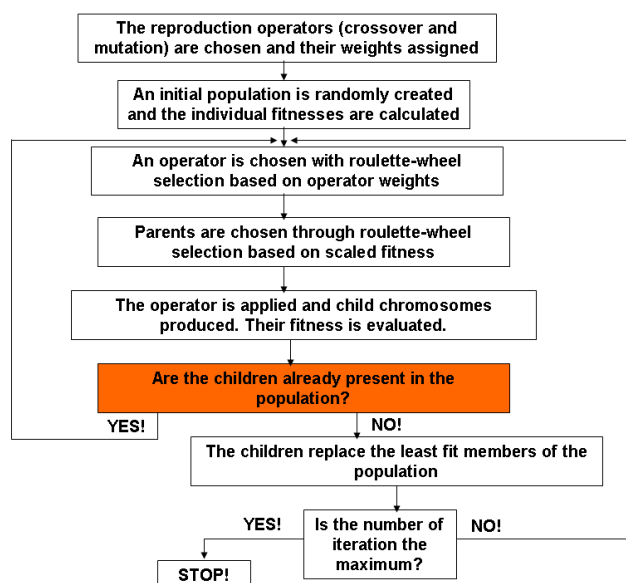


Figure 3.1. The block diagram of the GA as implemented in GOLD.

Genetic algorithm in AutoDock

The AutoDock adopts a GA in which it is implemented a local search method, initially proposed by Solis and Wets,¹⁵⁷ that allows to minimize the scoring function of selected individuals. The optimized atomic coordinates (phenotype) are stored back in the chromosome (genotype). Then, the new chromosome enters into a new iteration of genetic operators employed by GA. Given this transfer of information from phenotype to genotype this algorithm is called Lamarckian genetic algorithm (LGA).¹⁵⁴ In the LGA the local search (see Figure 3.2) is normally performed in phenotypic space and employs information about the fitness landscape. Sufficient iterations of the local search arrive at a local minimum, and an inverse mapping function is used to convert from its phenotype to its corresponding genotype. However, in the case of molecular docking, local search is performed by continuously converting from the genotype to the phenotype, so inverse mapping is not required. The genotype of the parent is replaced by the resulting genotype, however, in accordance with Lamarckian principles.

Moreover, in the LGA genotypic *mutation* has a different role with respect to the traditional GAs. Traditionally, *mutation* acting as a local search operator allows small refining changes not efficiently performed by *reproduction* and *crossover*. However, by using the explicit local search operator this role is not fundamental, but it allows to replace alleles that might disappear during the *reproduction*. Therefore, the *mutation* operator can have a multiple exploratory role.

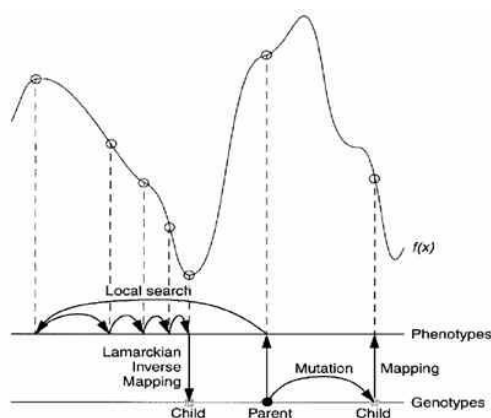


Figure 3.2. Genotypic and phenotypic search leading to a Darwinian and Lamarckian search.

Scoring functions

The evaluation and ranking of predicted ligand conformations is a crucial aspect of molecular docking. Thus, the design of reliable scoring functions is of fundamental importance. Scoring functions implemented in docking programs make various assumptions and simplifications in the evaluation of modelled complexes and do not fully account for a number of physical phenomena that determine molecular recognition for example, entropic effects. Essentially, three types or classes of scoring functions are currently applied: force-field-based, empirical and knowledge-based scoring functions.

Molecular mechanics force fields usually quantify the sum of two energies, the receptor–ligand interaction energy and internal ligand energy (such as steric strain induced by binding). Most force-field scoring functions only consider a single protein conformation, which makes it possible to omit the calculation of internal protein energy, which greatly simplifies scoring. Various force-field scoring functions are based on different force field parameter sets.

The empirical scoring functions are fit to reproduce experimental data, such as binding energies and/or conformations, as a sum of several parameterized functions. The design of these scoring functions is based on the idea that binding energies can be approximated by a sum of individual uncorrelated terms. The coefficients of the various terms are obtained from regression analysis using experimentally determined binding energies and, potentially, X-ray structural information.

There are also the scoring functions knowledge-based, which are designed to reproduce experimental structures rather than binding energies. In knowledge-based functions, ligand–protein complexes are modelled using relatively simple atomic interaction-pair potentials. A number of atom-type interactions are defined depending on their molecular environment. In common with empirical methods, knowledge-based scoring functions attempt to implicitly capture binding effects that are difficult to model explicitly.

Here, we revise the scoring functions implemented in the programs used in the thesis: GoldScore and ChemScore for GOLD, and the empirical scoring function from AutoDock

GoldScore (GS)

GS is a force-field-based scoring function implemented in GOLD and, in particular, it is defined as the weighted sum of the following components: the energy of the H-bonds between the protein and the ligand (E_{hb}), the internal energy of the ligand in the binding pose (E_{in}) and the van der Waals interaction energy of the bound complex (E_{vdw}) (see the equation reported below).^{152,155}

$$GS_{fitness} = -(c_{hb}E_{hb} + c_{in}E_{in} + c_{vdw}E_{vdw}) \quad (3.1)$$

GS is defined as a fitness function, where every single component is coupled to some given coefficients: c_{hb} , c_{in} and c_{vdw} . These are empirically determined on the basis of adjustments performed to best reproduce a series of known crystallographic ligand/protein complexes.

The H-bond term considers the difference between the interactions of protein and ligand in the complex and free in water, thus accounting for desolvation effect: initially the donor (d) and the acceptor (a) are considered in solution and, then, on coming together (da) water (w) is stripped off. Therefore, the H-bond energy E_{ij} between a donor i and an acceptor j between the ligand and the protein is composed by the following terms:

$$E_{ij} = (E_{da} + E_{ww}) - (E_{dw} + E_{aw}) \quad (3.2)$$

The interaction energies for each donor and acceptor types are pre-calculated with quantum mechanics and molecular mechanics approaches for a set of model fragments. For all the poses of ligand generated, the possible combinations of donors i and acceptors j between the ligand and the protein's are evaluated and a weight w_{ij} between 0 and 1 is assigned to each bond on the basis of both the distance between donor and acceptor and the angle formed by donor, H atom and acceptor:

$$w_{ij} = w_{dis(ij)} + w_{angl(iHj)} \quad (3.3)$$

$$w_{dis(ij)} = \begin{cases} 1, & d_{LP} \leq 0.25 \text{ \AA} \\ \left(-\frac{10}{33}d_{LP} + \frac{35}{33}\right)^2, & 0.25 < d_{LP} \leq d_{max} \text{ \AA} \\ 0, & d_{LP} > d_{max} \text{ \AA} \end{cases} \quad (3.4)$$

$$w_{angl(iHj)} = \begin{cases} 1, & \vartheta > 160^\circ \\ \left(-\frac{1}{150}\vartheta + \frac{1}{15}\right)^2, & 10^\circ < \vartheta \leq 160^\circ \\ 0, & \vartheta \leq 10^\circ \end{cases} \quad (3.5)$$

The distance d_{LP} is between the donor and the acceptor's lone pair. In default implementation of GOLD, d_{max} varies linearly from 4.0 Å at the first iterations to 1.5 Å after 75000 iterations to let only close-contacts H-bond contribute to GS fitness value of the final solutions. Similarly, ϑ is the angle between the donor, the H atom and the acceptor lone pair. The H-bond energy term in the scoring function is then given by the sum of all individual H-bond energies, multiplied by their weights:

$$E_{hb} = \sum_{ij} w_{ij} E_{ij} \quad (3.6)$$

The internal energy contribution is considered in GS function only when it is positive to avoid a lower minimization of the internal energy of ligand than of the one of reference conformation. It is the sum of the steric and torsional energies ligand: the steric energy is described by a sum over all the atoms $i \neq j$, separated by a distance d_{ij} , in the ligand of a 6-12 Lennard-Jones potential term:

$$E_{ij} = \frac{C}{d_{ij}^{12}} - \frac{D}{d_{ij}^6} \quad (3.7)$$

whereas the torsional one, associated with four consecutively bonded atoms I, j, k, l , is given by:

$$E_{ijkl} = \frac{1}{2} V_{ijkl} \left[1 + \frac{n_{ijkl}}{|n_{ijkl}|} + \cos\left(n_{ijkl} \cdot \omega_{ijkl}\right) \right] \quad (3.8)$$

where ω_{ijkl} is the torsional angle, n_{ijkl} the periodicity and V_{ijkl} the barrier of rotation.

The term E_{vdw} describes the close-contact interaction energy and it is calculated as the sum over all pairs of atoms i and j , respectively from ligand and protein, which are distanced between them less than 1.5 times the sum of their van der Waals radii. A 4-8 potential is used to describe this interaction:

$$E_{ij} = \frac{A}{d_{ij}^8} - \frac{B}{d_{ij}^4} \quad (3.9)$$

where d_{ij} is the distance between two atoms. If $E_{ij} > sE_{ij,min}$, a linear cut-off is applied to switch off this interaction, $E_{ij,min}$ being the minimum of E_{ij} and s being a scaling factor whose value increases logarithmically during the run in order to encourage the close contacts. A and B were chosen with the aim at reproducing the minimum of the standard 12-6 potential. The 4-8 potential is preferred because it is softer and allows the algorithm to easily form close-contacts with the protein.

ChemScore (CS)

The CS function was derived empirically from a set of 82 protein-ligand complexes from the PDB whose experimental binding affinities were determined.^{158,159} Unlike GS, CS was trained by multiple regression analysis against measured affinity data. The CS function attempts to estimate the total free energy of binding for a ligand-protein complex as a sum of different components:

$$\Delta G_{ChemScore} = c_0 + c_{Hbond}E_{Hbond} + c_{metal}E_{metal} + c_{lipo}E_{lipo} + c_{rot}H_{rot} \quad (3.10)$$

$$E_{Hbond} = \sum_{il} g_1(\Delta r)g_2(\Delta\alpha) \quad (3.11)$$

$$E_{metal} = \sum_{aM} f(r_{aM}) \quad (3.12)$$

$$E_{lipo} = \sum_{lL} f(r_{lL}) \quad (3.13)$$

In particular the function 3.10 uses contact terms to respectively estimate contributions from H-bonds (E_{Hbond}), metal-ligand (E_{metal}) and lipophilic interactions (E_{lipo}). The term H_{rot} indicates a penalty for flexibility of ligand and depending on its number of rotatable bonds.

The coefficients c_0 (it is a constant), c_{Hbond} , c_{lipo} , c_{metal} , and c_{rot} were empirically derived during the validation of the scoring function.

The H-bond term is calculated for all complementary possibilities of H-bonds between the ligand atoms, i , and target (and water) atoms, l . The functions g_1 and g_2 have the following form:

$$g_1(\Delta r) = \begin{cases} 1, & \Delta r \leq 0.25 \text{ \AA} \\ \left(1 - \frac{(\Delta r - 0.25)^2}{0.4}\right)^2, & 0.25 < \Delta r \leq 0.65 \text{ \AA} \\ 0, & \Delta r > 0.65 \text{ \AA} \end{cases} \quad (3.14)$$

$$g_2(\Delta\alpha) = \begin{cases} 1, & \Delta\alpha \leq 30^\circ \\ \left(1 - \frac{(\Delta\alpha - 30)^2}{50}\right)^2, & 30^\circ < \Delta\alpha \leq 80^\circ \\ 0, & \Delta\alpha > 80^\circ \end{cases} \quad (3.15)$$

where Δr is the deviation of bond length from 1.85 Å and $\Delta\alpha$ the deviation of bond angle from the ideal value of 180°.

The third term is eventually calculated for all acceptor/donors a in the ligand and the metal ion M in the target. This is described by the function $f(r)$, which has a simple contact form common for:

$$f(r) = \begin{cases} 1, & 0 < r < R_1 \\ \frac{1}{R_1 - R_2} - \frac{R_2}{R_1 - R_2}, & R_1 < r < R_2 \\ 0, & r > R_2 \end{cases} \quad (3.16)$$

where R_1 is 0.5 Å plus the sum of the two atoms' van der Waals radii and $R_2 = R_1 + 3.0$ Å. The same functional form is used to describe the lipophilic term, that is calculated for all lipophilic atoms in the ligand, l , and in the protein L .

The final term identifies the frozen rotatable bonds of ligand. All non-terminal sp^3 --- sp^3 and sp^2 --- sp^2 bonds are considered frozen if atoms on both sides of the bond are in contact with the target (two atoms are considered to be in contact if their distance is less than 0.5 Å).

H_{rot} estimates the flexibility penalty for molecules with frozen rotatable bonds:

$$H_{rot} = 1 + \left(1 - \frac{1}{N_{rot}}\right) \sum_r \frac{1}{2} (P_{nl}(r) + P'_{nl}(r)) \quad (3.17)$$

N_{rot} being the number of frozen rotatable bonds, and $P_{nl}(r)$ and $P'_{nl}(r)$ the percentages of polar atoms on either side of the rotatable bond.

AutoDock scoring function

In AutoDock¹⁵⁴ the implemented scoring function is defined as an empirical binding free energy function:

$$\begin{aligned} \Delta G_{AutoDock} = & \Delta G_{vdw} \sum_{i,j} \left(\frac{A_{ij}}{r_{ij}^{12}} - \frac{B_{ij}}{r_{ij}^6} \right) + \Delta G_{hb} \sum_{i,j} E(\varphi) \left(\frac{C_{ij}}{r_{ij}^{12}} - \frac{D_{ij}}{r_{ij}^{10}} \right) + \Delta G_{elect} \sum_{i,j} \left(\frac{q_i q_j}{\epsilon(r_{ij}) r_{ij}} \right) \\ & + \Delta G_{tor} N_{tor} + \Delta G_{sol} \sum_{i,j} (S_i V_j + S_j V_i) e^{\left(\frac{r_{ij}^2}{2\sigma^2} \right)} \end{aligned} \quad (3.18)$$

The summations are performed over all pairs of ligand atoms, i , and protein atoms, j , in addition to all pairs of atoms in the ligand separated by three or more bonds. r_{ij} is the distance between the atoms, φ is the H-bond angle, and q_i is the electrostatic charge of atom i . All five ΔG terms on the right hand side are coefficients empirically determined using linear regression analysis from a set of thirty protein-ligand complexes with known binding constants. The first three terms are in vacuo interaction terms: Lennard/Jones 12-6 dispersion repulsion term; a directional 12-10 hydrogen bonding term; screened Coulomb electrostatic potential. ΔG_{tor} is a measure of the unfavorable entropy of ligand binding due to the restriction of conformational degrees of freedom, and N_{tor} is the number of sp^3 bonds in the ligand. The last term approximately accounts for the desolvation free energy upon ligand binding. For each atom in the ligand, fragmental volumes of surrounding protein atoms (V_j) are weighted by an exponential function and then summed, evaluating the percentage of volume around the ligand atom that is occupied by protein atoms. This percentage is then weighted by the atomic salvation parameter of the ligand atom (S_i) to give the desolvation energy.

Cluster analysis

ACIAP implements a hierarchical agglomerative clustering algorithm.^{160,161} ‘‘Hierarchical’’ means that clusters at a higher level are union of clusters at lower levels, while ‘‘agglomerative’’ means that clusters never break apart during the formation process. The global hierarchy can be represented by means of a dendrogram, a tree showing different clustering levels, spanning from 1 to n . RMSD is taken as a measure of conformation-to-conformation distance. Therefore, the clustering algorithm starts with n unitary clusters; at each step, the two closest clusters are merged, until only one cluster containing all the poses is reached.¹⁶² The way the inter-cluster distance is evaluated by the average linkage method. Once the hierarchical tree is built, KGS penalty function is used to define the best clustering level and to prune it. At the end for each cluster, the representative conformation is calculated.

3.2. Molecular screening

Introduction

Among the different computational approaches available at present to complement or to succeed the array of HTS discovery technologies, virtual screening (VS) is one of the most popular. VS methods are mainly designed for searching large virtual compounds databases and selecting a limited number of candidate molecules for testing in order to identify NCEs with the desired biological activity.

The VS origins are protein-structure-based compounds screening or docking^{163,164} and chemical-similarity searching based on small molecules.¹⁶⁵ Although structures of target proteins are becoming increasingly available as templates for structure-based VS, small-molecule-based screening continues to dominate the field, owing to the fact that *hit* or *lead* information is still the predominant source of knowledge in many cases.

Chemical similarity search

In the context of VS, one of the most straightforward approaches is the similarity-search based on 2D molecular fragments as templates. This method aims at finding compounds that exhibit required chemical, structural, pharmacological or other properties. Such properties are represented as molecular descriptor sets and these descriptor sets are compared against each other by calculating a dissimilarity score between them. Thus, the goal of the screening procedure is often expressed as an allowed maximal dissimilarity score: structures with a dissimilarity score below such predefined *threshold* are accepted by the screening process, while others are rejected.

Dissimilarity metrics

The comparison of two descriptors involves the calculation of one or more dissimilarity coefficients using dissimilarity metrics. The following metrics have been employed: Tanimoto and Euclidean. Values of these metrics are non-negative numbers. A zero dissimilarity value indicates that the two descriptors are identical, and the larger the value of the dissimilarity coefficient the bigger the difference between the two structures is.

Tanimoto's dissimilarity metrics

In its original form, Tanimoto metrics¹⁶⁵ can be applied to binary fingerprints and it is a similarity metric:

$$T_{sim}(a,b) = \frac{B(a \& b)}{B(a) + B(b) - B(a \& b)} \quad (3.19)$$

where a and b are two binary fingerprints, $\&$ denotes binary bit-wise and-operator, $|$ denotes binary bit-wise or-operator and $B(x)$ is the number of 1 bits in any binary fingerprint x :

$$B(x) = |\{x_i = 1 \mid x \in \{0,1\}^n; i = 1, \dots, n\}| \sum_{i=1}^n x_i \quad (3.20)$$

The larger the number of common bits in a and b , the larger the value of similarity coefficient, T_{sim} , is. Therefore larger values represent higher similarity between a and b ; 1 is total similarity, when the two descriptors are the same, while 0 represents the absolute dissimilarity. From that it is straightforward to obtain a dissimilarity measure:

$$T_{dissim}(a,b) = 1 - T_{sim}(a,b) \quad (3.21)$$

However, extending binary Tanimoto dissimilarity to molecular descriptors other than binary fingerprints is less obvious.

The idea is to represent an integer value as a unary number, that is, replace it by as many 1 bits as its value is. This can be extended to a binary fingerprint by adding leading zeros to the series of 1 so as to make the length of all series the same. In this way, a binary fingerprint is generated and the original Tanimoto metric can be applied to it. For example the series 13, 4, 7, 9 can be represented as unary numbers as follows:

1111111111111, 1111, 1111111, 111111111

The binary form is:

111111111111, 0000000001111, 0000001111111, 0000111111111

which can simple be written as a binary fingerprint:

11111111111110000000000111100000011111110000111111111

for which applying Tanimoto is simple. With the above consideration in mind, Tanimoto can be rewritten for integer valued descriptor in the form below:

$$T_{sim}(a,b) = \sum_{i=1}^n \frac{\min(a_i, b_i)}{a_i + b_i - \min(a_i, b_i)} \quad (a = \langle a_1, \dots, a_n \rangle, b = \langle b_1, \dots, b_n \rangle) \quad (3.22)$$

Euclidean distance

The Euclidean distance, as a geometrical distance function, can be used to measure the distance (dissimilarity) between two non-spatial objects, in our case between two molecular descriptors. The formulation is straightforward:

$$d_E(a,b) = \sqrt{\sum_{i=1}^n (a_i - b_i)^2} \quad (3.23)$$

Note, that this distance is a dissimilarity function, and, on this basis, 0 value represents total similarity. However, the Euclidean distance of two molecular descriptors is not upper-bounded: the larger the distance the higher the dissimilarity between the two descriptors. One could think that this characteristic of the Euclidean metric allows more accurate measurement of dissimilarity, but in practice this is seldom needed. Instead, the direct comparability of dissimilarity values is important. This is hard to achieve with the use of Euclidean distance since dissimilarity values obtained for a large compound library are scattered in a wide range and one should not necessarily have *a priori* ideas about suitable threshold for the dissimilarity value for acceptance/rejection.

Chapter 4

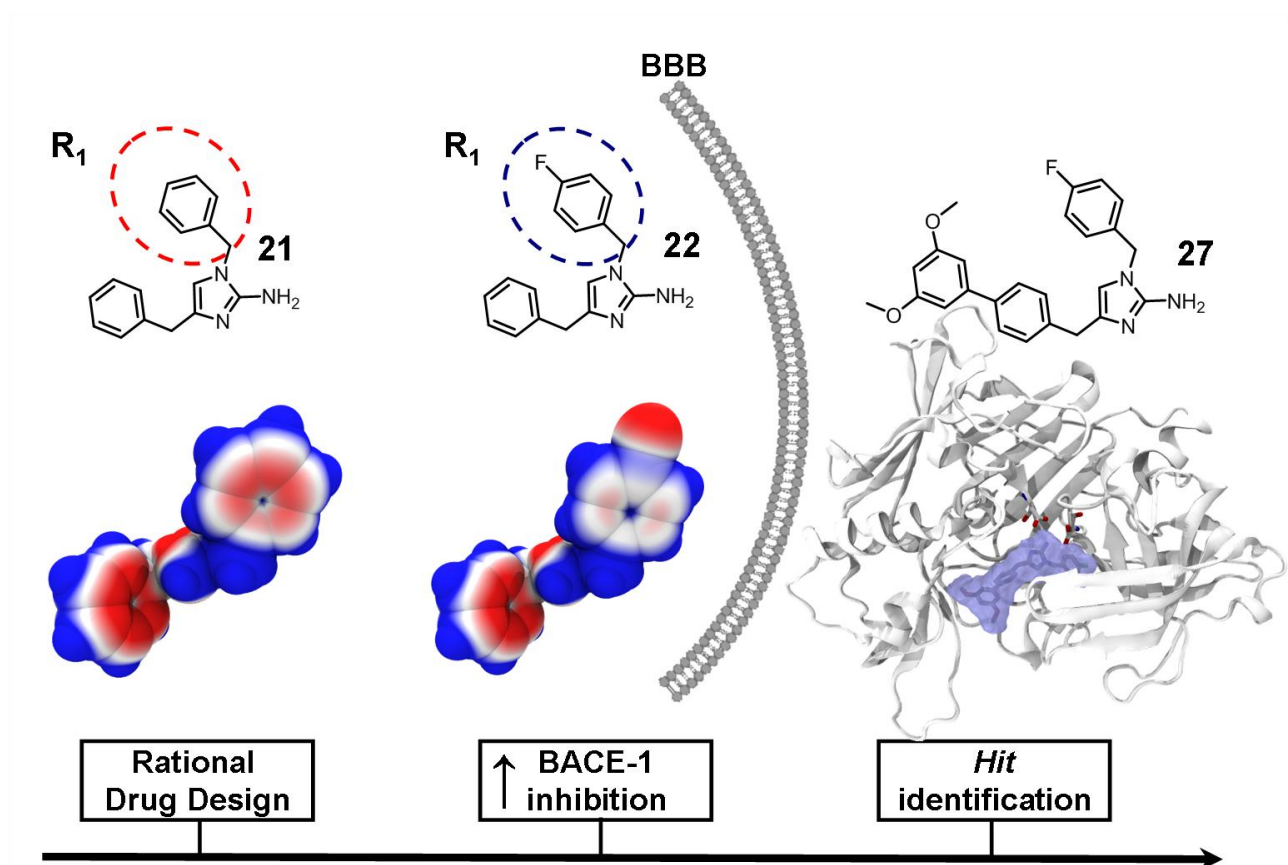
4. Novel classes of BACE-1 inhibitors as potential anti-Alzheimer's drugs

So far no compounds have been identified that can slow down or halt the progression of AD. Since it has been experimentally well assessed that the enzyme BACE-1 catalyses the rate-limiting step in the production of $A\beta$, it represents an attractive target for therapeutic intervention to arrest the disease. Investigation into role of BACE-1 in other physiological proteolytic processes is necessary to identify all possible risks of mechanism-based side effects, which might result from its inhibition. Although this remain a moot point, the experimental evidences discussed in the Chapter 2 and the fact that research groups both in academia and in pharmaceutical industry are currently pursuing BACE-1 as a viable therapeutic target suggest that there is a reasonable and suitable possibility that the benefits of BACE-1 inhibition outweigh the risks. Here, three different approaches employed and aimed at the discovery of novel BACE-1 inhibitors as potential anti-AD drugs are reported:

- i) structure-based design and synthesis (**Strategy 1**);
- ii) *in silico* discovery (**Strategy 2**);
- iii) design and synthesis of MTDLs (**Strategy 3**).

4.1. Strategy 1

A small chemical library of 2-aminoimidazole derivatives as BACE-1 inhibitors: structure-based design, synthesis, and biological evaluation



4.1.1. Introduction

The first BACE-1 inhibitors were peptide and peptidomimetic compounds successfully designed as substrate-based transition state analogs showing a nanomolar affinity for BACE-1.^{98,100} Unfortunately, as expected, these peptidic and peptidomimetic compounds, because of high molecular weight, low hydrophobicity and reduced capability to cross the BBB, do not present a valuable pharmacokinetic profile. However, the crystal structures of these inhibitors in complex with the enzyme have been utilized for structure-based projects that have led to the discovery of several classes of compounds with improved pharmacokinetics properties.¹²³ In particular, there was a boom in the development of non-peptidic BACE-1 inhibitors that have been discovered by means of different experimental screening approaches, such as HTS and fragment-based.^{11,151} Particularly compared with traditional HTS, a significantly higher *hit* rate can be obtained by using a computational structure-based approach, which can fully exploit the large amount of structural information making BACE-1, despite the largeness of its active site, a suitable target for rational drug design purposes.⁶

Here, we report on the structure-based design and microwave-assisted synthesis of a novel small library of 2-aminoimidazoles as BACE-1 inhibitors.

4.1.2. Structure-based design

Initially, we aimed at identifying a moiety potentially interacting with the catalytic aspartic dyad of the enzyme. In particular, among the possible scaffolds, the 2-aminoimidazole appeared to be a very attractive moiety for the following reasons: i) it contains the guanidinium function, which can provide optimal interactions with the catalytic aspartic dyad (see Figure 4.1), as also demonstrated by the crystal structures of several guanidinium-carrying inhibitors in complex with BACE-1;^{131,133,166} ii) it is a privileged structure;¹⁶⁷ iii) it allows the parallel synthesis of differently polysubstituted derivatives.^{168,169} Therefore, the 2-aminoimidazole was docked to validate its capability to interact with the catalytic dyad of BACE-1.

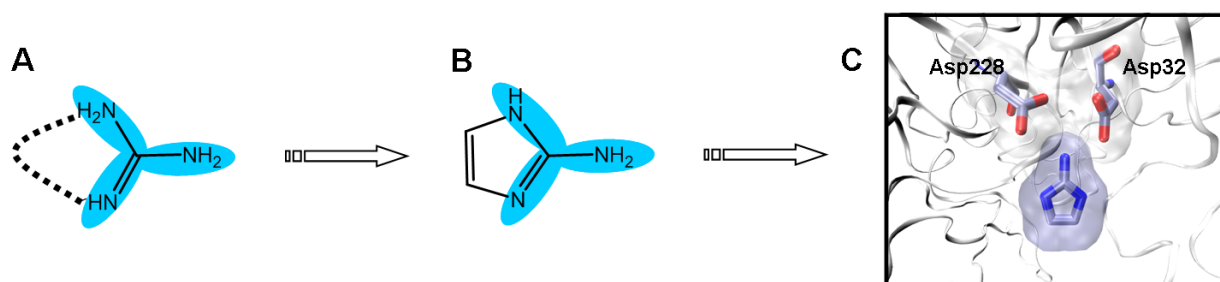


Figure 4.1. The guanidinium function (A) is contained in the 2-aminoimidazole moiety (B) which is a valuable interacting counterpart with the catalytic dyad, Asp32 and Asp228, as shown by the docking BACE-1/2-aminoimidazole complex (C)

As expected, the 2-aminoimidazole turned out to be oriented in the center of the rather large BACE-1 binding pocket by interacting with both catalytic aspartic acids, Asp32 and Asp228, via electrostatic and H-bond interactions (see Figure 4.1). Then, among the 2-aminoimidazoles reported in the literature, the fragment **21** shown in Figure 4.2 turned out to be particularly well-suited for drug discovery purposes for the following reasons: **21** has a low molecular weight (MW = 263.34) and displays a rather good chemical accessibility, which could allow for generating library of compounds. This fragment was preliminary investigated by means of docking simulations. The binding mode of **21** at BACE-1 binding pocket is reported in Figure 4.2. The following interactions were identified: i) the guanidinium moiety of **21** interacted with both aspartic acids (Asp32 and Asp228) side chains and with Thr232; ii) one of the two phenyl rings formed hydrophobic interactions (with Val69, Trp76, Phe108) and a π - π stacking with Tyr71; iii) the second phenyl ring established a cation- π interaction with the side chain of Arg235.

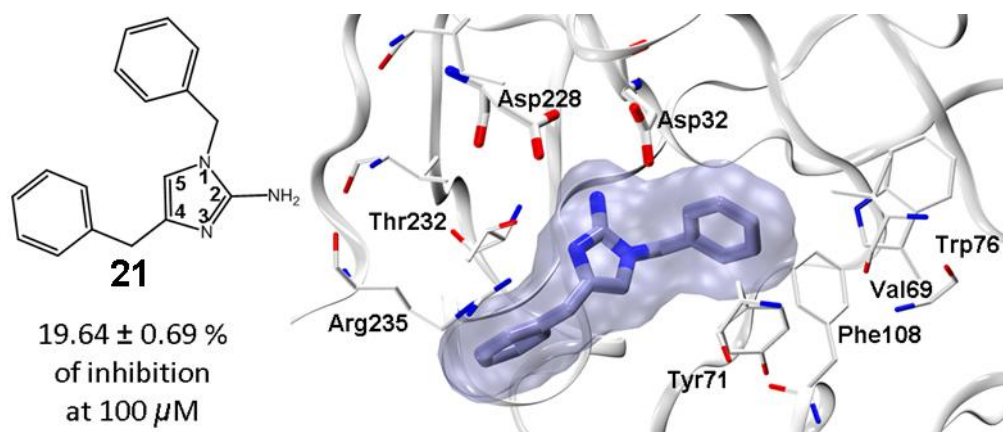


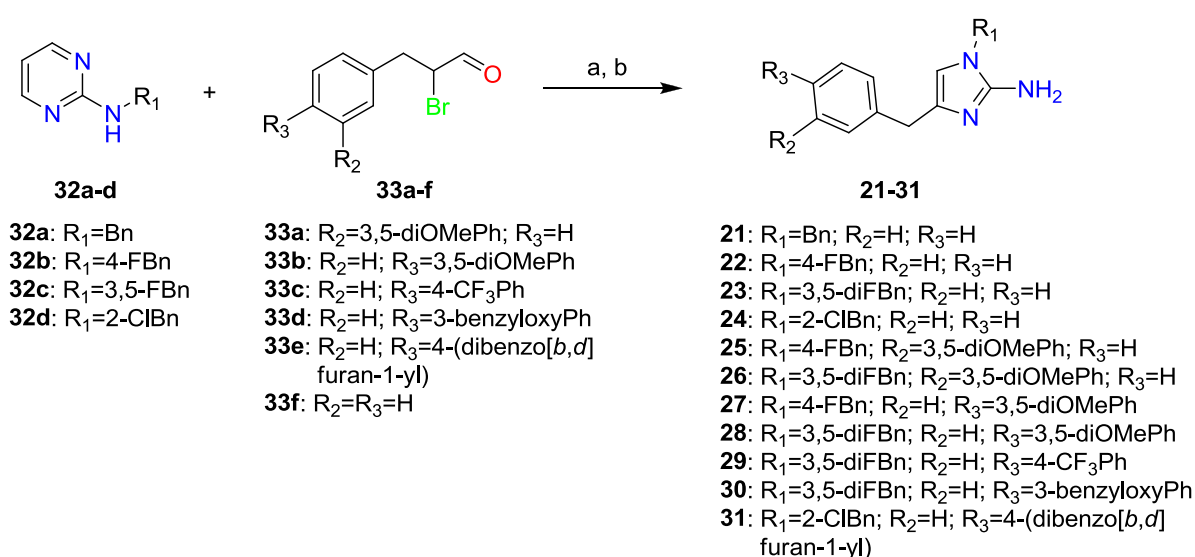
Figure 4.2. Low-energy docking model of the BACE-1/**21** complex.

In light of this computational result, **21** was tested against BACE-1 using an enzymatic assay.¹⁷⁰ It exhibited a moderate-to-low inhibitor potency at 100 μM concentration (BACE-1 inhibition % = 19.64 ± 0.69). On these bases, decorating fragment **21**, we designed and synthesized a small library of 2-aminoimidazoles.

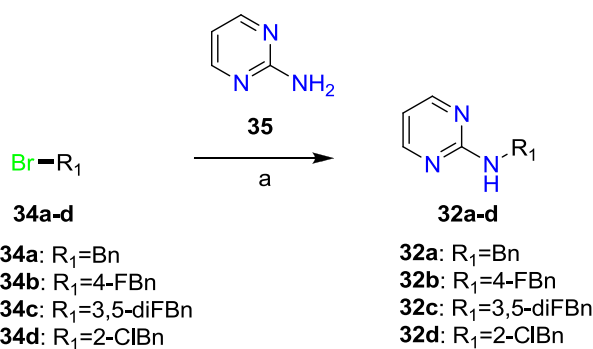
4.1.3. Chemistry

The 2-aminoimidazoles, **21-31**, were obtained taking advantage of a microwave-assisted, one-pot, two-step protocol¹⁶⁹ based on the cyclocondensation of 2-benzylaminopyrimidines **32a-d** and appropriate 3-substituted- α -bromopropyl aldehydes **33a-f**, followed by the cleavage of the corresponding not isolated intermediate imidazo[1,2-a]pyrimidin-1-ium salts with an excess of hydrazine (Scheme 4.1). The 2-benzylaminopyrimidines **32a-d** were synthesized in parallel by reaction of commercially available benzylbromides **34a-d** with excess of 2-aminopyrimidine **35** and sodium hydride (Scheme 4.2). The α -bromo aldehydes **33a-f** were obtained in a parallel fashion using the following synthetic pathway. A cross-coupling Suzuki reaction between the 3-(bromophenyl)-propionic methyl esters **36-37**, which can be easily accessed from the corresponding 3-(bromophenyl)-propanoic acids, and the appropriate boronic acids **38-41** in the presence of a catalytic amount of tetrakis (triphenylphosphine) palladium Pd(PPh₃)₄ gave the 3-biphenyl propanoic methyl esters **42a-e**, respectively. These were reduced to the corresponding 3-biphenyl propyl alcohols **43a-e**. Oxidation of **43a-e** and commercially available 3-phenylpropanol **43f** gave the corresponding 3-substituted propyl aldehydes **44a-f**, which were brominated in mild conditions using 0.5 equivalent of 5,5-dibromobarbituric acid (DBBA) to provide the required 3-substituted- α -bromopropyl aldehydes **33a-f** (Scheme 4.3).

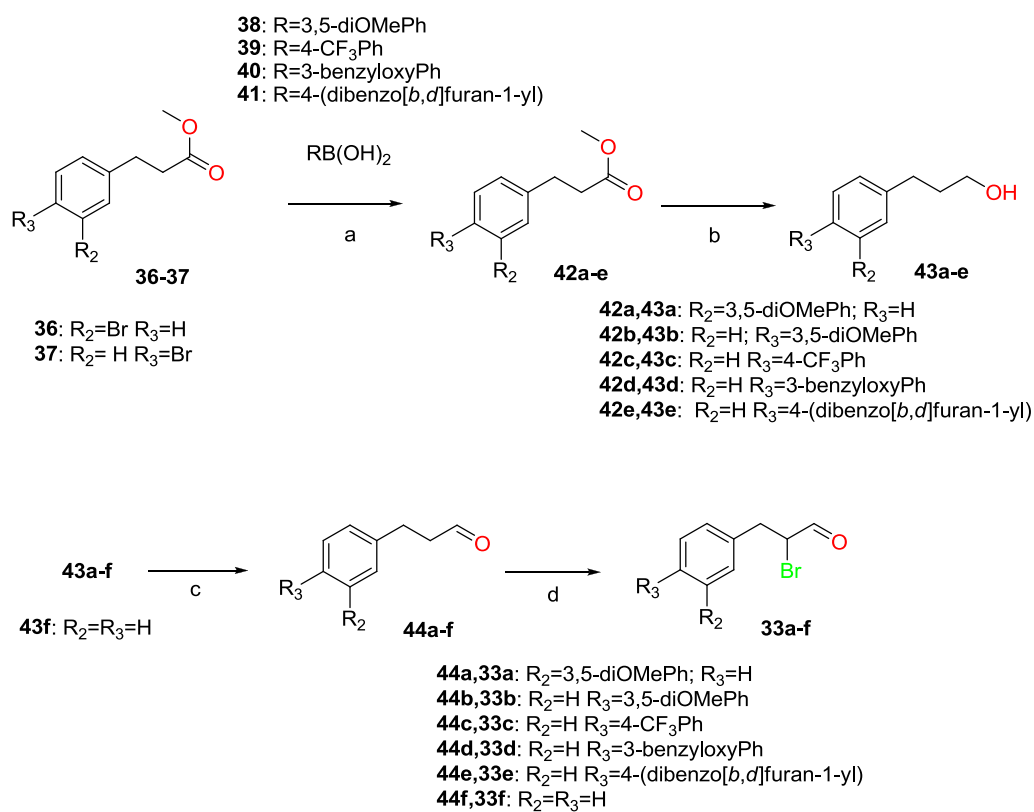
Schemes



Scheme 4.1. Reagents and conditions: (a) MeCN, 150 °C, 150 W; (b) 60% hydrazine (5 eq), MeCN, 100 °C, 100 W.



Scheme 4.2. Reagents and conditions: (a) NaH, THF, 24 h, room temperature.



Scheme 4.3. Reagents and conditions: (a) Pd(PPh₃)₄, Na₂CO₃ (aq), toluene:EtOH (2:1), 5 h, reflux; (b) LiAlH₄, Et₂O, 0 °C, 5 h; (c) PCC (1.4 eq), CH₂Cl₂, 0 °C, 3 h; (d) DBBA (0.5 eq), Et₂O, HCl (cat).

4.1.4. Results and discussion

22-31 were first tested in biochemical assays performed using the fluorescence resonance energy transfer (FRET) methodology.¹⁷⁰ The BACE-1 inhibition studies were based on the cleavage of peptide substrate mimicking the human APP sequence with the Swedish mutation (Methoxycoumarin-Ser-Glu-Val-Asn-Leu-Asp-Ala-Glu-Phe-Lys-dinitrophenyl, M-2420, Bachem, Germany)¹⁷⁰ (see Experimental section (ES)). **22-31** were tested at a concentration of 5 μ M and their BACE-1 inhibition percentages are reported in Table 4.1. The IC_{50} values of most active compounds (**27-29** and **31**) were determined by using the linear regression parameters. Subsequently, the capability of **27-29** and **31** to modulate APP processing was examined by performing a cell-based ELISA assay. This study was carried out in primary chicken telencephalon neurons to assess the effect of the most active inhibitors on secretion of $A\beta_{38}$, $A\beta_{40}$ and $A\beta_{42}$ ¹⁷⁰ (see ES).

As previously described, our strategy was based on **21** as the starting fragment for generating a new series of BACE-1 inhibitors. In particular, we attempted to improve the low potency of **21** (see Figure 4.2) by initially modifying the electronic and hydrophobic properties of the benzyl group in position R_1 (see Scheme 4.1) through the introduction of fluorine and chlorine atoms in different positions (see compounds **22-24** in Table 4.1).

Table 4.1. BACE-1 inhibition profile of compounds **22-31**.

Cpds	Chemical Structure	BACE-1 Inhibition (%) ^{a,b}	BACE-1 IC ₅₀ (μM) ^a
22		26.40 ± 0.02	n.d. ^c
23		20.27 ± 0.01	n.d.
24		23.31 ± 0.01	n.d.
25		32.51 ± 0.01	n.d.
26		32.48 ± 0.01	n.d.
27		40.25 ± 0.01	7.40 ± 1.20
28		38.17 ± 0.05	7.32 ± 0.54
29		41.34 ± 0.01	5.59 ± 0.06
30		24.25 ± 0.02	n.d.
31		37.78 ± 0.01	5.95 ± 0.17

^a Values are mean ± S.D. of two independent experiments for BACE-1 inhibition.¹⁷⁰ ^b % inhibition of BACE-1 activity at the concentration of 5 μM of the tested compounds **22-31**. ^c n. d. = not determined.

Especially, when compared to **21**, **22-24** appeared to have an electron-poorer benzyl group (R₁) (see Figure 4.3) that could allow this moiety to establish more favourable π-π stacking with electron-rich aromatic residues located in the binding pocket (i.e. Tyr71 and Trp76).

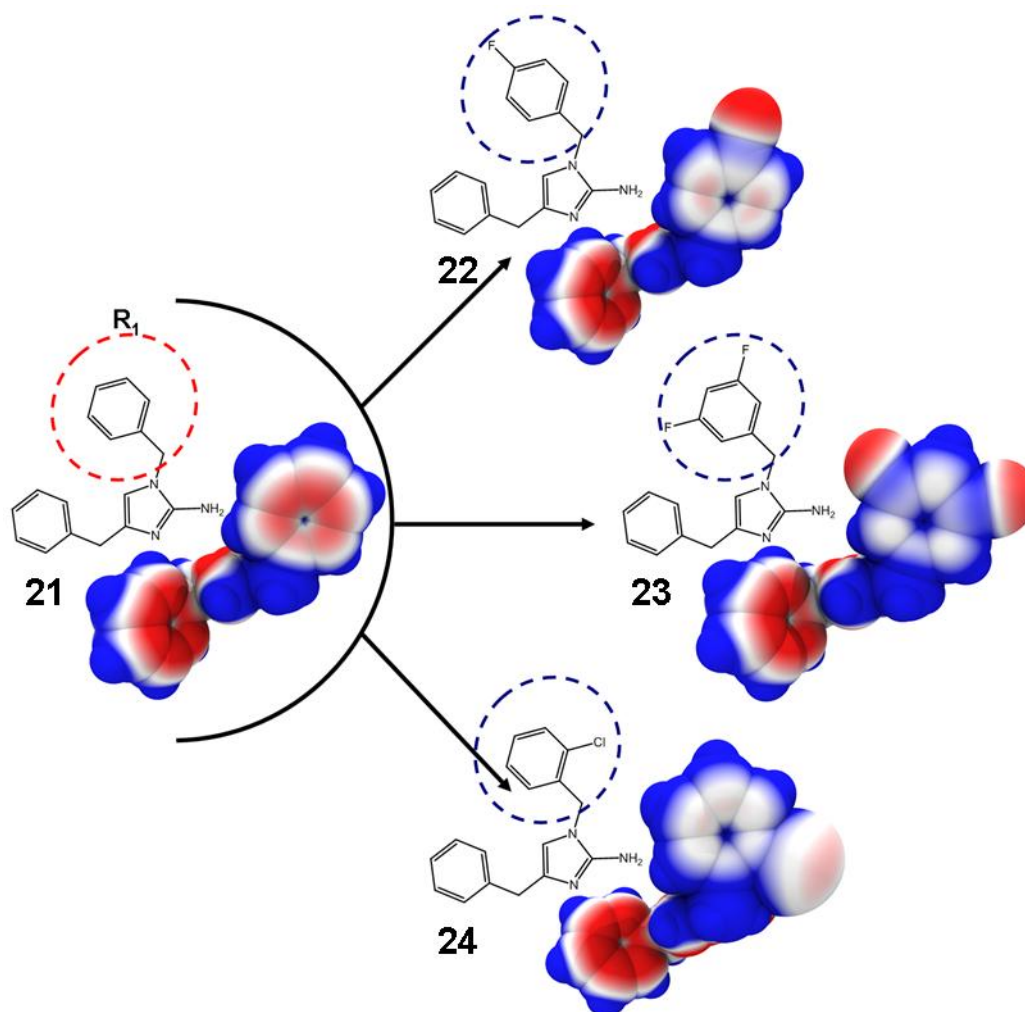


Figure 4.3. ESP surfaces of compounds **21** and **22-24** differently substituted at the crucial R_1 position (shown inside the red and blue dashed lines for compounds **21** and **22-24**, respectively). According to the BACE-1 inhibition data, a concurrent decrease in negative charge (i.e., electron density) of the attached aromatic system can be seen, represented in the ESP surface as a gradual colour change from red→white→blue over the benzene ring.

In addition, from a pharmacokinetic perspective, the presence of fluorine atoms on an aromatic ring could improve the metabolic stability, by avoiding a probable aromatic hydroxylation mechanism.¹⁷¹

To increase the chemical diversity, we then synthesized a second series of derivatives, **25-31**, maintaining a halogenated benzyl group in R_1 and bearing differently substituted aromatic rings in R_2 and R_3 (meta and para positions, see Scheme 4.1). All compounds showed a BACE-1 inhibitory profile. In particular, **27-29** and **31** showed IC_{50} values in the low micromolar range (see Table 4.1). To characterize the binding mode of one of the most active inhibitors, docking and molecular dynamics (MD) simulations were carried out using BACE-1 (PDB id: 1SGZ)⁹⁷ and **27** (see Figure 4.4 and ES).

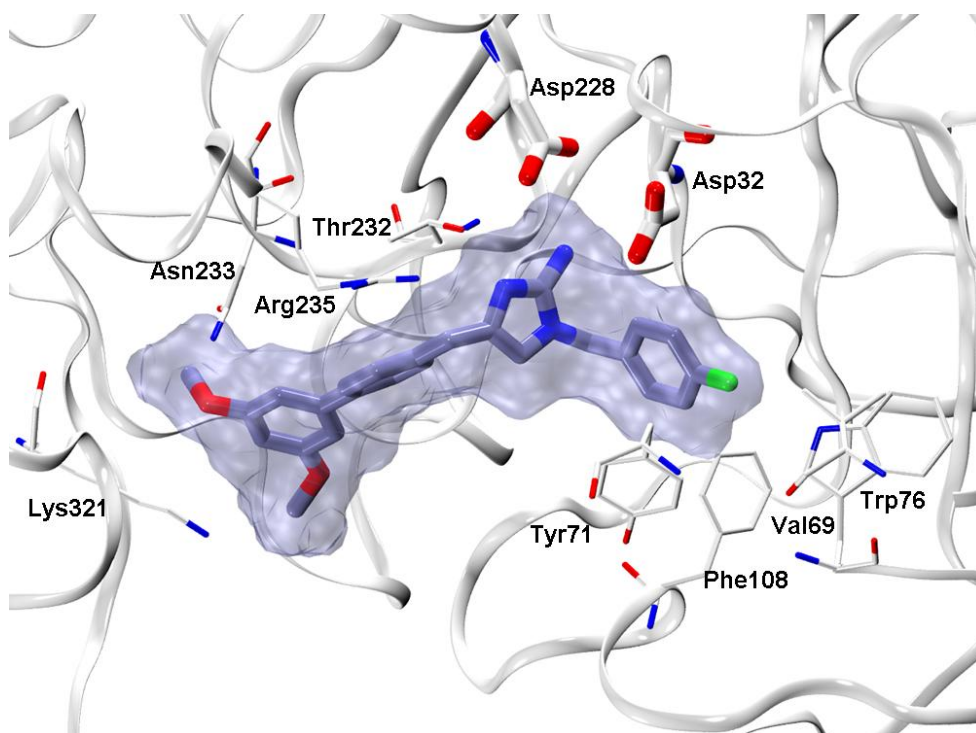


Figure 4.4. The binding mode of **27** at the protease domain of BACE-1 (PDB id: 1SGZ).⁹⁷

The following interactions were observed for the best-ranked pose as obtained using the Goldscore scoring function (see ES): i) the amino group (NH₂) of **27** interacts via H-bond with the catalytic dyad; ii) the N3 nitrogen of the imidazole ring establishes electrostatic and H-bond interactions with the side chains of Asp228 and Thr232, respectively; iii) the fluorine atom interacts with the NH of Trp76 side chain; iv) the benzyl ring establishes favorable π - π stacking with the side chain of Tyr71 and hydrophobic interactions with Val69, Trp76, and Phe108; v) the phenyl group mounted on the C4 of the imidazole ring interacts via cation- π with the Arg235; vi) the polymethoxylated substituent in R₃ might establish H-bond interactions with the side chains of Asn233 and Lys321, both residues located in a solvent-exposed region of the active site. Notably, once this complex was already computationally generated, the X-ray structure of a 2-aminoimidazole derivative in complex with BACE-1 was published by researchers from Merck.^{172,173} Interestingly enough, our predicted binding mode was remarkably similar to that reported^{172,173} showing as pivotal interactions the salt-bridge between the guanidinium moiety and the aspartic dyad. To further investigate the role of these electrostatic interactions, we monitored the stability of these salt bridges throughout two independent runs of 50 ns each (overall 100 ns) of MD simulations (see Figures 4.5) (see ES for further details).

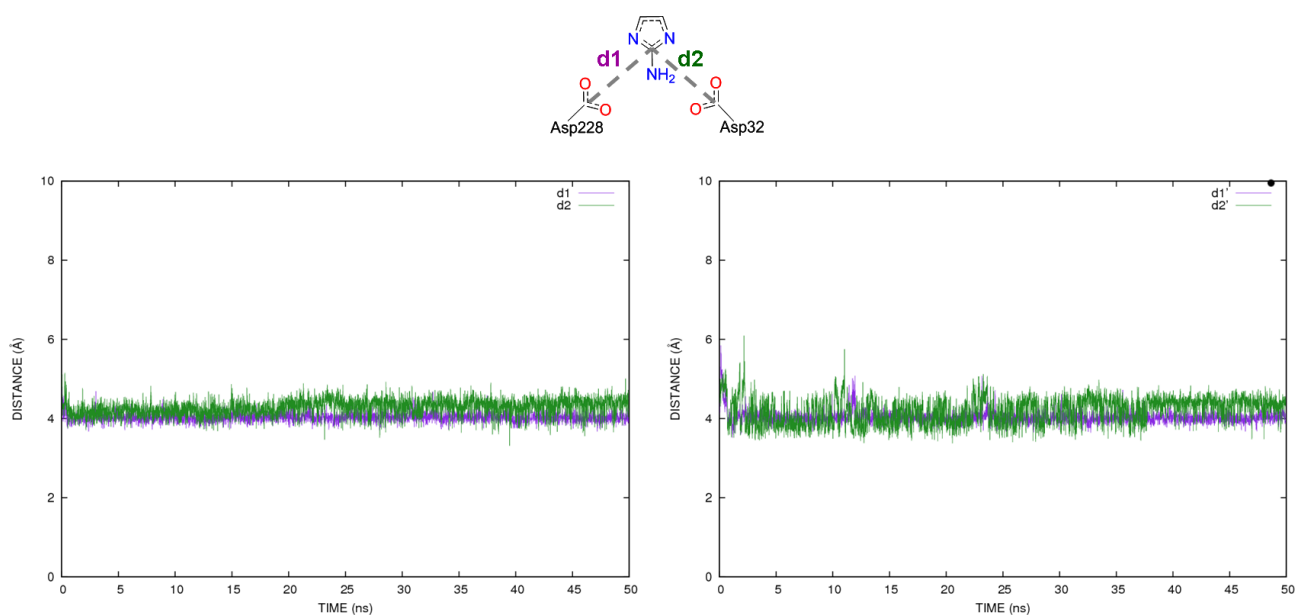


Figure 4.5. The two distances (Å) $d1/d1'$ (C γ @Asp228---Ccat@2-aminoimidazole) and $d2/d2'$ (C γ @Asp32---Ccat@2-aminoimidazole) are plotted as a function of the simulated time (ns).

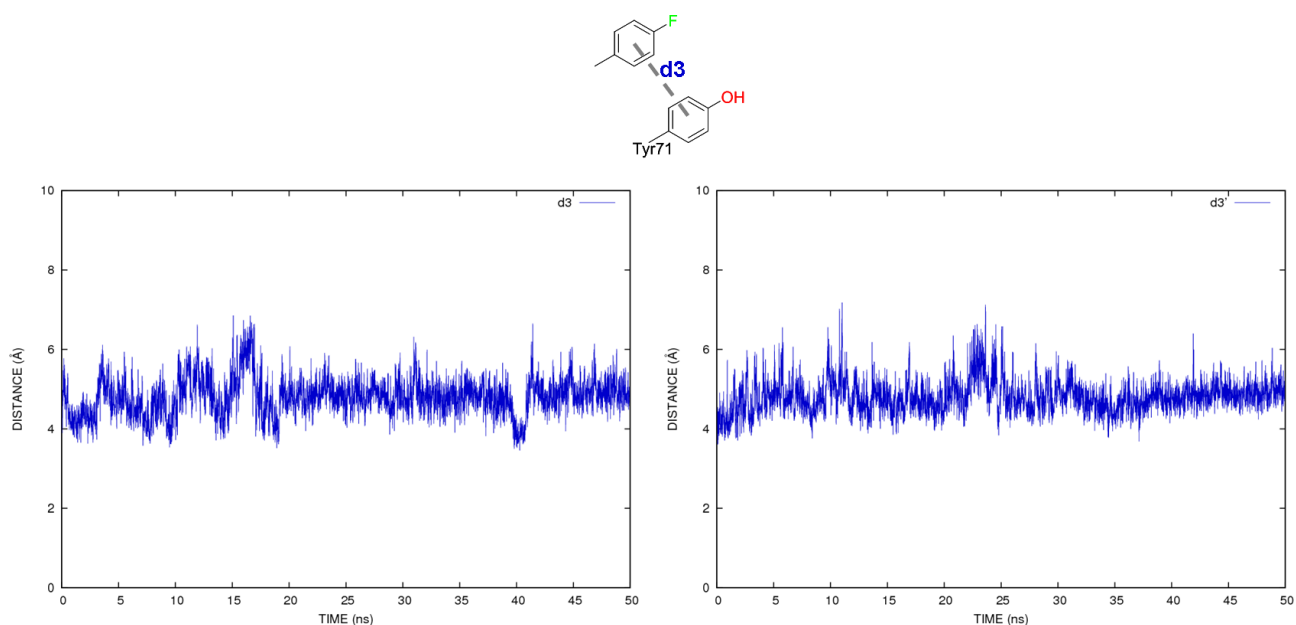


Figure 4.6. The distance (Å) $d3/d3'$ (centroid@Tyr71---centroid@phenyl moiety) is plotted as a function of the simulated time (ns).

Both interactions were remarkably stable showing that the guanidinium was the anchoring point of our inhibitors at BACE-1 active site. In addition, as shown in Figure 4.6, also a stable π - π stacking has been observed between the fluorinated-benzyl ring and the side chain of Tyr71. In light of these results, **27-29** and **31** were tested using cellular assays based on the secretion of $A\beta_{38}$, $A\beta_{40}$ and $A\beta_{42}$ and on cell viability in primary chicken telencephalon neurons.¹⁷⁴ The reduction of $A\beta_{38}$, $A\beta_{40}$, and $A\beta_{42}$ formation was evident for **27** and **28** up to concentrations of 5 μ M (IC₅₀ values are

reported in Table 4.2); in contrast, **29** and **31** resulted inactive. Notably, **7** displayed some moderate toxicity at 25 μM , while **28** started to become toxic at 50 μM (see Figure 4.7).

Table 4.2. Inhibition of $A\beta_{38}$, $A\beta_{40}$ and $A\beta_{42}$ secretion,^a *in vitro* permeability (*Pe*) values^b with related predictive penetration into the CNS^c and molecular descriptors^d of compounds **27-29** and **31**.

Cpds	$A\beta_{38}$ IC ₅₀ (μM) ^a	$A\beta_{40}$ IC ₅₀ (μM) ^a	$A\beta_{42}$ IC ₅₀ (μM) ^a	<i>Pe</i> (10^{-6} cm s ⁻¹) ^b	Prediction ^c	cLogP (prot.) ^d	cLogP (not prot.) ^d	TPSA (prot.) ^d	TPSA (not prot.) ^d
27	15	23	19	4.0 \pm 1.0	CNS+	2.572	5.593	63.562	62.317
28	33	35	27	3.2 \pm 0.2	CNS+/-	2.663	5.685	63.562	62.317
29	n. a. ^e	n. a.	n. a.	n. d. ^f	n. d.	3.517	6.539	45.094	43.849
31	n. a.	n. a.	n. a.	4.0 \pm 0.7	CNS+	4.581	7.602	58.234	56.989

^a Values are mean of three independent experiments for reduction of $A\beta$ secretion. All data were corrected with mean neurons viability obtained in the MTT reduction assay, performed after 24 h of treatment with these BACE-1 inhibitors to evaluate their potential cell toxicity. ^b Values are mean \pm S.D. of two independent experiments (PBS/EtOH = 70/30 was used as solvent). ^c The compounds were classified¹⁷⁵ as CNS+ when they present a *Pe* value $>$ 3.55×10^{-6} cm s⁻¹, and as CNS+/- when the *Pe* value is between 3.55×10^{-6} and 2.00×10^{-6} cm s⁻¹. ^d cLogP and TPSA in both protonated and not protonated were calculated by Molinspiration, a free-online cheminformatics tool (<http://www.molinspiration.com>). ^e n. a. = not active. ^f n. d. = not determined.

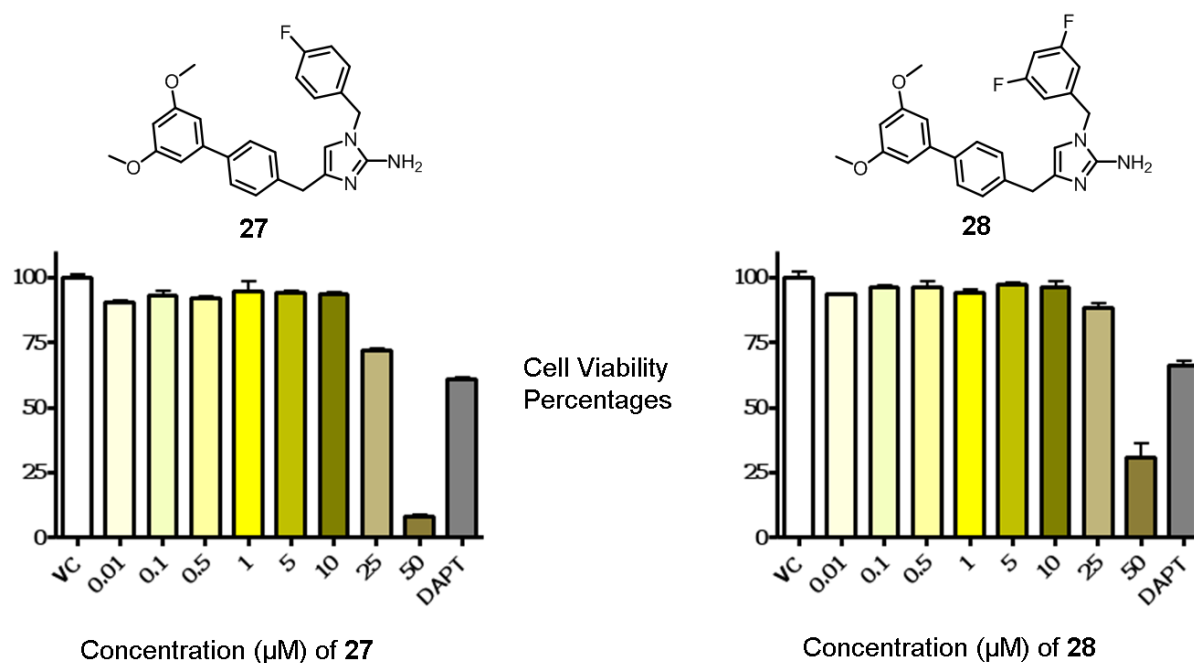


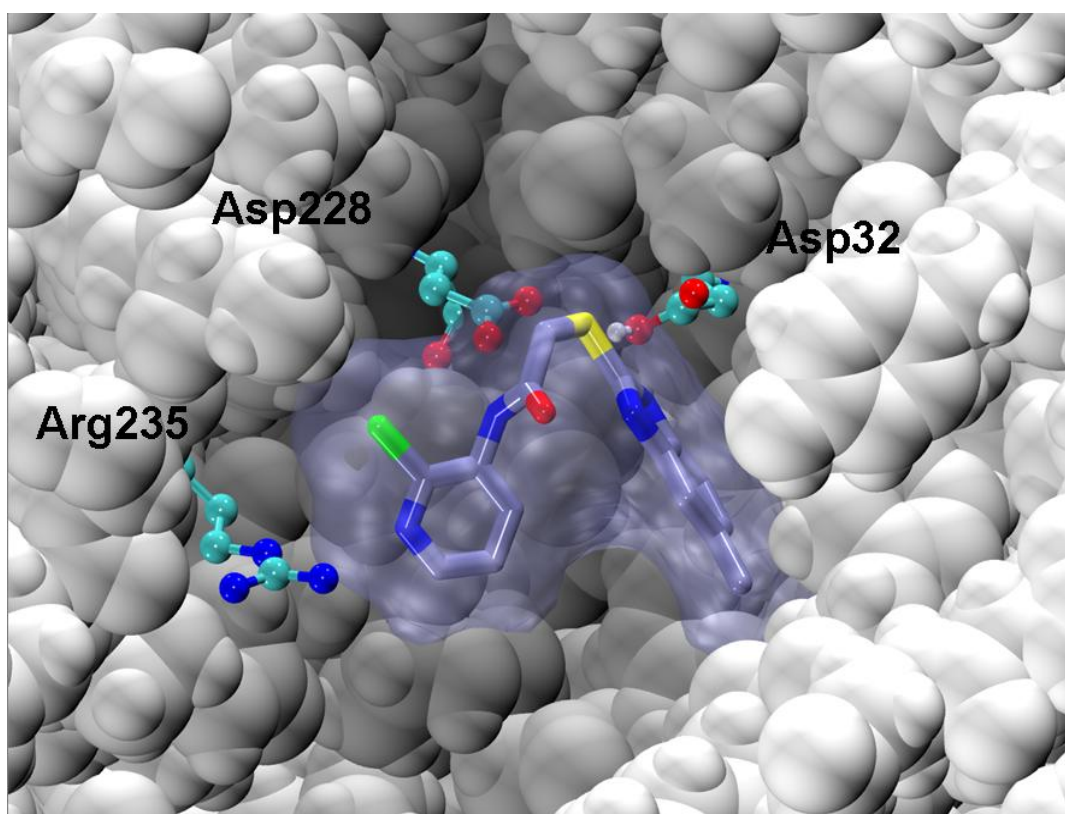
Figure 4.7. Neurotoxicity of T.I., compounds **27** and **28**, after 24 h of treatment. Values represent the mean neuronal viability in percent and the S.E.M. from one independent experiment performed in 96-well plates ($n = 6$ per experiment)

for each T.I. concentration and for controls. The vehicle control group was set as 100%. Statistical analysis was performed using one-way ANOVA analysis followed by Bonferroni's Multiple Comparison Test.

To explain the different activity of derivatives **27-29** and **31** in cellular assays, we explored some of their molecular descriptors such as calculated decimal logarithm of octanol/water partition coefficient (cLogP) and topological polar surface area (TPSA). **29** and **31** showed higher cLogP and lower TPSA values when compared to **27** and **28** (see Table 4.2). Finally, since an anti-AD drug candidate must work at central nervous system (CNS) level, we studied the capability of **27-29** and **31** to cross the blood brain barrier (BBB) by using the parallel artificial membrane permeability assay (PAMPA), as described by Di et al.¹⁷⁵ (see ES). As shown by the in vitro permeability (*Pe*) values (Table 4.2), **28** BBB permeation was predicted to be low, **29** was not examined because of its insolubility in the experimental conditions here employed, whereas **27** and **31** were predicted to be able to cross the BBB by passive permeation. In light of this series of experiments, it turned out that **27** was a promising *hit* to undergo to a subsequent *hit-to-lead* campaign. Interestingly, structurally similar compounds recently reported by Hills et al.¹⁷³ have shown relatively low Pgp efflux, pointing to this class of molecules as promising BACE-1 *lead* candidates.

4.2. Strategy 2

Sequential virtual screening approach to the identification of small organic molecules as potential BACE-1 inhibitors



4.2.1. Introduction

As previously mentioned, most of the non-peptidic BACE-1 inhibitors have been discovered by means of different screening approaches. Among these, the virtual screening method was particularly exploited in the straightforward and random search for novel and structurally diverse compounds as BACE-1 inhibitors covering a broad range of the chemical space.

Several computational groups have successfully identified novel *hit* candidates,^{136,176,177} most of which have been resulted active at low micromolar range. Notably, given the considerable largeness of the active site of BACE-1, these inhibitors presented a relatively high molecular weight (MW) being out of range (> 500 Daltons (Da)).

In contrast to this, here, we report on the sequential application of VS approaches to identify novel scaffolds towards the discovery of new BACE-1 inhibitors with a reduced MW and, thus, valuable ligand efficiency (LE).

4.2.2. Results and discussion

As a prerequisite for the blood-brain barrier (BBB) permeability, we searched for molecules matching the following physicochemical properties: a MW < 450 Da; a number of H-bonds < 8; a logP from 2 to 5; a polar surface area (PSA) < 100 Å².¹⁷⁸ In this way, we focused only on those molecules putatively endowed of pharmacokinetic properties appropriate for CNS penetration.

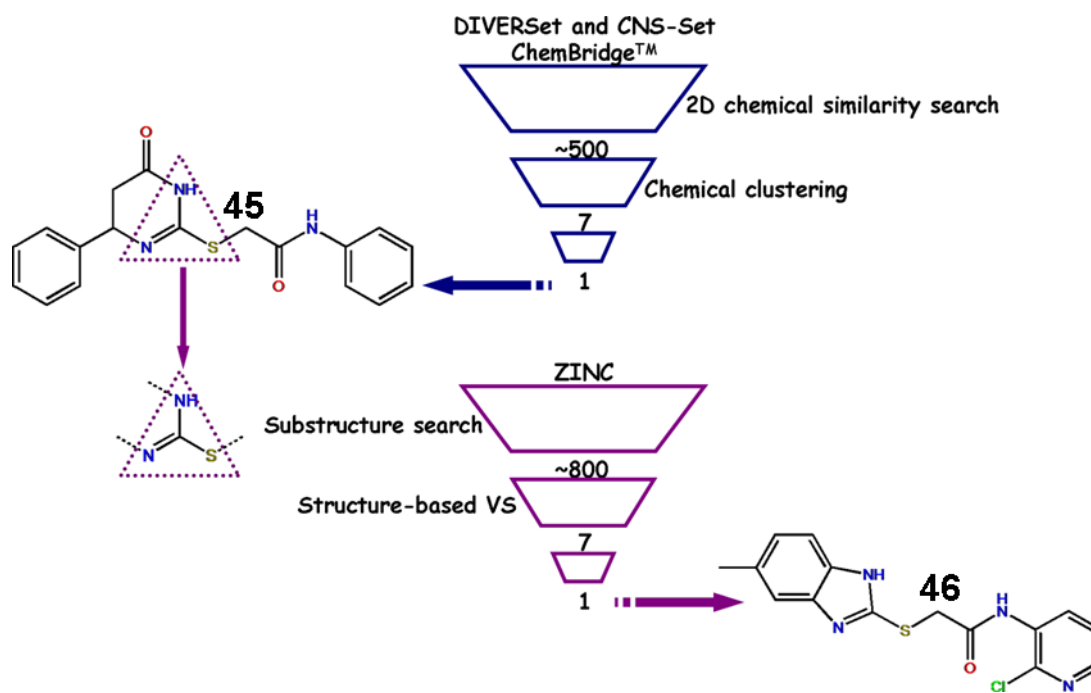


Figure 4.8. Schematic representation of the sequential virtual screening approach. Identification of new high-micromolar and micromolar hits: compounds **45** and **46**, respectively.

In Figure 4.8, our VS funnel is reported. Starting from two different databases of commercially available compounds, we were able to identify two micromolar inhibitors through two subsequent steps of VS simulations. To initially reduce the high dimensionality of the database, we biased the VS procedure focusing on small molecules bearing a guanidinium moiety. Indeed, such a moiety provides optimal interactions with the catalytic aspartic dyad, as shown by the crystal structures of guanidinium-carrying inhibitors in complex with BACE-1.^{131,133,166}

In particular, we focused on dihydroisocytosine derivatives, which were designed by a fragment-based *lead* generation and structure-guided evolution.¹³³ For instance, compound **47** (Figure 4.9) was shown to be a rather potent BACE-1 inhibitor as assessed by biochemical and cell-based assays: IC₅₀ = 0.38 μM using the FRET methodology; IC₅₀ = 0.59 μM using whole-cell assays. Furthermore, otherwise from many BACE-1 inhibitors, **47** displays a good value of LE,¹⁷⁹ 0.36,¹³³ and promising physicochemical features.

47 was actually here exploited as a template for the first step of our protocol. In particular, by employing ScreenMD, a tool from Chemaxon, we performed a 2D chemical similarity search by using the Tanimoto's metric calculated using the molecular similarity index (<http://www.chemaxon.com>). TPSA (topological polar surface area, see Figure 4.9) and a calculated logP (cLogP) were also used as pre-screening parameters to focus only on those compounds, matching the criteria of BBB permeability, as previously described. We screened databases from ChemBridgeTM (<http://www.chembridge.com>) which provides a highly diverse collection of compounds. In particular, we considered DIVERSetTM and CNS-SetTM libraries containing a total of ~110,000 compounds.

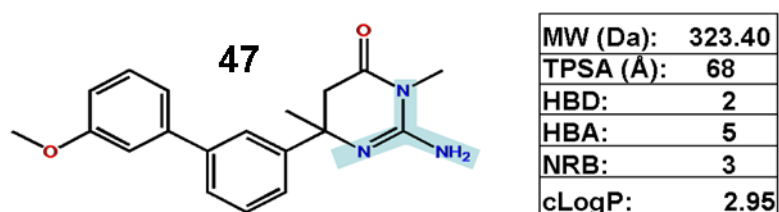


Figure 4.9. The dihydroisocytosine derivative BACE-1 inhibitor (PDB id: 2VA6), **47**, and its molecular descriptors: molecular weight (MW); topological polar surface area (TPSA); H-bond donors (HBD); H-bond acceptors (HBA); number of rotatable bonds (NRB); calculated decimal logarithm of octanol/water partition coefficient (cLogP).

We selected only those molecules with a similarity index more than 50%, thus obtaining ~500 compounds. The molecules were clusterized on the basis of maximum common substructures, and classified by the hierarchical tool LibMCS (<http://www.chemaxon.com>). Depending on the cutting level, a variable number of chemically different clusters could be obtained. In our approach, seven clusters were finally pinpointed by visual inspection, and seven new compounds, **45** and **48-53**, representative of each cluster, submitted to biological evaluation (see ES).

Most of the molecules were able to slightly inhibit BACE-1 being the isothiourea derivative, **45**, the most promising *hit* (Figure 4.8) with an IC₅₀ value equal to 92.5 μM ± 9.7 (according to the “Sigma Assay”, see ES). Furthermore, **45** was also tested using the “Invitrogen Assay”, confirming the previous inhibition potency (see Table 6.3 in ES). Interestingly enough, **45** was characterized by new structural features rather different from those of the dihydroisocytosine template **47**, still keeping a similarity level more than 50% as far as the guanidine moiety was concerned. In light of this, we launched a campaign of similarity search using **45** as reference compound for the following main reasons: i) **45** was the sole compound showing a consistent inhibition profile according to both biochemical assays (see Table 6.3 in ES); ii) **45** has a relatively low molecular weight (MW = 339.42), and therefore, possible *hit* compounds structurally related to it can represent promising starting point for identifying potential *lead* candidates; iii) the molecular structure of **45** is relatively

new in the field of BACE-1 drug discovery, and therefore it can open up new chemical opportunities in the search for novel BACE-1 inhibitors.

On these bases, we performed the second step of our protocol, by virtual screening all the isothiourea derivatives present in the ZINC database (<http://zinc.docking.org/>). The resulting subset of molecules, ~800, was used to perform structure-based VS into the active site of BACE-1. This was performed by employing the GOLD 4.1.1 software (CCDC, Cambridge, UK),¹⁵² and the crystal structure of BACE-1 in complex with OM99-2 (PDB id: 1FKN).¹⁰⁰ Seven new compounds, **46** and **54-59**, were retrieved by this procedure (the chemical structures are reported in Table 6.4 of ES) and one of them, **46**, showed an $IC_{50} = 3.5 \pm 0.1 \mu M$ (according to the “Sigma Assay”).

To further validate this result, a new experiment, based on increasing 10-fold the enzyme concentration, was employed to verify the binding specificity of compound **46**. In fact, no shift in IC_{50} of **46** was observed.

A possible mode of binding of **46** into the active site of the protein target is reported in Figure 4.10. In particular, the following main interactions between the ligand and the proteasic domain of BACE-1 were identified: i) the ligand NH group, belonging to the benzoimidazole moiety, H-bonded to Asp32 side chain; ii) the carbonyl group interacted via H-bond with both the Thr72 side-chain and backbone; iii) the NH group, belonging to the acetamide moiety, formed an H-bond with both Asp228 and Thr231 side chains; iv) the pyridinic nitrogen atom H-bonded to Arg235 side chain; v) the thioacetamidic sulfur atom weakly H-bonded to protonated Asp32 side chain; vi) the chlorine atom formed hydrophobic interactions with Ile226 and Val332; vii) the methyl-benzimidazole moiety was stabilized by hydrophobic interactions mainly with Leu30, Tyr71, Phe108, Ile110, Trp115, and Ile118.

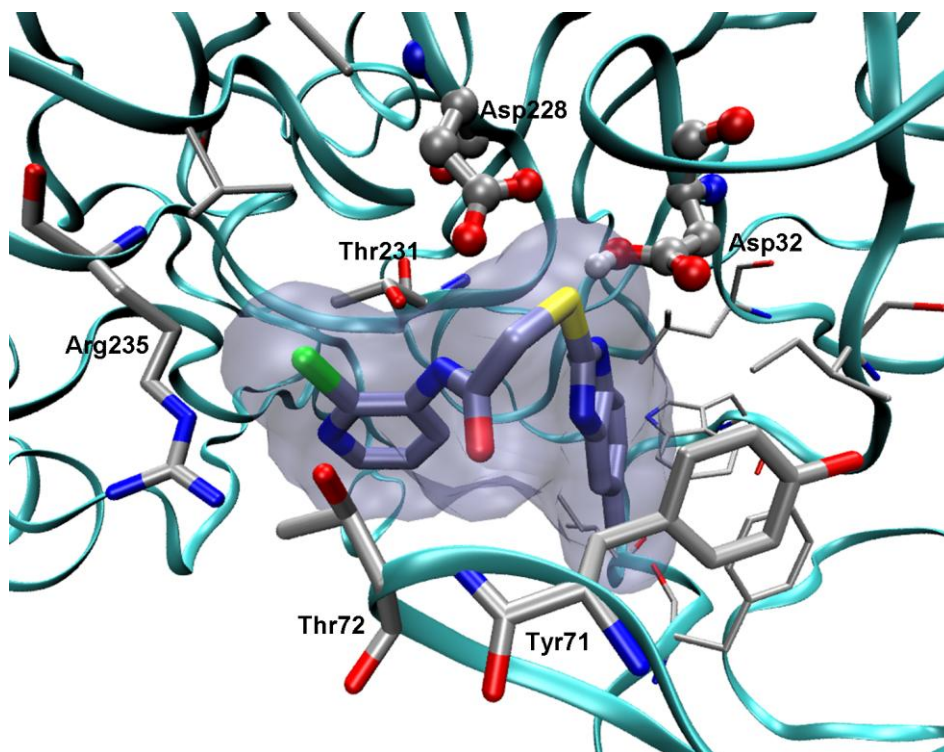


Figure 4.10. Low-energy docking pose of the BACE-1/**46** complex.

Interestingly, **46**, which displayed micromolar affinity, possessed relatively high LE of 0.34, more than that of known nanomolar peptide-based inhibitors (LE < 0.2), and similar to that of the dihydroisocytosine inhibitor **47** (LE = 0.36). Moreover, the proposed binding mode for **46** is predicting that the H-bond donors of the guanidine NH₂ in known inhibitors, as the compound **47**, can be replaced by a S atom, which is normally considered a weak H-bond acceptor (see Figure 4.11).

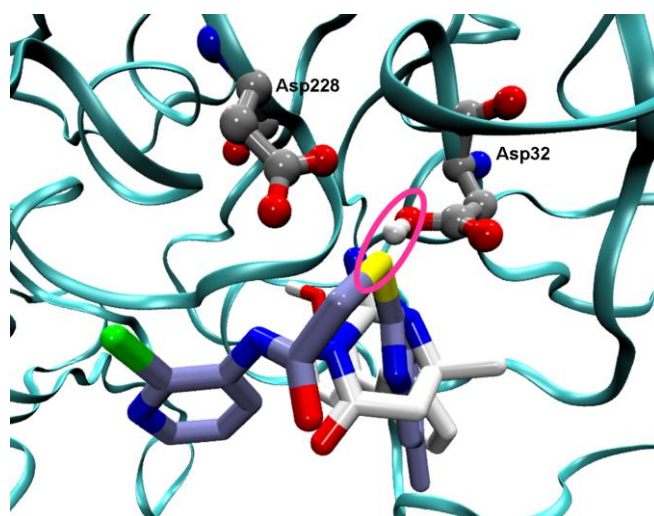


Figure 4.11. Superimposition of **46** (iceblue) and **47** (white) highlighting with a magenta ellipse the weak H-bond between the sulfur atom and the Asp32 side chain is reported.

Furthermore, both new *hit* compounds, **45** and **46**, had a low molecular weight and were compliant with both the requirements of BBB permeability¹⁷⁸ and the Lipinski's rule (Figure 4.12).

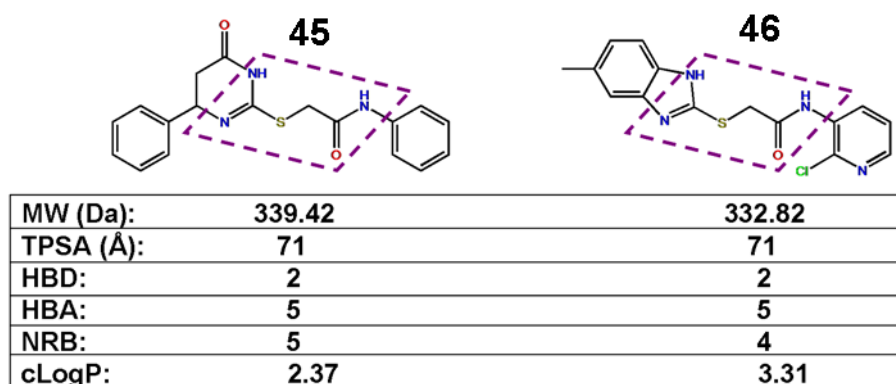


Figure 4.12. Molecular descriptors of the inhibitors **45** and **46**: the common structural motif of **45** and **46** is shown inside the violet dashed lines.

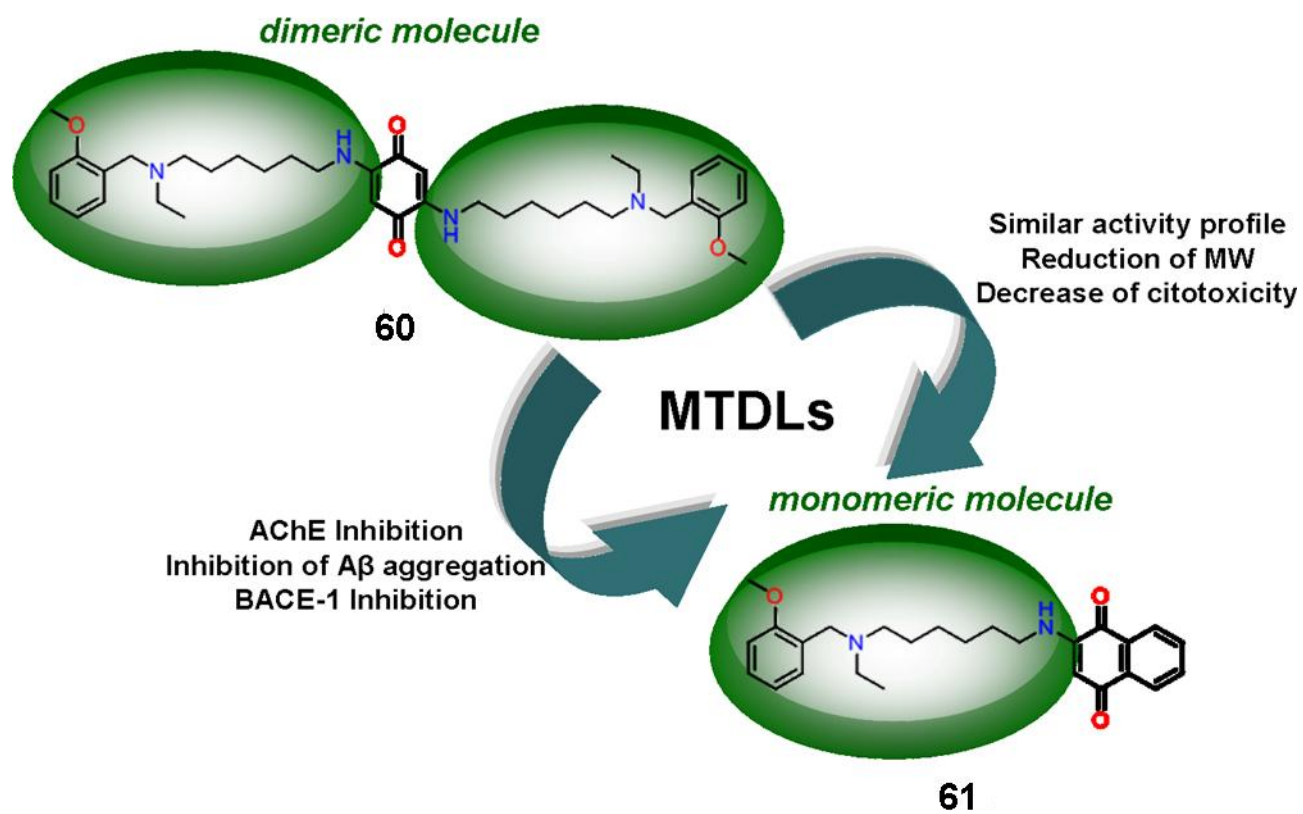
Finally, we noticed that **45** and **46** displayed a new common structural motif able to interact with the aspartic catalytic dyad as shown in Figure 4.12. In this context, the higher activity of **46** compared to **45** could be likely due to the presence of the pyridine ring, which can establish an electrostatic interaction with Arg235 thus improving its affinity for the enzyme.^{180,181}

In addition, thioureas as BACE-1 inhibitors have very recently been reported by Schering-Plough¹⁸² However, in this case, since the molecules are acyclic, the H-bond donor plays a major role in the binding with Asp32, as also demonstrated by the x-ray structure of the complex. Conversely, we report on cyclic isothioureas that represents a new chemotype showing a quite novel mode of binding.

Finally, the present compounds might represent promising non-peptidic *hits* to undergo subsequent optimization steps to improve BACE-1 inhibiting profile and eventually afford novel anti-AD *lead* candidates.

4.3. Strategy 3

Synthesis of monomeric derivatives to probe memoquin's bivalent interactions



4.3.1. Introduction

In the field of medicinal chemistry the multi target directed ligand (MTDL) theory is emerging as an interesting approach, being particularly used to combat multi-factorial diseases, such as AD. Compared with the well-accepted clinical use of multi-medication therapy (MMT), the MTDL design strategy might represent its natural evolution, and MTDLs emerge as valuable tools for hitting the multiple targets implicated in AD aetiology. Several MTDLs have been developed by academia and industry in recent years as an alternative way to develop effective anti-AD drugs.¹⁸³⁻¹⁸⁹

In this scenario, one MTDL, which resulted able to affect several mechanisms relevant to AD, was memoquin (**60**), a molecule developed by the Department of Pharmaceutical Sciences at the University of Bologna.

60 was rationally designed with the aim of creating a NCE with a poly-pharmacological profile against AD.^{190,191} An *in vitro* and *in vivo* characterization revealed its multifunctional mechanism of action, and its interaction with three molecular targets involved in AD pathology, namely acetylcholinesterase (AChE), A β , and BACE-1.¹⁹² **60** is thus the successful product of one of the first AD multitarget drug discovery efforts.

From a medicinal chemistry point of view, **60** is a bivalent ligand, with a symmetrical structure composed of two 2-methoxybenzyl-diamino moieties connected by a benzoquinone spacer.

With the aim of verifying if a dimeric structure is essential for activity and incorporating activity at diverse targets into a single molecule, a novel series of monomeric congeners, related to the multi-target *lead* candidate **60**, was synthesized and, then, their potential multifunctional profile biologically evaluated.

4.3.2. Design

As well in the field of opioids, where several examples of linking two pharmacophoric units via spacers of different length and flexibility were reported by Portoghese,¹⁹³ the bivalent ligand strategy has received attention over the past decade for the design of anti-AD drugs. This was mostly motivated by the peculiar topology of a classical AD target, the enzyme AChE, which has two recognition sites sharing common molecular features.¹⁹⁴ Consequently, improved potency is shown by drugs that simultaneously bind the catalytic and the peripheral anionic (PAS) sites of AChE.¹⁹⁵⁻¹⁹⁹

The multitarget approach could be considered an evolution of the bivalent ligands concept. This is because combining structural elements from two ligands is the simplest way of incorporating activity at two targets into a single molecule.²⁰⁰ The rationale for using the bivalent ligand approach in AD also stems from the possibility that dimeric structures may be capable of bridging independent recognition sites on other validated targets (such as $A\beta$ and BACE-1), resulting in a binding interaction that is thermodynamically more favourable than the monovalent binding of two molecules. In principle, this would be particularly advantageous in view of the complexity of the recognition mechanism of protein-protein interactions in amyloidosis.²⁰¹ As a matter of fact, several amyloid binding compounds share a common bivalent structure and bivalent 'molecular tweezers' have been envisaged as the next generation of ligands.²⁰² Another positive feature of anti-AD bivalent ligands is that, due to their high hindrance, they can efficiently fit the extended substrate binding site of BACE-1.²⁰³ However, their high MW has negative consequences for the pharmacokinetic profile.

For **60**, we could verify absorption through oral administration and access to the central nervous system.²⁰⁴ Nevertheless, if we strictly reason in terms of Lipinski's rule,²⁰⁵ **60** violates the MW parameter, being out of range (632 vs. 500 Da). On this basis, we sought to generate analogs of **60** with a reduced MW, yet maintaining its promising multitarget profile.

To this end, we prepared and then evaluated at multiple targets (AChE, $A\beta$, BACE-1) five congeners (**61-65**), which we formally obtained by cutting the dimeric structure of **60** in two halves. In the resulting monomeric compounds, one 2-methoxybenzyl-diamino chain is always preserved, with the ending fragments being a naphthoquinone (**61**), a quinolinoquinone (**62**), a 2,3-dimethylbenzoquinone (**63**), and a 2-methoxy-benzoquinone (**64**), respectively. Moreover, we reduced the flexibility at the polymethylene chain of **64**, because a conformationally restricted analogue (**65**) might show improved potency. Notably, all compounds displayed an MW below the 500 Da cut-off (see Chart 4.1 for design strategy).

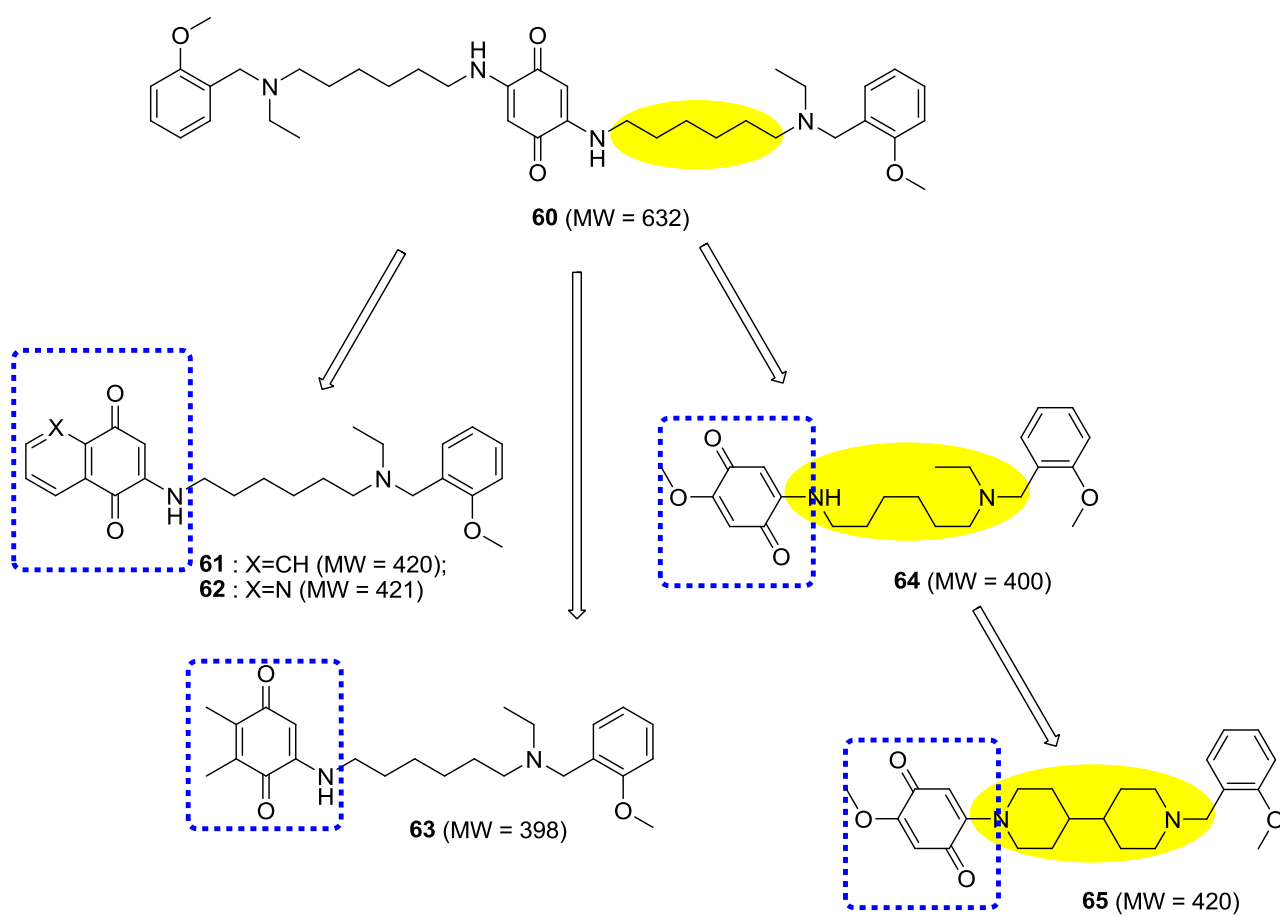


Chart 4.1. Design strategy for monovalent ligand **61-65**.

4.3.3. Results and discussion

To characterize the multi-target profile of **61-65**, their inhibitory activity at human AChE and butyrylcholinesterase (BChE) (Table 4.3) was tested. Kinetic and molecular modelling evidence have demonstrated that **60** is a dual binding cholinesterases inhibitor, which accounts for its remarkable nanomolar activity.^{190,191} Interestingly, all compounds, except **65**, were effective inhibitors of AChE, with **61** being just six times less potent than **60**.

Table 4.3. Inhibitory activity on human AChE and BuChE, BACE-1 and A β aggregation by **61-65** and reference compound **60**.

Cpds	IC ₅₀ AChE	IC ₅₀ BuChE	BACE-1	Inhibition of A β aggregation (%)	
	(nM) ^a	(nM) ^a	inhibition (%) ^b	AChE-induced ^c	Self-induced ^d
60	1.55 ± 0.11	144 ± 100	> 80	87.1 ± 1.7	66.8 ± 4.4
61	9.73 ± 0.44	1490 ± 100	60.2 ± 1.6	69.1 ± 3.2	27.3 ± 4.3
62	27.9 ± 1.6	2560 ± 170	Na	41.3 ± 0.7	15.4 ± 6.7
63	29.0 ± 4.0	314 ± 21	12.8 ± 2.0	60.6 ± 0.2	30.2 ± 1.4
64	65.3 ± 2.2	22800 ± 1600	32.8 ± 2.4	n.t.	45.7 ± 3.4
65	24400 ± 1400	3580 ± 150	32.9 ± 1.0	n.t.	20.5 ± 1.0

^aHuman recombinant AChE and BuChE from human serum were used. IC₅₀ values ± SEM represent the concentration of inhibitor required to decrease enzyme activity by 50% and are the mean of two independent measurements, each performed in duplicate. ^bInhibition of BACE-1. The concentration of the tested inhibitor was 3 μ M. Experimental conditions as in the work reported by Bolognesi et al.²⁰⁶ For **61** IC₅₀ = 2.8 ± 0.1 μ M. IC₅₀ value represents the concentration of inhibitor required to decrease enzyme activity by 50% and is the mean of two independent measurements, each performed in duplicate; na = not active. ^cInhibition of AChE-induced A β (1–40). The concentration of the tested inhibitor and A β ₄₀ was 100 μ M and 230 μ M, respectively, whereas the A β ₄₀: AChE ratio was equal to 100:1. Values are the mean of two independent experiments each performed in duplicate; n.t. = not tested. ^dInhibition of A β ₄₂ 50 μ M self-aggregation when [I] = 10 μ M was used. The A β ₄₂/inhibitor ratio was equal to 5/1. Values are the mean of two independent experiments each performed in duplicate.

This suggests that even the monovalent structures of **61-64** could establish interactions with both sites of the enzyme, whereas it is plausible that the constrained structure of **65** did not allow an optimal docking into the AChE gorge. Figure 4.13A reports the bound conformation of **61**, resulting from docking simulations carried out at the active site of hAChE (PDB id: 1B41,²⁰⁷ see ES). Here, we see that **61** was able to interact with the catalytic region and, at the same time, to protrude towards the solvent exposed gorge entrance.

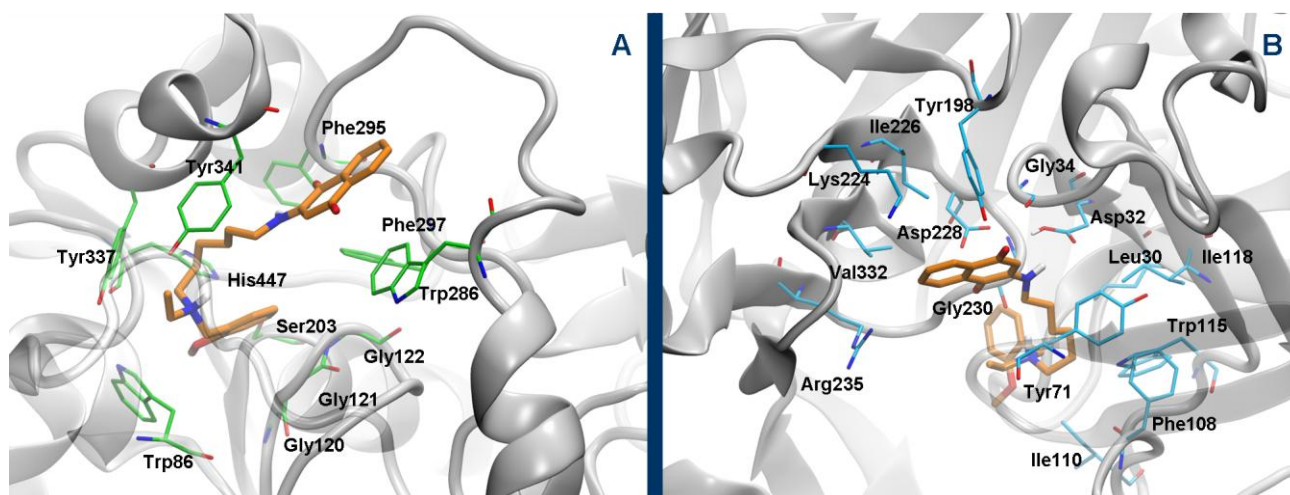


Figure 4.13. Low energy docking model of **61** (orange) into the active sites of AChE (A: residues displayed in light green) and BACE-1 (B: residues displayed in light cyan).

The following interactions between **61** and hAChE were observed: i) the ligand protonated nitrogen established a cation- π interaction with the indole ring of Trp86 and the phenol ring of Tyr337; ii) the oxygen in position 1 of the quinone moiety established an H-bond interaction with the backbone of Phe295; iii) the naphthalen-dione moiety established a favorable π - π stacking with the indole ring of Trp286 of the PAS. This last finding was relevant in the context of previous reports that linked inhibition of AChE-induced $A\beta$ aggregation with a binder's ability to interact with the PAS of the enzyme.²⁰⁸ Indeed, the AChE-induced $A\beta$ aggregation experiments,²⁰⁸ performed on the three most active AChEIs **61-63**, are in agreement with the proposed binding mode at AChE. Activities in the AChE-induced aggregation and AChE inhibition were highly correlated for **61**, which was the most potent in both assays. A different pattern was found for **62** and **63**.

In light of the remarkable anti-aggregating properties of **60**²⁰⁹ and several other bivalent ligands,^{206,210} the ability of **61-65** to reduce $A\beta_{42}$ spontaneous aggregation was then investigated. Data in Table 4.3 show that **61-65** at 10 μ M inhibited $A\beta$ self-aggregation in a range varying from 15% to 46%. At the same concentration, **60** displayed a percentage of 68%, which is less than two times higher than that of the most potent compound **64**.

Interestingly, two protonable diamino chains of **60** do not appear to be necessary for $A\beta$ binding. Conversely, these data pinpoint to the quinone core as an essential feature for potent aggregation inhibition, in agreement with the well-documented inhibitory capability of quinones towards $A\beta$ assembly.²¹¹⁻²¹³ Spacer flexibility also seems to be important, with **65** showing halved percent inhibition with respect to **64**. As part of its multi-target profile, **60** inhibits BACE-1 quite effectively.¹⁹⁰ Therefore, preliminary studies were carried out to assess whether the monomeric derivatives retained the ability to inhibit BACE-1 in vitro. **61-65** were tested at a concentration of 3

μM and their inhibition percentages are reported in Table 4.3. The most potent compound was **61**, which inhibited enzyme activity by 60%, whereas **60** by a percentage higher than 80%. For **61** we also calculated an IC_{50} value of 2.8 μM . To check for nonspecific effects, additional experiments were performed on **60** and **61** with a different source of enzyme, type of substrate, and in the presence of a detergent (CHAPS, 0.1% w/v). In this second assay, **61** showed a similar potency (IC_{50} value of 3.0 μM) while **60** was less active ($\text{IC}_{50} = 4.6 \mu\text{M}$). The discrepancy of results between the two assays for **60** is likely to be a consequence of differences in the substrate, protein, and assay buffer.

Docking simulations were performed to elucidate, at molecular level, the BACE-1 inhibitory activity of **61**. Figure 4.13B reports the binding mode of **61** at BACE-1 proteasic site (PDB id 2QZL).²¹⁴ The leading interactions that characterized the bound complex were: i) the proximal nitrogen of the spacer established two H-bond interactions with the side chain of catalytic Asp32, and the carbonyl oxygen of Gly34 backbone; ii) the oxygen in position 4 of naphthalen-dione moiety interacted via H-bond with the side chain of Tyr198; iii) the protonated nitrogen established an H-bond interaction with the carbonyl oxygen of Gly230 backbone; iv) the aliphatic chain of the spacer was lodged in a hydrophobic subpocket described by Tyr71, Phe108, Ile110, Leu30, Ile118, and Trp115; and v) the quinone formed hydrophobic contacts with Ile226 and Val332.

To further substantiate the secretase inhibitory activity, we also tested whether **61** affects APP processing in a cellular context. This study was carried out in primary chicken telencephalon neurons to assess the effect on secretion of $A\beta_{38}$, $A\beta_{40}$ and $A\beta_{42}$.¹⁷⁴ Thus, intrinsic cell toxicity of **61** was first evaluated, using **60** as reference compound. Treating primary neurons for 24 h with **61** (0.01–50 μM) did not lead to modified viability, whereas treatment with high concentration of **60** (25 and 50 μM) significantly abolished neuronal viability (see Figure 4.14).

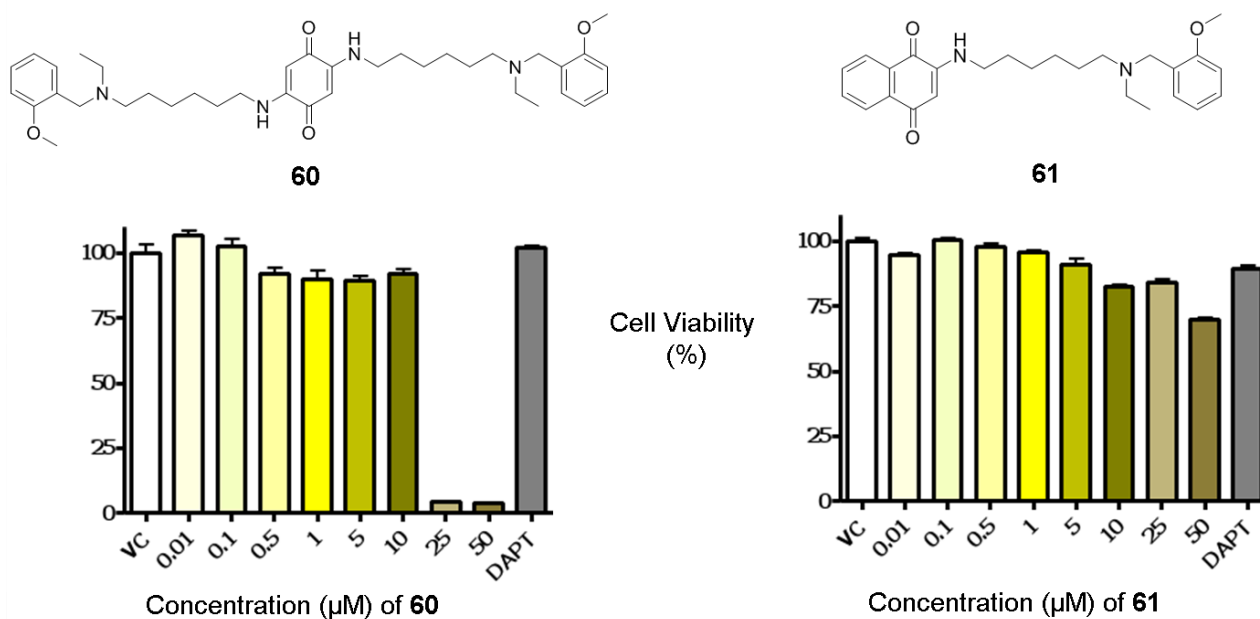


Figure 4.14. Neurotoxicity of compounds **60** and **61** after 24 h of treatment. Values represent the mean neuronal viability in percent and S.E.M. (n = 6 per experiment) for each concentration and for controls. The vehicle control group (VC) was set as 100%. Statistical analysis was performed using one-way ANOVA analysis followed by Bonferroni's Multiple Comparison Test.

Notably, **60** exhibited a similar toxicity in SH-SY5Y cell line.²¹⁵ These data are encouraging because they disprove possible concerns about a potential toxicity of these molecules linked to their quinone portion: the presence of a quinone in both **60** and **61** points to a molecule-related rather than a chemotype-related toxicity profile. Concerning studies on amyloid peptides production, **61** inhibited $A\beta_{38}$, $A\beta_{40}$ and $A\beta_{42}$ secretion, with IC_{50} values of 19, 21 and 46 μ M, respectively. These values were corrected with mean neurons viability, obtained in the MTT reduction assay. Conversely, due to its toxicity, a concentration-dependent decrease in $A\beta$ secretion could not be observed for **60**. There is a growing body of evidence that MTDLs¹⁸³ provide a viable area for AD drug discovery. One limitation to this approach is that most of the hits discovered so far tend to have high MW, resulting in new NCEs that are eventually associated with poor oral bioavailability.²¹⁶ The low ligand efficiency of MTDLs is a critical issue. This is because affinity at the different targets usually parallels the increase in MW, whereas pharmacokinetic properties are improved by reducing the MW.²¹⁶ Interestingly, in the present series of **60**-derivatives, the reduction of MW did not correspond to a reduction in the multiple activities. In fact, for the most active compound **61**, the MTDL activity profile remains almost unchanged with respect to **60**, with the toxicity profile actually being improved.

In conclusion, if the decrease in MW translates into the expected superior bioavailability, **61** could be a promising starting point in the search for new MTDLs against AD.

Chapter 5

5. Concluding remarks and future perspectives

AD has no current cure, although treatments for symptoms are available. These can temporarily slow the worsening of dementia symptoms and improve quality of life for patients suffering AD and their caregivers. Currently, there is a worldwide effort to find better ways to treat the disease, delay its onset, and prevent it from developing (<http://www.alz.org/>).

From a drug discovery perspective, human BACE-1 has appeared to be a suitable target for the following reasons: i) BACE-1 catalyzes the rate-limiting step in the production of A β ; ii) it has widely been structurally characterized; iii) a BACE-1 inhibitor, CTS-21666 from CoMentis, advanced up to Phase II clinical trials.

Here, I have presented my theoretical and experimental work towards the successful identification, by two different strategies (see Strategies 1 and 2), of new chemical entities (NCEs) able to inhibit BACE-1. In particular, in contrast with traditional high-throughput screening (HTS), particularly employed by big pharmaceutical companies with a tremendously high level of costs, we have performed a significantly higher *hit* rate by using structure-based and computer-aided drug discovery approaches. In addition, I have been engaged in another study (Strategy 3) based on the rational design and synthesis of novel multitarget-directed ligands (MTDLs) as an alternative therapeutic strategy against AD, and a novel *lead* candidate has been identified. Notably, BACE-1 turned out to be one of the selected molecular targets.

Strategy 1

In the first study, I have described a rational structure-based approach, integrated with a synthetic protocol amenable to parallel synthesis, aimed at discovery of new 2-aminoimidazole derivatives as BACE-1 inhibitors. Among 10 derivatives *ex novo* synthesised (Table 4.1, paragraph 4.1.4), **27** has emerged as a promising anti-BACE-1 *hit* because of the following reasons:

- i) the rather good chemical accessibility that allows to carry out extensive SAR studies;
- ii) the low micromolar inhibitory profile against BACE-1, as assessed by enzymatic and cellular assays;

iii) the capability to cross *in vitro* the BBB as assessed by the PAMPA test.

Furthermore, we have identified the potential binding mode of **27** through molecular docking and molecular dynamics simulations (Figure 4.4, paragraph 4.1.4). The pivotal interactions with BACE-1 might be the basis for the future design of compounds with higher affinity.

In conclusions, **27** can represent a suitable starting point for an extensive campaign of *hit-to-lead* and, eventually, *lead* optimization. Indeed, these results are promising in the context of the 2-aminoimidazole-based BACE-1 inhibitors, where a major issue is the blood brain barrier (BBB) penetration.²¹⁷

Strategy 2

In the second strategy, we have adopted another drug discovery approach based on the sequential application of two different computational tools, a random chemical-similarity search and structure-based screening, together with experimental biochemical assays.

This *in silico* approach has allowed me to identify two novel small drug-like organic molecules as potential BACE-1 inhibitors (Figure 4.8, paragraph 4.2.2). Both these new *hits* have a low MW and are compliant with the requirements of BBB permeability and the Lipinski's rule.²⁰⁵ Moreover, they show common physicochemical properties and novel structural motif able to interact with the aspartic catalytic dyad. Beside this "primary interaction", we could also identify accessory moieties, in particular for the most active compound **46**, whose binding mode was well-characterized through docking simulations (Figure 4.10, paragraph 4.2.2), likely able to modulate the affinity of this class of ligands towards their biological counterpart.

These compounds might represent promising non-peptidic *hits* to undergo subsequent optimization steps to improve BACE-1 inhibiting profile and eventually afford novel anti-AD *lead* candidates.²¹⁸

Notably, **46** has a relatively high value of ligand efficiency (LE), especially compared to other BACE-1 inhibitors reported in the literature,^{136,176,177,219} which have been identified by virtual screening procedures and resulted active at the similar micromolar range, but characterized by a high MW.

Strategy 3

There is a growing body of evidence that an alternative strategy to target the multi-factorial nature of AD is represented by MTDLs. One limitation to this approach is that most of the *hits* discovered so far tend to have high MW, resulting in new NCEs that are eventually associated with poor oral bioavailability. The low LE of MTDLs is a critical issue. This is because affinity at the different targets usually parallels the increase in MW, whereas pharmacokinetic properties are improved by

reducing the MW. Interestingly, in the present series of memoquin (**60**) derivatives (Chart 4.1, paragraph 4.3.2.), the reduction of MW did not correspond to a reduction in the multiple activities. In fact, for the most active compound **61**, the MTDL activity profile remains almost unchanged with respect to **60**, with the toxicity profile actually being improved. In conclusion, if the decrease in MW translates into the expected superior bioavailability, **61** may be a promising starting point in the search for new MTDLs against AD.

We conclude that this work represents an excellent initial step towards the development of new potent BACE-1 inhibitors and MTDLs for the treatment of AD. The combined and parallel use of computer-aided drug design tools together with focused synthetic strategies may further contribute to carry out a straightforward and innovative research with a lower expense of economic resources, compared to the costs of the HTS approach. In particular, the MTDL strategy is intended to have a crucial role in the design and development of effective anti-Alzheimer's drugs.

Chapter 6

6. Experimental section

6.1. Computational studies

6.1.1. Methods in Strategy 1

Molecular docking

The model of BACE-1 was constructed by removing all water molecules from its crystal structure (X-ray structure of human BACE1 “apo” form; PDB id: 1SGZ)⁹⁷ and adding all hydrogen atoms and minimized by Amber force field Parm99.²²⁰ Histidines were protonated in according to their putative H-bond patterns in the crystal structure. The 3D models of ligands were built using Sybyl 7.1.1 (Tripos Associates Inc, USA) and then optimized at the density functional level of theory (B3LYP/6-31G*) by means of the Gaussian09²²¹ software. Docking simulations were carried out by means of GOLD,¹⁵² 4.1.1 version. The outcomes from docking were clusterized by using ACIAP.^{160,161}

Before running simulations with **27**, the docking protocol was validated by assessing the capability of GOLD¹⁵² and AutoDock¹⁵³ to reproduce the crystallographic structures of guanidinium-carrying BACE-1 inhibitors in complex with the enzyme (PDB id: 2VA5, 2VA6, and 2VA7).¹³³ When our studies were almost completed, the X-ray structure of BACE-1 in complex a 2-aminoimidazole derivative appeared in the literature.¹⁷² Therefore, to further strengthen our protocol, this complex (PDB id: 3H0B)¹⁷² was investigated by docking simulations. In particular, three different protonation states of catalytic aspartates were taken into account using three different scoring functions: GS, CS, and the empirical function from AutoDock. The results are shown in the Table 6.1. All these results clearly showed that GOLD employing the GS scoring function was superior to both CS and AutoDock, in terms of reproducibility of crystallographic complexes (as far as the 2-aminoimidazole moiety was concerned). For this reason the following setup was defined: i) BACE-1 in the di-deprotonated state (overall charge of the catalytic dyad -2); ii) GOLD for docking simulations; iii) GS scoring function for ranking.

Table 6.1. Validation results of docking protocol.

	GS RMSD ^a (Å)	CS RMSD ^a (Å)	AutoDock RMSD ^a (Å)
Asp32 and Asp228 dideprotonated (net charge:-2)	0.082	0.693	0.436
Asp32 protonated Asp228 deprotonated (net charge:-1)	0.100	0.929	2.125
Asp228 protonated Asp32 deprotonated (net charge:-1)	0.118	1.641	0.481

^aRMSD related to the 2-aminoimidazole moiety of the best-ranked docking pose as obtained by the three different scoring functions with respect to the crystallographic 2-aminoimidazole derivative in complex with the enzyme BACE-1 (PDB id: 3H0B).¹⁷²

GOLD

GOLD 4.1.1 adopts a search genetic algorithm to generate lowest binding ligand-protein complex energies. Genetic algorithm default parameters were set: the population size was 100, the selection pressure was 1.1, the number of operations was 10^5 , the number of islands was 5, the niche size was 2, migrate was 10, mutate was 95, and crossover was 95. Docking calculations were computed to obtain 250 randomly seeded runs for each ligand. Binding-site cavity was set as a spherical region of 15 Å radius centered on C γ of Asp32. To evaluate the single poses resulted by search algorithm both GS and CS scoring functions were used.

AutoDock

To perform better docking experiments, the ligands were docked using AutoDock 4.0. The parameters for the molecules were calculated adopting its standard parameterization procedure. The LGA was applied as a search method for the different docking results. The potential grid map for each atom type was calculated using a cubic box (center: C γ of Asp32) of 76 grid points in each direction, with a distance of 0.425 Å between grid points. For each ligand 100 docking runs were performed.

Cluster analysis

The results both from GOLD and AutoDock were rationalized by means of the clustering algorithm ACIAP.¹⁶¹ This cluster analysis program employs hierarchical agglomerative method by a user-independent cutting rule to give the most representative poses.

Electrostatic Potential (ESP)

The ESP surfaces were calculated by using the SMP version of the Gaussian 09²²¹ package and, in particular, employing the B3LYP functional, and the 6-311G(d,p) basis set. Optimisations of **21** and **22-24** were carried out *in vacuo*, and ESP surfaces were plotted between -0.02 and +0.02 atomic units by using VMD (as previously shown in Figure 4.3, paragraph 4.1.4).²²²

Molecular dynamics (MD)

The binary complex between BACE-1 and compound **27** was investigated by means of MD simulations carried out with the NAMD-2.7 software.²²³ MD simulations (two independent runs of 50 ns each, overall 100 ns) of the BACE-1/**27** complex were carried out in explicit solvent and periodic boundary conditions. Indeed, the BACE-1/**27** complex as outcome of docking simulations was immersed in a water box with a size of $80 \times 85 \times 75 \text{ \AA}^3$. Overall charge neutrality in the system was achieved by adding five Na^+ counterions. The Amber Force Field parm99SB²²⁴ was used to describe the protein and the counterions, while the TIP3P model was used for water.²²⁵ The ligand was treated with the General Amber Force Field.²²⁶

Firstly, water shells and counterions were minimized using steepest descent and conjugate gradient algorithms. Then, a minimization of the entire complex was performed setting a convergence criterion on the gradient of $0.001 \text{ Kcal}^{-1} \text{ \AA}^{-1}$. Equilibration runs were carried out by heating the system to 300 K in 100 ps. This was followed by MD simulations in the NPT ensemble (constant temperature and pressure).

The simulations were carried out by means of Langevin dynamics using a damping coefficient of 5 ps^{-1} and a uniform integration time step of 2 fs. Bonds involving hydrogen atoms were restrained to their equilibrium geometry with the SHAKE algorithm.²²⁷ Short-range non-bonded interactions were treated using a cut-off radius of 10.0 \AA as long as a zero switching function active at distances larger than 8.0 \AA . A neighbour list having a radius of 12.0 \AA was used and updated every 10 integration time steps. Periodic boundary conditions were employed, and long-range electrostatics was estimated by means of the Particle-Mesh Ewald method²²⁸ using a grid spacing of less than 1.0 \AA in each dimension.

The analyses performed by visual inspection with VMD software²²² allowed us to observe a rather good stability of some key interactions. In particular the aspartic dyad and the guanidinium moiety have shown a quite stable electrostatic interaction throughout the simulations (see Figure 4.5, paragraph 4.1.4). In addition, also a stable π - π stacking has been observed between the fluorinated-benzyl ring and the side chain of Tyr71 (see Figure 4.6, paragraph 4.1.4).

6.1.2. Methods in Strategy 2

Chemical similarity screening

The Tanimoto similarity was computed according to the following equation:

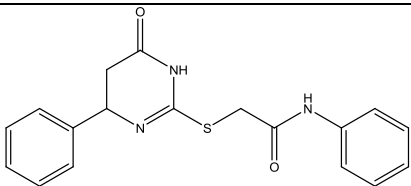
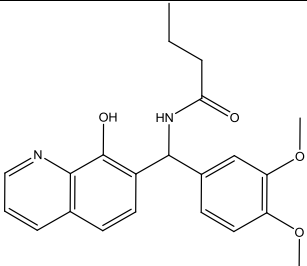
$$T_{sim}(a,b) = \frac{B(a \& b)}{B(a) + B(b) - B(a \& b)}$$

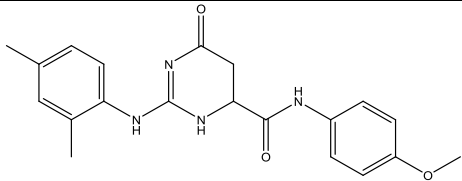
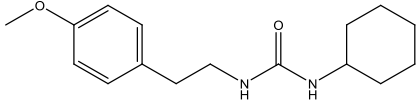
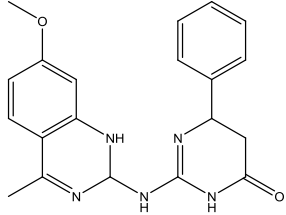
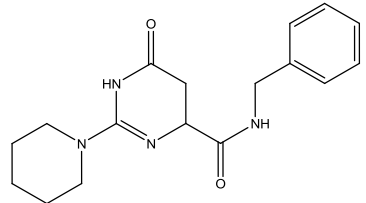
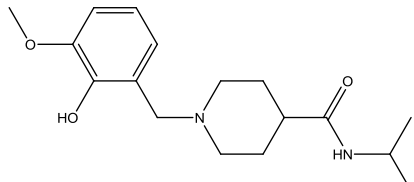
Where a and b stand for two binary fingerprints, representing respectively the molecule template (a) and each molecule from ChemBridge database (b), and $\&$ denotes binary bit-wise and-operator. As a consequence, the larger the number of common bits in a and b , the larger the value of T_{sim} . No-scaling factors were adopted.

We selected a similarity cut-off of 0.8, which did not provide any novel scaffolds. Therefore, we increased the similarity cut-off up to 0.5, which turned out to be the best compromise between chemical similarity and diversity. In this way, starting from dihydroisocytosine we discover an isothiourea derivative (compound **1**) with a promising BACE-1 affinity.

All molecules selected, **45** and **48-53**, from 2D chemical similarity search were tested using two different biochemical assays (“Invitrogen Assay” and “Sigma Assay”). Only the results obtained with **45** were found comparable in both assays (see Table 6.2).

Table 6.2. All molecules, **45** and **48-53**, selected from 2D chemical similarity search were tested using two different biochemical assays (“Invitrogen Assay” and “Sigma Assay”). Only the results obtained with **45** were found comparable in both assays.

Cpds	Chemical structures	Invitrogen Assay		Sigma Assay	
		Concentration (μM)	Inhibition (%)	Concentration (μM)	Inhibition (%)
45		29.80	20.22 ± 2.30	30.70	20.31 ± 1.60
48		30.36	9.67 ± 0.55	31.06	44.12 ± 6.42

49		30.17	n.a*	34.50	62.31 ± 13.05
50		31.98	n.a	28.80	24.54 ± 5.73
51		30.00	n.a.		n.d. #
52		30.00	67.37 ± 13.50	27.18	n.a
53		30.00	57.48 ± 8.53	34.00	n.a

* n.a. = not active; # n.d. = not determined.

Molecular docking

Protein preparation

The protein model for docking simulations was based on the PDB id 1FKN.¹⁰⁰ Water molecules, ions, and ligands were removed, and hydrogen atoms were added by using the BIOPOLIMERS module of Sybyl 7.3. Histidines were protonated accordingly to their putative H-bond patterns in the crystal structure. Asp32 was neutral, protonated on inner oxygen of side chain, and the Asp228 negatively charged in agreement with a previous study.²²⁹

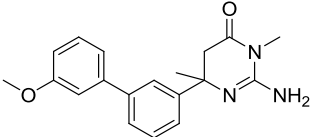
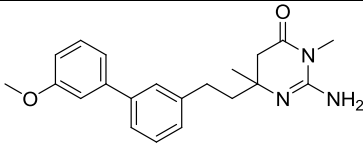
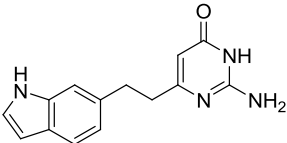
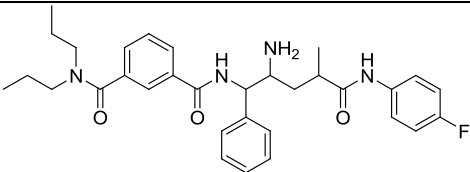
Ligands Preparation

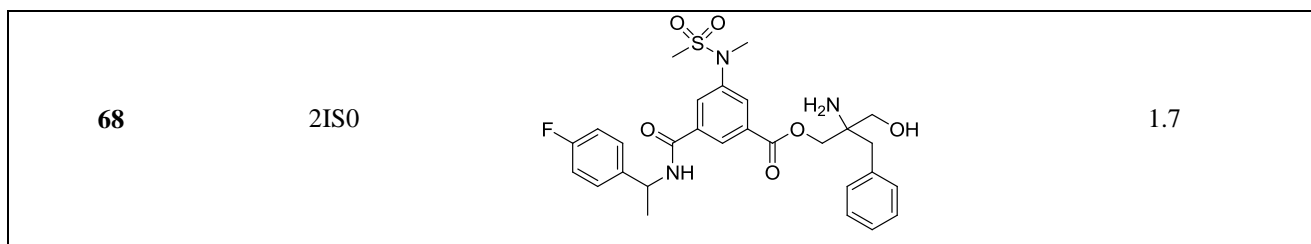
The 3D models of ligands were generated by Sybyl 7.3 and then optimized at the density functional level of theory (B3LYP/6-31G*) by means of the Gaussian09 software.²²¹

Docking Protocol

All the docking simulations were performed by GOLD 4.1.1 software. The active site was defined as a sphere of 15 Å centered on the atom C γ of the Asp32. Automatic settings with an accuracy of 100% for genetic algorithm were used: the population size was 100, the selection pressure was 1.1, the number of operations was 10⁵, the number of islands was 5, the niche size was 2, migrate was S4 10, mutate was 95, and crossover was 95. Both the scoring functions (Goldscore and Chemscore) were applied separately in two independent runs of docking simulations for the subset of molecules from ZINC database. Our protocol was preliminary validated by assessing the capability of GOLD to reproduce the BACE-1/**47** complex (PDB id: 2VA6).¹³³ To further confirm this result, two analogues of **47**, **19** and **66**, (respectively PDB id: 2VA7 and 2VA5)¹³³ were docked with GOLD, showing the suitability of the program to study this class of compounds against BACE-1. Moreover, two additional BACE-1 experimental complexes (PDB id: 2FDP²³⁰ and 2IS0)²³¹ were studied with the same protocol, further demonstrating the capability of GOLD to reproduce crystallographic complexes of BACE-1/inhibitors. Obtained results are shown in the Table 6.3.

Table 6.3. Validation results of docking protocol.

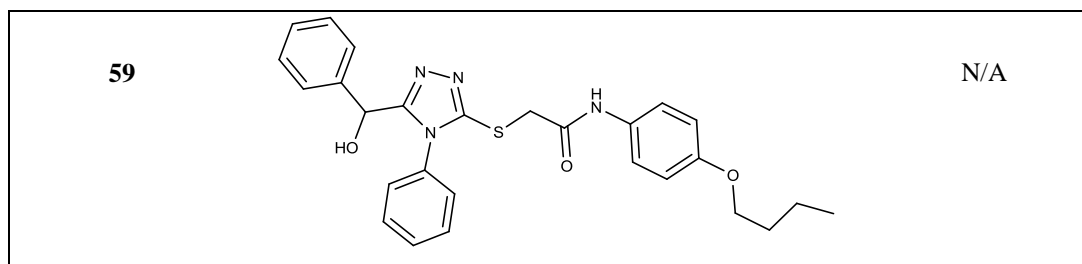
Cpds	PDB id	Chemical Structure	Docking RMSD (Å)
47	2VA6		0.7
19	2VA7		0.2
66	2VA5		1.2
67	2FDP		1.8



All compounds selected from structure-based virtual screening, **46** and **54-59**, (see Table 6.4) were tested using the “Sigma Assay”. Because of their intrinsic fluorescence, except compound **46**, it was not possible to determine the putative BACE-1 inhibition percentages.

Table 6.4. Compounds selected from structure-based virtual screening.

Cpds	Chemical Structure	IC ₅₀ (μM)
46		3.5 ± 0.1
54		> 5 [#]
55		N/A [§]
56		N/A
57		N/A
58		N/A



Determined by "Invitrogen Assay".

§ Not Available (N/A)

This work was carried out in collaboration with Prof. Recanatini's group.

6.1.3. Methods in Strategy 3

Molecular docking

The docking simulations were carried out by means of ICM 3.7.

AChE was modelled starting from the crystallographic structure of human AChE in complex with fasciculin (PDB id: 1B41).²⁰⁷ Fasciculin and other non protein molecules were deleted and only the enzyme chain was retained. Hydrogen atoms and missing heavy atoms were added. Zero occupancy side chains, polar hydrogen atoms, and the positions of asparagine and glutamine side chain amidic groups were optimized and assigned the lowest energy conformation. After optimization, histidines were assigned the tautomerization state which improved the hydrogen bonding pattern.

The residues defining the boundaries of the binding box were assumed to be known and directly derived from the bound poses of the two inhibitors: propidium (in complex with mouse AChE; PDB id: 1N5R) and donepezil (in complex with torpedo AChE; PDB id: 1EVE).^{232,233} Likewise, BACE-1 was modelled starting from the crystallographic structure of the human enzyme in complex with a peptide-mimetic inhibitor (PDB id: 2QZL).²¹⁴

Ligands were built defining the right bond orders, hydrogen bonds, and protonation states. Each ligand was assigned the MMFF force field²³⁴ atom types and charges.

The docking engine employed was the Biased Probability Monte Carlo (BPMC) stochastic optimizer as implemented in ICM.^{235,236} The ligand binding site at the receptor was represented by precalculated 0.5 Å spacing potential grid maps, representing van der Waals potentials for hydrogen and heavy probes, electrostatics, hydrophobicity, and hydrogen bonding.

The molecular conformation was described by means of internal coordinate variables. The adopted force field was a modified version of the ECEPP/3 force field.²³⁷ The binding energy was assessed by means of the standard ICM empirical scoring function.²³⁸

This work was performed in collaboration with Dr. Bottegoni from IIT of Genova.

6.2. Chemistry

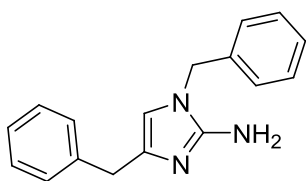
6.2.1. General chemical methods

Reaction progress was monitored by TLC on precoated silica gel plates (Kieselgel 60 F254, Merck) and visualized by UV254 light. Flash column chromatography was performed on silica gel (particle size 40-63 μM , Merck). Tetrahydrofuran (THF) and Et_2O were freshly distilled over sodium/benzoketal. Unless otherwise stated, all reagents were obtained from commercial sources and used without further purification. Compounds were named relying on the naming algorithm developed by CambridgeSoft Corporation and used in Chem-BioDraw Ultra 11.0. ^1H -NMR and ^{13}C -NMR spectra were recorded at 200-400 and 50-100 MHz, respectively. All the NMR experiments were performed by using CDCl_3 as solvent. Chemical shifts (δ) are reported in parts per millions (ppm) relative to TMS as internal standard. Coupling constants (J), when given, are reported in Hertz (Hz). For microwave-assisted organic synthesis a CEM Discover BenchMate reactor was used in the standard configuration as delivered, including proprietary software. All microwave-assisted reactions were carried out in sealed quartz process vials (15 mL). IR-FT spectra were performed in Nujol and obtained on a Nicolet Avatar 320 E.S.P. instrument; ν_{max} is expressed in cm^{-1} . Mass spectra were recorded on a V.G. 7070 E spectrometer or on a Waters ZQ 4000 apparatus operating in electrospray (ES) mode. Purity of compounds was determined by elemental analyses; purity for all the tested compounds was $\geq 95\%$.

6.2.2. General procedure for the microwave-assisted synthesis of 2-aminoimidazoles 21-31 and their characterization

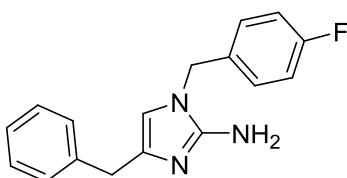
In a 10 mL microwave vial, 2-benzylaminopyrimidines **32a-d** (1.0 equiv) and 3-substituted- α -bromopropyl aldehydes **33a-f** (1.35 eq) were successively dissolved in dry CH_3CN (2-3 mL). The microwave reactor was irradiated by maximum power of 150 W at the temperature of 150 $^\circ\text{C}$ for 75 min. After the reaction mixture was cooled with an air flow for 15 min, a hydrazine hydrate 60% solution (5 equiv) was added, and the mixture was irradiated at 100 W to heat at the temperature of 100 $^\circ\text{C}$ for 15 min. The reaction mixture was diluted by CH_2Cl_2 (20 mL), washed with a saturated NH_4Cl solution (10 mL), brine (10 mL) and H_2O (2 x 10 mL). The organic layer was dried over Na_2SO_4 , then filtered and concentrated. The resulting residue was purified by flash chromatography on silica gel ($\text{CH}_2\text{Cl}_2/\text{MeOH} = 9.5/0.5$) (Scheme 4.1).

1,4-Dibenzyl-1*H*-imidazol-2-amine (**21**).



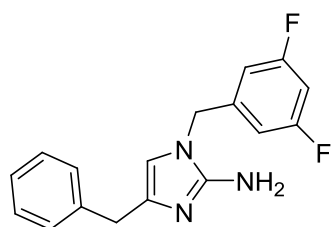
Reaction of *N*-benzylpyrimidin-2-amine **32a** (0.28 g, 1.53 mmol) and 2-bromo-3-phenylpropanal **33f** (0.44 g, 2.07 mmol) gave the crude final product **21** that was purified by flash chromatography (CH₂Cl₂/MeOH = 9.5/0.5). Yield 31%; brown solid; ESI-MS (*m/z*): 264 (M+H⁺); ¹H-NMR (200 MHz): δ 7.37-7.14 (m, 10H), 6.10 (s, 1H), 5.61 (br-s, 2H, NH₂), 4.87 (s, 2H), 3.76 (s, 2H) ppm; ¹³C-NMR (50 MHz): δ 147.4, 136.4, 133.9, 129.0, 128.8, 128.7, 128.5, 128.0, 127.8, 127.0, 111.2, 49.0, 31.4 ppm. IR: ν = 3420 cm⁻¹.

4-Benzyl-1-(4-fluorobenzyl)-1*H*-imidazol-2-amine (**22**).



Reaction of *N*-(4-fluorobenzyl)pyrimidin-2-amine **32b** (0.25 g, 1.25 mmol) and 2-bromo-3-phenylpropanal **33f** (0.36 g, 1.68 mmol) gave the crude final product **22** that was purified by flash chromatography (CH₂Cl₂/MeOH = 9.5/0.5). Yield 29%; brown solid; ESI-MS (*m/z*): 282 (M+H⁺); ¹H-NMR (200 MHz): δ 7.28-7.12 (m, 7H), 7.05-6.96 (m, 2H), 6.04 (s, 1H), 5.94 (br-s, 2H, NH₂), 4.87 (s, 2H), 3.73 (s, 2H) ppm; ¹³C-NMR (50 MHz): δ 164.7, 159.8, 147.4, 138.3, 131.0, 130.9, 129.2, 129.1, 128.7, 128.3, 126.3, 116.0, 115.5, 111.5, 47.8, 33.0 ppm. IR: ν = 3422 cm⁻¹.

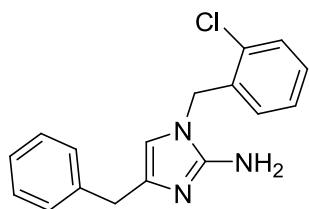
4-Benzyl-1-(3,5-difluorobenzyl)-1*H*-imidazol-2-amine (**23**).



Reaction of *N*-(3,5-difluorobenzyl)pyrimidin-2-amine **32c** (0.27 g, 1.25 mmol) and 2-bromo-3-phenylpropanal **33f** (0.36 g, 1.68 mmol) gave the crude final product **23** that was purified by flash chromatography (CH₂Cl₂/MeOH = 9.5/0.5). Yield 21%; brown solid; ESI-MS (*m/z*): 300 (M+H⁺); ¹H-NMR (200 MHz): δ 7.29-7.20 (m, 5H), 6.71-6.67 (m, 3H), 6.10 (s, 1H), 5.10 (br-s, 2H, NH₂), 4.89 (s, 2H), 3.77 (s, 2H) ppm; ¹³C-NMR (50 MHz): δ 165.8 (d, *J* = 12.5), 160.8 (d, *J* =

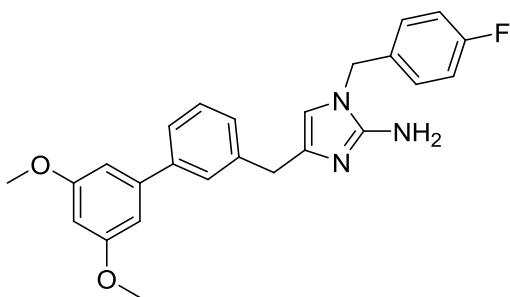
12.5), 148.2, 139.0, 138.7, 137.7, 132.2, 128.8, 128.5, 126.6, 111.2, 110.0, 103.8 (t, $J = 25$), 47.6, 32.6 ppm. IR: $\nu = 3421 \text{ cm}^{-1}$.

4-Benzyl-1-(2-chlorobenzyl)-1H-imidazol-2-amine (24).



Reaction of *N*-(2-chlorobenzyl)pyrimidin-2-amine **32d** (0.27 g, 1.25 mmol) and 2-bromo-3-phenylpropanal **33f** (0.36 g, 1.68 mmol) gave the crude final product **34** that was purified by flash chromatography ($\text{CH}_2\text{Cl}_2/\text{MeOH} = 9.5/0.5$). Yield 11%; brown solid; ESI-MS (m/z): 299 ($\text{M}+\text{H}^+$); $^1\text{H-NMR}$ (200 MHz): δ 7.40-7.23 (m, 8H), 7.07-7.02 (m, 1H), 5.96 (s, 1H), 4.95 (s, 2H), 4.80 (br-s, 2H, NH_2) 3.80 (s, 2H) ppm; $^{13}\text{C-NMR}$ (50 MHz): δ 148.1, 137.8, 133.0, 132.3, 131.5, 129.9, 129.8, 128.9, 128.7, 128.5, 127.5, 126.6, 111.3, 46.2, 32.5 ppm. IR: $\nu = 3420 \text{ cm}^{-1}$.

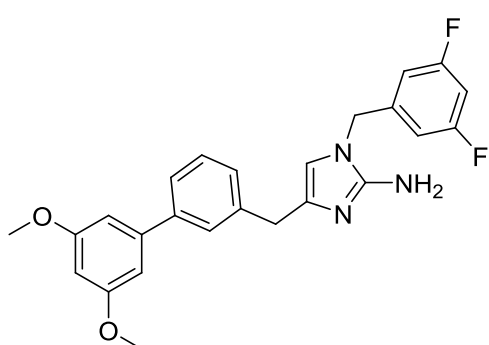
1-(4-Fluorobenzyl)-4-((3',5'-dimethoxybiphenyl-3-yl)methyl)-1H-imidazol-2-amine (25).



Reaction of *N*-(4-fluorobenzyl)pyrimidin-2-amine **32b** (0.25 g, 1.25 mmol) and 2-bromo-3-(3',5'-dimethoxybiphenyl-3-yl)propanal **33a** (0.58 g, 1.68 mmol) gave the crude final product **25** that was purified by flash chromatography ($\text{CH}_2\text{Cl}_2/\text{MeOH} = 9.5/0.5$).

Yield 21%; orange solid; ESI-MS (m/z): 418 ($\text{M}+\text{H}^+$); $^1\text{H-NMR}$ (200 MHz): δ 7.48-7.25 (m, 4H), 7.15-6.99 (m, 4H), 6.74-6.73 (m, 2H), 6.48-6.46 (m, 1H), 6.21 (s, 1H), 4.79 (s, 2H), 3.99 (br-s, 2H, NH_2), 3.85 (s, 6H), 3.82 (s, 2H) ppm; $^{13}\text{C-NMR}$ (50 MHz): δ 164.8, 161.0, 159.9, 147.5, 143.5, 141.1, 140.4, 136.7, 131.8, 131.7, 128.7, 128.5, 128.1, 127.7, 124.9, 116.1, 115.7, 112.4, 105.5, 99.1, 55.4, 47.8, 34.8 ppm. IR: $\nu = 3414 \text{ cm}^{-1}$.

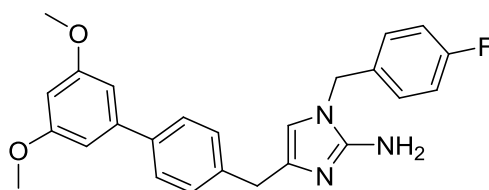
1-(3,5-Difluorobenzyl)-4-((3',5'-dimethoxybiphenyl-3-yl)methyl)-1H-imidazol-2-amine (26).



Reaction of *N*-(3,5-difluorobenzyl)pyrimidin-2-amine **32c** (0.27 g, 1.25 mmol) and 2-bromo-3-(3',5'-dimethoxybiphenyl-3-yl)propanal **33a** (0.58 g, 1.68 mmol) gave the crude final product **26** that was purified by flash chromatography (CH₂Cl₂/MeOH = 9.5/0.5). Yield 22%;

brown solid; ESI-MS (*m/z*): 436 (*M*+*H*⁺); ¹H-NMR (400 MHz): δ 7.46-7.44 (m, 1H), 7.42-7.40 (m, 1H), 7.35-7.31 (m, 1H), 7.24-7.21 (m, 2H), 6.75-6.70 (m, 2H), 6.69-6.61 (m, 2H), 6.44-6.43 (m, 1H), 6.04 (s, 1H), 4.79 (s, 2H), 4.82 (s, 6H), 3.80 (s, 2H), 2.78 (br-s, 2H, NH₂) ppm; ¹³C-NMR (50 MHz): δ 165.7 (d, *J* = 12.5), 161.7 (d, *J* = 12.5), 148.0, 143.3, 141.0, 140.3, 140.2, 136.9, 128.6, 128.1, 127.7, 124.9, 112.0, 109.8, 109.6, 109.3, 105.4, 103.3 (t, *J* = 25), 99.2, 55.3, 47.4, 34.7 ppm. IR: ν = 3415 cm⁻¹.

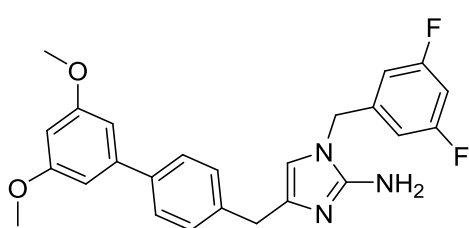
1-(4-Fluorobenzyl)-4-((3',5'-dimethoxybiphenyl-4-yl)methyl)-1H-imidazol-2-amine (27).



Reaction of *N*-(4-fluorobenzyl)pyrimidin-2-amine **32b** (0.25 g, 1.25 mmol) and 2-bromo-3-(3',5'-dimethoxybiphenyl-4-yl)propanal **33b** (0.58 g, 1.68 mmol) gave the crude final product **27** that was purified by flash

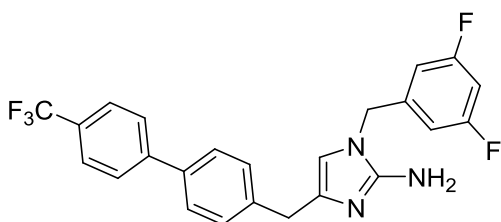
chromatography (CH₂Cl₂/MeOH = 9.5/0.5). Yield 30%; yellow solid; ESI-MS (*m/z*): 418 (*M*+*H*⁺); ¹H-NMR (400 MHz): δ 7.47 (d, *J* = 8.4, 2H), 7.31 (d, *J* = 8.4, 2H), 7.10-7.08 (m, 2H), 7.04-6.99 (m, 2H), 6.70-6.69 (m, 2H), 6.44-6.43 (m, 1H), 6.02 (s, 1H), 4.79 (s, 2H), 3.82 (s, 6H), 3.79 (s, 2H), 1.96 (br-s, 2H, NH₂) ppm; ¹³C-NMR (50 MHz) δ 164.0, 161.0, 159.0, 147.4, 143.3, 139.3, 139.0, 136.6, 131.7, 129.2, 128.7, 128.5, 127.1, 116.2, 115.8, 112.4, 105.3, 99.1, 55.4, 47.9, 34.3 ppm. IR: ν = 3414 cm⁻¹.

1-(3,5-Difluorobenzyl)-4-((3',5'-dimethoxybiphenyl-4-yl)methyl)-1*H*-imidazol-2-amine (28).



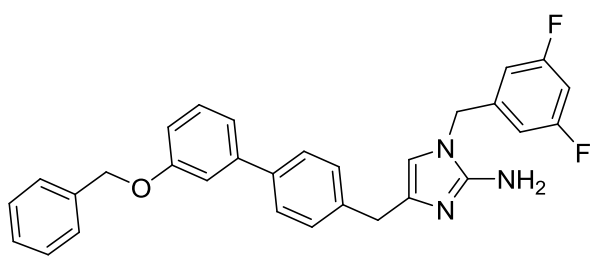
Reaction of *N*-(3,5-difluorobenzyl)pyrimidin-2-amine **32c** (0.28 g, 1.25 mmol) and 2-bromo-3-(3',5'-dimethoxybiphenyl-4-yl)propanal **33b** (0.59 g, 1.69 mmol) gave the crude final product **28** that was purified by flash chromatography (CH₂Cl₂/MeOH = 9.5/0.5). Yield 31%; yellow solid; ESI-MS (*m/z*): 436 (M+H⁺); ¹H-NMR (400 MHz): δ 7.49 (d, *J* = 8.4, 2H), 7.32 (d, *J* = 8.4, 2H), 6.73-6.70 (m, 1H), 6.69-6.68 (m, 2H), 6.65-6.62 (m, 2H), 6.43-6.42 (m, 1H), 6.21 (s, 1H), 4.81 (s, 2H), 3.83 (s, 2H), 3.82 (s, 6H), 1.64 (br-s, 2H, NH₂) ppm; ¹³C-NMR (50 MHz) δ 165.8 (d, *J* = 12.5), 161.0 (d, *J* = 12.5), 147.7, 143.2, 140.4, 140.2, 140.1, 139.4, 138.9, 137.2, 129.2, 127.1, 112.2, 109.8, 109.3, 105.2, 103.4 (t, *J* = 25), 99.0, 55.3, 47.6, 34.3 ppm. IR: ν = 3415 cm⁻¹.

1-(3,5-Difluorobenzyl)-4-((4'-(trifluoromethyl)biphenyl-4-yl)methyl)-1*H*-imidazol-2-amine (29).



Reaction of *N*-(3,5-difluorobenzyl)pyrimidin-2-amine **32c** (0.15 g, 0.70 mmol) and 2-bromo-3-(4'-(trifluoromethyl)biphenyl-4-yl)propanal **33c** (0.34 g, 0.95 mmol) gave the crude final product **29** that was purified by flash chromatography. Yield 26%; yellow solid; ESI-MS (*m/z*): 444 (M+H⁺); ¹H-NMR (400 MHz): δ 7.66-7.64 (m, 4H), 7.53 (d, *J* = 8.4, 2H), 7.36 (d, *J* = 8.4, 2H), 6.76-6.75 (m, 1H), 6.66-6.65 (m, 2H), 6.08 (s, 1H), 4.81 (s, 2H), 3.83 (s, 2H), 3.06 (br-s, 2H, NH₂) ppm; ¹³C-NMR (100 MHz): δ 164.6 (d, *J* = 12.3), 162.1 (d, *J* = 12.3), 148.3, 144.3, 138.5, 138.1, 137.9, 132.1, 129.5, 129.1, 127.5, 127.2, 125.7, 125.6, 122.1, 111.2, 110.1, 109.9, 104.0 (t, *J* = 24.6), 47.6, 32.2 ppm. IR: ν = 3418 cm⁻¹.

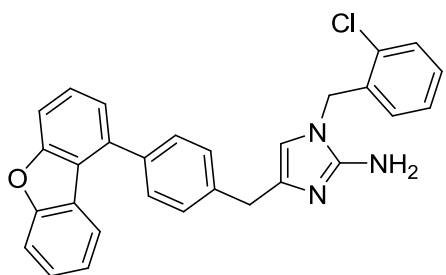
1-(3,5-Difluorobenzyl)-4-((3'-(benzyloxy)biphenyl-4-yl)methyl)-1*H*-imidazol-2-amine (30).



Reaction of *N*-(3,5-difluorobenzyl)pyrimidin-2-amine **32c** (0.18 g, 0.82 mmol) and 2-bromo-3-(3'-(benzyloxy)biphenyl-4-yl)propanal **33d** (0.44 g, 1.11 mmol) gave the crude final product **30** that

was purified by flash chromatography ($\text{CH}_2\text{Cl}_2/\text{MeOH} = 9.5/0.5$). Yield 23%; yellow solid; ESI-MS (m/z): 482 ($\text{M}+\text{H}^+$); $^1\text{H-NMR}$ (200 MHz): δ 7.56-7.29 (m, 10H), 7.21-7.18 (m, 2H), 6.99-6.96 (m, 1H), 6.82-6.98 (m, 3H), 6.01 (s, 1H), 5.14 (s, 2H), 4.88 (s, 2H), 3.84 (s, 2H), 2.02 (br-s, 2H, NH_2) ppm; $^{13}\text{C-NMR}$ (50 MHz): δ 160.8 (d, $J = 12.5$), 159.1 (d, $J = 12.5$), 147.3, 142.6, 139.2, 138.8, 137.6, 137.0, 130.9, 129.7, 129.3, 128.6, 128.0, 127.5, 127.2, 119.8; 113.7, 113.3, 112.6, 109.9, 109.4, 103.6 (t, $J = 25$), 70.1, 47.7, 34.5 ppm. IR: $\nu = 3415 \text{ cm}^{-1}$.

1-(2-Chlorobenzyl)-4-(4-(dibenzo[b,d]furan-1-yl)benzyl)-1*H*-imidazol-2-amine (31).



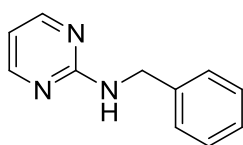
Reaction of *N*-(2-chlorobenzyl)pyrimidin-2-amine **32d** (0.15 g, 0.68 mmol) and 2-bromo-3-(4-(dibenzo[b,d]furan-1-yl)phenyl)propanal **33e** (0.35 g, 0.92 mmol) gave the crude final product **31** that was purified by flash chromatography

($\text{CH}_2\text{Cl}_2/\text{MeOH} = 9.5/0.5$). Yield 13%; yellow solid; ESI-MS (m/z): 465 ($\text{M}+\text{H}^+$); $^1\text{H-NMR}$ (400 MHz): δ 7.97-7.95 (m, 1H), 7.91-7.88 (m, 1H), 7.83-7.81 (m, 2H), 7.58-7.55 (m, 2H), 7.46-7.31 (m, 6H), 7.25-7.22 (m, 2H), 6.94-6.92 (m, 1H), 6.25 (s, 1H), 4.92 (s, 2H), 3.87 (s, 2H), 2.63 (br-s, 2H, NH_2) ppm; $^{13}\text{C-NMR}$ (100 MHz): δ 156.1, 153.3, 148.2, 136.9, 135.0, 133.1, 131.8, 130.3, 130.0, 129.9, 129.1, 129.0, 128.8, 127.6, 127.2, 126.7, 125.4, 124.9, 124.1, 123.2, 122.8, 120.6, 119.6, 111.8, 111.3, 46.4, 31.8 ppm. IR: $\nu = 3413 \text{ cm}^{-1}$.

6.2.2. General parallel procedure for the synthesis of 2-benzylaminopyrimidines 32a-d and their characterization

In distinct reactors, 2-aminopyrimidine **35** (4 equiv) was dissolved in dry THF (12 mL) and the resulting solution was cooled in an ice bath. To these solutions NaH (4 equiv) was added resulting in effervescence and in the formation of suspensions. The mixtures were stirred in the ice bath for 15 min, and then the appropriate benzyl bromide derivatives **34a-d** (1 equiv) were added dropwise to each reactor. The mixtures were stirred at room temperature for 24 h and each one was treated as follow. The solvent was evaporated under vacuo, and H₂O (25 mL) was added. The resulting aqueous solution was extracted with CH₂Cl₂ (3 x 25 mL) and the combined organic layers were washed with H₂O (25 mL), saturated NaHCO₃ solution (25 mL) and brine (25 mL), dried over anhydrous Na₂SO₄ and concentrated under vacuo. Each crude residue was purified by flash chromatography on silica gel (petroleum ether/EtOAc = 1/1) (Scheme 4.2).

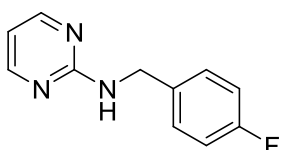
N-benzylpyrimidin-2-amine (**32a**).



Reaction of 2-aminopyrimidine **35** (1.5 g, 15.75 mmol) and the benzyl bromide **34a** (0.46 mL, 3.96 mmol) afforded compound **32a** that was purified on silica gel (petroleum ether/EtOAc = 1/1). Yield 93%; yellow solid; ¹H-

NMR (200 MHz): δ 8.20 (d, $J = 4.4$, 2H), 7.40-7.28 (m, 5H), 6.52 (t, $J = 4.8$, 1H), 6.28 (br-s, 1H, NH), 4.66 (d, $J = 5.8$, 2H) ppm.

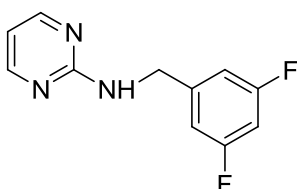
N-(4-fluorobenzyl)pyrimidin-2-amine (**32b**).



Reaction of 2-aminopyrimidine **35** (1.5 g, 15.75 mmol) and the benzyl bromide **34b** (0.49 mL, 3.96 mmol) afforded compound **32b** that was purified on silica gel (petroleum ether/EtOAc = 1/1). Yield 83%; white

solid; ¹H-NMR (200 MHz): δ 8.29 (d, $J = 4.6$, 2H), 7.38-7.29 (m, 2H), 7.08-6.99 (m, 2H), 6.58 (t, $J = 4.8$, 1H), 5.62 (br-s, 1H, NH), 4.63 (d, $J = 6.0$, 2H) ppm.

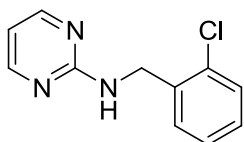
N-(3,5-difluorobenzyl)pyrimidin-2-amine (**12c**).



Reaction of 2-aminopyrimidine **35** (1.5 g, 15.75 mmol) and the benzyl bromide **34c** (0.50 mL, 3.96 mmol) afforded compound **32c** that was

purified on silica gel. Yield 85%; white solid; $^1\text{H-NMR}$ (400 MHz): δ 8.24 (d, $J = 4.8$, 2H), 6.85 (d, $J = 6.4$, 2H), 6.69-6.64 (m, 1H), 6.56 (t, $J = 4.8$, 1H), 5.90 (br-s, 1H, NH), 4.62 (d, $J = 6.4$, 2H) ppm.

***N*-(2-chlorobenzyl)pyrimidin-2-amine (32d).**



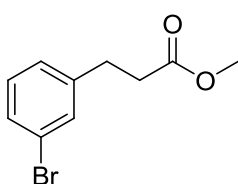
Reaction of 2-aminopyrimidine **35** (1.5 g, 15.75 mmol) and the benzyl bromide **34d** (0.50 mL, 3.96 mmol) afforded compound **32d** that was purified on silica gel (petroleum ether/EtOAc = 1/1). Yield 95%; yellow solid; $^1\text{H-NMR}$ (200

MHz): δ 8.23 (d, $J = 4.8$, 2H), 7.46-7.28 (m, 2H), 7.24-7.18 (m, 2H), 6.54 (t, $J = 4.8$, 1H), 6.40 (br-s, 1H, NH), 4.75 (d, $J = 6.2$, 2H) ppm.

6.2.3. General parallel procedure for the synthesis of 3-(bromophenyl)-propionic methyl esters 36-37 and their characterization

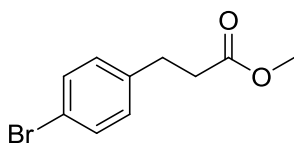
In distinct reactors, solutions of the appropriate 3-(3-bromophenyl)-propionic acid or 3-(4-Bromophenyl)-propionic acid in MeOH were prepared and concentrated H_2SO_4 was added to each reactor. The resulting mixtures were stirred under reflux for 16h. Each crude mixture was reduced under vacuo and the residues were partitioned with dichloromethane (20 mL) and saturated NaHCO_3 solution (20 mL). The organic layers of each reaction was dried with Na_2SO_4 , filtered and evaporated. The resulting compounds were used in a further reaction without any further purification.

Methyl 3-(3-bromophenyl)propanoate (36).



3-(3-Bromophenyl)-propanoic acid (0.4 g, 1.74 mmol) led to compound **36**. Yield 99%; white oil; $^1\text{H-NMR}$ (200 MHz): δ 7.36-7.32 (m, 2H), 7.16-7.13 (m, 2H), 3.68 (s, 3H), 2.93 (t, $J = 7.4$, 2H), 2.62 (t, $J = 7.8$, 2H) ppm.

Methyl 3-(4-bromophenyl)propanoate (**37**).



3-(4-Bromophenyl)-propanoic acid (0.4 g, 1.74 mmol) led to compound

37. Yield 99%; white oil; $^1\text{H-NMR}$ (400 MHz): δ 7.32 (d, $J = 8.2$, 2H),

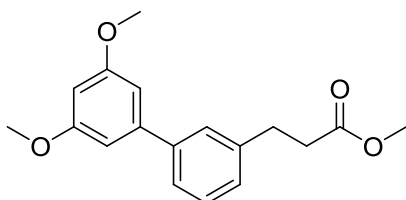
7.01 (d, $J = 8.0$, 2H), 3.60 (s, 3H), 2.83 (t, $J = 7.6$, 2H), 2.62 (t, $J = 8.0$,

2H) ppm.

6.2.4. General parallel procedure for the synthesis of biphenyl propanoic acid methyl esters **42a-e** and their characterization.

In distinct reactors, 3-(bromophenyl)-propionic methyl esters **36-37** (1.0 equiv) were dissolved in toluene (7 mL). Phenyl boronic acids **38-41** (2 equiv) in EtOH (3.5 mL) and Na_2CO_3 2M (2M, aq, 3.0 equiv) were then added to the corresponding reactors, and the resulting mixtures were deoxygenated with a stream of N_2 . After 10 min, $\text{Pd}(\text{PPh}_3)_4$ (0.005 equiv) was added and each mixture was stirred at reflux temperature for 5 h under N_2 , then cooled to room temperature and treated as follows. Each solution was poured into a mixture of H_2O (5 mL) and Et_2O (5 mL), and the two phases were separated. The aqueous layer was washed with Et_2O (5 mL), and the organic phases were combined and washed with 1M NaOH (5 mL), followed by brine (5 mL), then dried over Na_2SO_4 and evaporated. Purification of each crude product performed by flash chromatography on silica gel (petroleum ether/ $\text{EtOAc} = 8/2$) yielded the corresponding biphenyl propanoic acid methyl esters **42a-e** (Scheme 4.3).

Methyl 3-(3',5'-dimethoxybiphenyl-3-yl)propanoate (**42a**).



Reaction of 3-(bromophenyl)-propionic methyl ester **36** (0.3 g,

1.23 mmol) and boronic acid **38** (0.45 g, 2.46 mmol) afforded

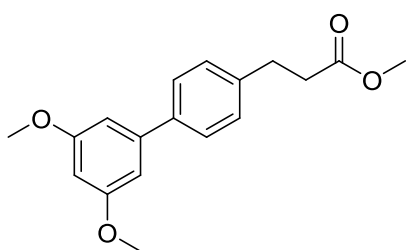
compound **42a** that was purified by flash chromatography on silica

gel (petroleum ether/ $\text{EtOAc} = 8/2$). Yield 97%; white powder; $^1\text{H-}$

NMR (400 MHz): δ 7.42-7.40 (m, 2H), 7.36-7.33 (m, 1H), 7.19-7.17 (m, 1H), 6.72-6.70 (m, 2H),

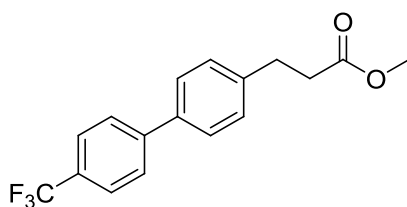
6.47-6.46 (m, 1H), 3.83 (s, 6H), 3.67 (s, 3H), 3.01 (t, $J = 8.0$, 2H), 2.67 (t, $J = 7.6$, 2H) ppm.

Methyl 3-(3',5'-dimethoxybiphenyl-4-yl)propanoate (42b).



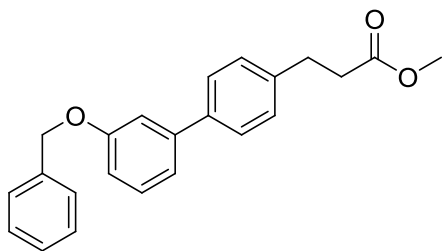
Reaction of 3-(bromophenyl)-propionic methyl ester **37** (0.3 g, 1.23 mmol) and boronic acid **38** (0.45 g, 2.46 mmol) afforded compound **42b** that was purified by flash chromatography on silica gel (petroleum ether/EtOAc = 8/2). Yield 94%; white powder; ¹H-NMR (200 MHz): δ 7.52 (d, $J = 7.8$, 2H), 7.29 (d, $J = 8.0$, 2H), 6.75-6.74 (m, 2H), 6.49-6.48 (m, 1H), 3.87 (s, 6H), 3.71 (s, 3H), 3.02 (t, $J = 7.6$, 2H), 2.69 (t, $J = 7.6$, 2H) ppm.

Methyl 3-(4'-(trifluoromethyl)biphenyl-4-yl)propanoate (42c).



Reaction of 3-(4-bromophenyl)-propionic methyl ester **37** (0.3 g, 1.23 mmol) and boronic acid **39** (0.47 g, 2.46 mmol) afforded compound **42c** that was purified by flash chromatography on silica gel. Yield 95%; white powder; ¹H-NMR (200 MHz): δ 7.72-7.70 (m, 4H), 7.56-7.53 (m, 2H), 7.35-7.31 (m, 2H), 3.71 (s, 3H), 3.04 (t, $J = 8.0$, 2H), 2.71 (t, $J = 7.0$, 2H) ppm.

Methyl 3-(3'-(benzyloxy)biphenyl-4-yl)propanoate (42d).

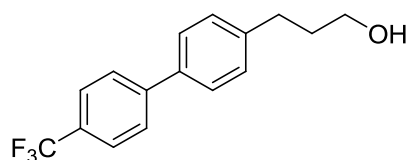


Reaction of 3-(bromophenyl)-propionic methyl ester **37** (0.3 g, 1.23 mmol) and boronic acid **40** (0.56 g, 2.46 mmol) afforded compound **42d** that was purified by flash chromatography on silica gel (petroleum ether/EtOAc = 8/2). Yield 99%; ¹H-NMR (200 MHz): δ 7.54-7.18 (m, 12H), 6.97 (d, $J = 7.2$, 2H), 5.14 (s, 2H), 3.71 (s, 3H), 3.02 (t, $J = 7.8$, 2H), 2.69 (t, $J = 7.6$, 2H) ppm.

Methyl 3-(4-(dibenzo[b,d]furan-1-yl)phenyl)propanoate (42e).

7.40 (d, $J = 8.2$, 2H), 7.14 (d, $J = 7.8$, 2H), 6.63-6.62 (m, 2H), 6.36-6.34 (m, 1H), 3.73 (s, 6H), 3.58 (t, $J = 6.6$, 2H), 2.64 (t, $J = 7.2$, 2H), 1.88-1.74 (m, 2H), 1.82 (br-s, 1H, OH) ppm.

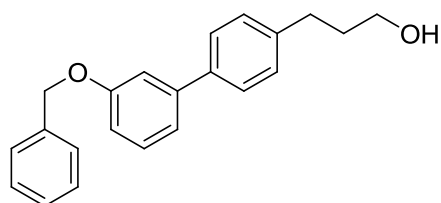
3-(4'-(Trifluoromethyl)biphenyl-4-yl)propan-1-ol (43c).



Biphenyl propanoic methyl ester **42c** (0.24 g, 0.94 mmol) led to compound **43c**. Yield 87%; white powder; $^1\text{H-NMR}$ (200 MHz): δ 7.72-7.70 (m, 4H), 7.57 (d, $J = 8.0$, 2H), 7.34 (d, $J = 8.2$, 2H),

3.75 (t, $J = 6.2$, 2H), 2.81 (t, $J = 7.2$, 2H), 2.05-1.91 (m, 2H), 1.67 (br-s, 1H, OH) ppm.

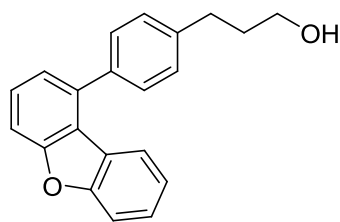
3-(3'-(Benzyloxy)biphenyl-4-yl)propan-1-ol (43d).



Biphenyl propanoic methyl ester **42d** (0.16 g, 0.46 mmol) led to compound **43d**. Yield 99%; white solid; $^1\text{H-NMR}$ (200 MHz): δ 7.57-7.21 (m, 12H), 7.02-6.97 (m, 2H), 5.16 (s, 2H), 3.75 (t, J

= 6.2, 2H), 2.80 (t, $J = 8.0$, 2H), 2.04-1.94 (m, 2H), 1.48 (br-s, 1H, OH) ppm.

3-(4-(Dibenzo[b,d]furan-1-yl)phenyl)propan-1-ol (43e).



Biphenyl propanoic methyl ester **42e** (0.30 g, 0.91 mmol) led to compound **43e**. Yield 98%; white solid; $^1\text{H-NMR}$ (400 MHz): δ 7.99-7.97 (m, 1H), 7.92-7.90 (m, 1H), 7.86-7.83 (m, 2H), 7.60-7.58 (m, 2H), 7.57-7.44 (m, 1H), 7.43-7.33 (m, 4H), 3.74 (t, $J = 6.0$, 2H), 2.80 (t, J

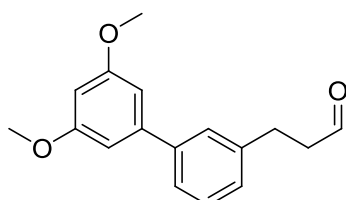
= 7.6, 2H), 2.01-1.94 (m, 2H), 1.40 (br-s, 1H, OH) ppm.

6.2.6. General procedure for the synthesis of 3-substituted propyl aldehydes 44a-f and their characterization

A solution of the appropriate 3-biphenyl propyl alcohols **43a-f** (1.0 equiv) in CH_2Cl_2 (5 mL) was added dropwise to the suspension of PCC (1.4 equiv) in CH_2Cl_2 (15 mL) cooled to 0 °C. The

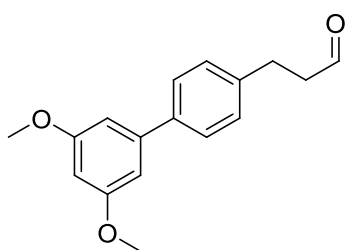
reaction mixture was stirred in an ice bath for 3-4h, then filtered on silica gel and evaporated to dryness. All the compounds were used in the next step without any further purification (Scheme 4.3).

3-(3',5'-Dimethoxybiphenyl-3-yl)propanal (44a).



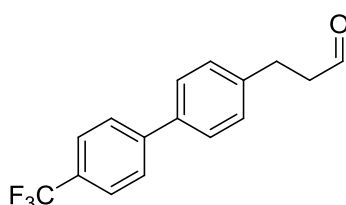
3-Biphenyl propyl alcohol **43a** (0.42 g, 1.54 mmol) lead to compound **44a**. Yield 90%; yellow oil; $^1\text{H-NMR}$ (200 MHz): δ 9.83 (t, $J = 1.2$, 1H), 7.50-7.35 (m, 3H), 7.23-7.20 (m, 1H), 6.79-6.78 (m, 2H), 6.55-6.53 (m, 1H), 3.88 (s, 6H), 3.05 (t, $J = 7.0$, 2H), 2.86 (t, $J = 7.4$, 2H) ppm.

3-(3',5'-Dimethoxybiphenyl-4-yl)propanal (44b).



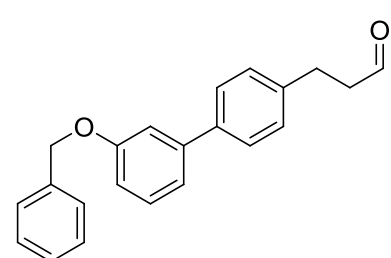
3-Biphenyl propyl alcohol **43b** (0.42 g, 1.54 mmol) lead to compound **44b**. Yield 72%; yellow oil; $^1\text{H-NMR}$ (400 MHz): δ 9.82 (t, $J = 1.2$, 1H), 7.50 (d, $J = 6.8$, 2H), 7.24 (d, $J = 7.6$, 2H), 6.72-6.71 (m, 2H), 6.47-6.45 (m, 1H), 3.83 (s, 6H), 2.98 (t, $J = 7.6$, 2H), 2.79 (t, $J = 7.2$, 2H) ppm.

3-(4'-(Trifluoromethyl)biphenyl-4-yl)propanal (44c).



3-Biphenyl propyl alcohol **43c** (0.23 g, 0.82 mmol) led to compound **44c**. Yield 88%; yellow oil; $^1\text{H-NMR}$ (200 MHz): δ 9.89 (t, $J = 1.6$, 1H), 7.71-7.70 (m, 4H), 7.57 (d, $J = 8.0$, 2H), 7.34 (d, $J = 8.4$, 2H), 3.06 (t, $J = 7.2$, 2H), 2.87 (t, $J = 6.8$, 2H) ppm.

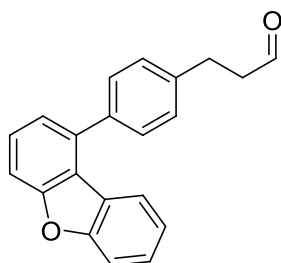
3-(3'-(Benzyloxy)biphenyl-4-yl)propanal (44d).



3-Biphenyl propyl alcohol **43d** (0.26 g, 0.81 mmol) lead to compound **44d**. Yield 94%; yellow oil; $^1\text{H-NMR}$ (200 MHz): δ

9.88 (t, $J = 1.6$, 1H), 7.57-7.35 (m, 6H), 7.31-7.23 (m, 6H), 7.02-6.96 (m, 1H), 5.15 (s, 2H), 3.03 (t, $J = 7.2$, 2H), 2.85 (t, $J = 7.4$, 2H) ppm.

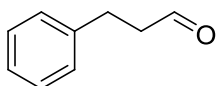
3-(4-(Dibenzo[b,d]furan-1-yl)phenyl)propanal (**44e**).



3-Biphenyl propyl alcohol **43e** (0.39 g, 1.29 mmol) lead to compound **44e**.

Yield 98%; yellow oil; $^1\text{H-NMR}$ (400 MHz): δ 9.86 (t, $J = 1.2$, 1H), 7.99-7.97 (m, 1H), 7.93-7.91 (m, 1H), 7.90-7.84 (m, 2H), 7.60-7.57 (m, 2H), 7.48-7.43 (m, 1H), 7.41-7.33 (m, 4H), 3.04 (t, $J = 7.6$, 2H), 2.85 (t, $J = 7.6$, 2H) ppm.

3-Phenylpropanal (**44f**).



3-Phenyl propyl alcohol **43f** (2.0 g, 14.6 mmol) lead to compound **44f**. Yield 81%; yellow oil; $^1\text{H-NMR}$ (200 MHz): δ 9.79 (t, $J = 1.0$, 1H), 7.40-7.23 (m, 5H),

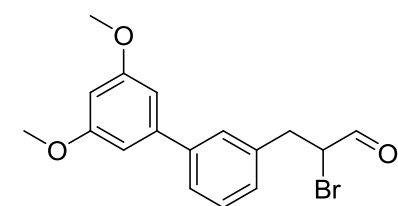
2.98 (t, $J = 7.4$, 2H), 2.75 (t, $J = 7.0$, 2H) ppm.

6.2.7. General procedure for the synthesis of 3-substituted- α -bromopropyl aldehydes **33a-f** and their characterization

A solution of the appropriate 3-substituted propyl aldehydes **44a-f** (1.0 equiv) in dry Et_2O (2 mL) was added dropwise to a solution of DBBA (0.5 equiv) in dry Et_2O (4 mL). Successively, a solution 4N of HCl in 1,4-dioxane (0.028 mL, 0.1equiv) was added dropwise and the reaction mixture was stirred at room temperature for 20 h. The resulting suspension was extracted with a saturated NaHCO_3 solution (10 mL) and Et_2O (3 x 10 mL). The combined organic layers were washed with H_2O (10 mL), and brine (10 mL), then dried over Na_2SO_4 and evaporated to dryness (Scheme 4).

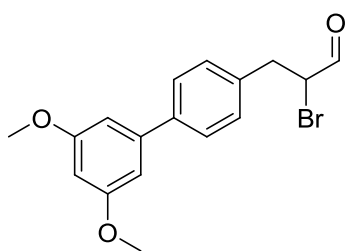
3).

2-Bromo-3-(3',5'-dimethoxybiphenyl-3-yl)propanal (**33a**).



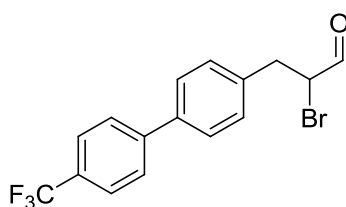
The 3-substituted propyl aldehyde **44a** (0.64 g, 2.36 mmol) led to the brominated product **33a**. Yield 99%; thick yellow oil; $^1\text{H-NMR}$ (200 MHz): δ 9.52 (d, $J = 1.4$, 1H), 7.53-7.20 (m, 4H), 6.74-6.73 (m, 2H), 6.51-6.50 (m, 1H), 4.54-4.47 (m, 1H), 3.87 (s, 6H), 3.62-3.52 (m, 1H), 3.29-3.18 (m, 1H) ppm.

2-Bromo-3-(3',5'-dimethoxybiphenyl-4-yl)propanal (**33b**).



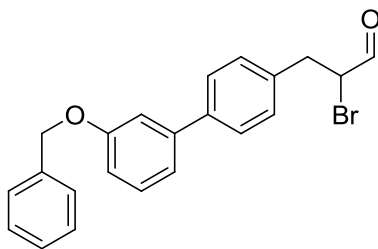
3-substituted propyl aldehyde **44b** (0.47 g, 1.73 mmol) led to the brominated product **33b**. Yield 99%; thick yellow oil; $^1\text{H-NMR}$ (200 MHz): δ 9.55 (d, $J = 1.8$, 1H), 7.57-7.54 (m, 1H), 7.40-7.28 (m, 3H), 6.74-6.73 (m, 1H), 6.53-6.49 (m, 2H), 4.57-4.46 (m, 1H), 3.87 (s, 6H), 3.62-3.45 (m, 2H) ppm.

2-Bromo-3-(4'-(trifluoromethyl)biphenyl-4-yl)propanal (**33c**).



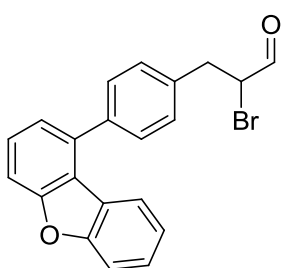
The 3-substituted propyl aldehyde **44c** (0.20 g, 0.72 mmol) led to the brominated product **33c**. Yield 83%; thick yellow oil; $^1\text{H-NMR}$ (200 MHz): δ 9.55 (d, $J = 2.2$, 1H), 7.71-7.70 (m, 4H), 7.57 (d, $J = 8.0$, 2H), 7.33 (d, $J = 8.4$, 2H), 4.42-4.31 (m, 1H), 3.41-3.19 (m, 2H) ppm.

2-Bromo-3-(3'-(benzyloxy)biphenyl-4-yl)propanal (**33d**).



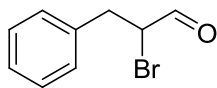
The 3-substituted propyl aldehyde **44d** (0.24 g, 0.76 mmol) led to the brominated product **33d**. Yield 96%; thick yellow oil; $^1\text{H-NMR}$ (200 MHz): δ 9.54 (d, $J = 2.4$, 1H), 7.58-7.18 (m, 12H), 7.02-6.96 (m, 1H), 5.15 (s, 2H), 4.55-4.46 (m, 1H), 3.60-3.45 (m, 1H), 3.29-4.18 (m, 1H) ppm.

2-Bromo-3-(4-(dibenzo[b,d]furan-1-yl)phenyl)propanal (33e).



The 3-substituted propyl aldehyde **44e** (0.25 g, 0.83 mmol) led to the brominated product **33e**. Yield 98%; $^1\text{H-NMR}$ (400 MHz): δ 9.53 (d, $J = 2.4$, 1H), 7.98-7.96 (m, 1H), 7.94-7.92 (m, 1H), 7.89-7.86 (m, 2H), 7.60-7.57 (m, 2H), 7.66-7.28 (m, 5H), 4.54-4.51 (m, 1H), 3.60-3.54 (m, 1H), 3.28-3.22 (m, 1H) ppm.

2-Bromo-3-phenylpropanal (33f).



3-Phenyl propyl aldehyde **44f** (1.15 g, 8.57 mmol) led to the brominated product **33f**. Yield 93%; $^1\text{H-NMR}$ (200 MHz): δ 9.51 (d, $J = 2.6$, 1H), 7.36-7.21 (m, 5H), 4.48-4.44 (m, 1H), 3.56-3.45 (m, 1H), 3.25-3.13 (m, 1H) ppm.

6.3. Biology

6.3.1. BACE-1 inhibition: enzymatic procedures

Method A: M-2420 substrate and Sigma enzyme

Human recombinant BACE-1, sodium acetate, CHAPS and DMSO were purchased from Sigma Aldrich (Milan, Italy). The substrate, M-2420, was from Bachem, (Torrance, CA, USA). Purified water from Milli-RX system (Millipore, Milford, MA, USA) was used to prepare buffers and standard solutions. Spectrofluorometric analyses were carried out on a Fluoroskan Ascent multiwell spectrofluorimeter (excitation: 320 nm; emission: 405 nm) by using black microwell (96 wells) Corning plates (Sigma, Italy).

Stock solutions of the tested compounds were prepared in DMSO and diluted with DMSO. Specifically, 175 μ L of BACE1 enzyme (25 nM in NaOAc 20 mM pH 4.5, containing 0.1% w/v CHAPS) were incubated with 5 μ L of test compound for 60 minutes. To start the reaction, 20 μ L of M-2420 (3 μ M in Hepes 10 mM pH 7.5) were added to the well. The mixture was incubated at room temperature for 15 minutes and the fluorescence signal was read at 405 nm.

Assays were done with a blank containing all components except BACE1 in order to account for non enzymatic reaction. The reaction rates were compared and the percent inhibition due to the presence of test compounds was calculated. Each concentration was analyzed in duplicate. The percent inhibition of the enzyme activity due to the presence of increasing test compound concentration was calculated by the following expression: $100 - (v_i/v_o \times 100)$, where v_i is the initial rate calculated in the presence of inhibitor and v_o is the enzyme activity. To demonstrate inhibition of BACE-1 activity, inhibitor IV (Calbiochem, Darmstadt, Germany) was used as reference inhibitor ($IC_{50} = 13.61$ nM).

Method B: Panvera peptide and Invitrogen Enzyme

Purified Baculovirus-expressed BACE-1 and rhodamine derivative substrate were purchased from Panvera (Madison, WI, U.S). Sodium acetate and DMSO were from Sigma Aldrich (Milan, Italy). Purified water from Milli-RX system (Millipore, Milford, MA, USA) was used to prepare buffers and standard solutions. Spectrofluorometric analyses were carried out on a Fluoroskan Ascent multiwell spectrofluorimeter (excitation: 544 nm; emission: 590 nm) by using black microwell (96 wells) Corning plates (Sigma, Italy). Stock solutions of the tested compounds were prepared in DMSO and diluted with 50 mM sodium acetate buffer pH = 4.5. Specifically, 20 μ L of BACE1 enzyme (25 nM) were incubated with 20 μ L of test compound for 60 minutes. To start the reaction, 20 μ L of substrate (0.25 μ M) were added to the well. The mixture was incubated at 37 °C for 60

minutes. To stop the reaction, 20 μL of BACE-1 stop solution (sodium acetate 2.5 M) were added to each well. Then the spectrofluorometric assay was performed by reading the fluorescence signal at 590 nm.

Assays were done with a blank containing all components except BACE-1 in order to account for non enzymatic reaction. The reaction rates were compared and the percent inhibition due to the presence of test compounds was calculated. Each concentration was analyzed in triplicate. The percent inhibition of the enzyme activity due to the presence of increasing test compound concentration was calculated by the following expression: $100 - (v_i/v_o \times 100)$, where v_i is the initial rate calculated in the presence of inhibitor and v_o is the enzyme activity. To demonstrate inhibition of BACE-1 activity, inhibitor IV (Calbiochem, Darmstadt, Germany) was used as reference inhibitor ($\text{IC}_{50} = 12.89 \text{ nM}$).

6.3.2. Inhibition of AChE and BuChE activities

The method of Ellman et al. was followed.²³⁹ Five different concentrations of each compound were selected in order to obtain inhibition of AChE or BuChE activities comprised between 20 and 80%. The assay solution consisted of a 0.1 M potassium phosphate buffer pH 8.0, with the addition of 340 μM 5,5'-dithio-bis(2-nitrobenzoic acid), 0.02 unit/mL of human recombinant AChE or BuChE from human serum (Sigma Chemical), and 550 μM of substrate (acetylthiocholine iodide or butyrylthiocholine iodide, respectively). Test compounds were added to the assay solution and preincubated at 37 °C with the enzyme for 20 min before the addition of substrate. Enzyme reaction was followed at 412 nm for five min by a double beam spectrophotometer (Jasco V-530). Assays were carried out with a blank containing all components except AChE or BuChE in order to account for non-enzymatic reaction. The reaction rates were compared, and the percent inhibition due to the presence of test compounds was calculated. Each concentration was analyzed in triplicate, and IC_{50} values were determined graphically from inhibition curves (percent inhibition vs log inhibitor concentration).

6.3.3. Inhibition of AChE-induced A β -amyloid aggregation

Aliquots of 2 μL A β_{40} peptide (Bachem AG, Germany), lyophilized from a 2 mg mL⁻¹ HFIP (1,1,1,3,3,3-hexafluoro-2-propanol) solution and dissolved in DMSO, were incubated for 24 h at room temperature in 0.215 M sodium phosphate buffer (pH 8.0) at a final concentration of 230 μM . For co-incubation experiments aliquots (16 μL) of human recombinant AChE (final concentration 2.30 μM , A β /AChE molar ratio 100:1) and AChE in the presence of 2 μL of tested inhibitor (final concentration = 100 μM) were added. Blanks containing A β , AChE, and A β plus inhibitor, in 0.215

M sodium phosphate buffer pH 8.0 were prepared. The final volume of each vial was 20 μ L. Each assay was run in duplicate. To quantify amyloid fibril formation, the thioflavin T fluorescence method was then applied.^{208,240,241}

Analyses were performed with a Jasco Spectrofluorometer FP-6200 using a 3 ml quartz cell. After incubation, the samples containing $A\beta$, or $A\beta$ plus AChE, or $A\beta$ plus AChE in the presence of inhibitors were diluted with 50 mM glycine-NaOH buffer (pH 8.5) containing 1.5 μ M thioflavin T to a final volume of 2.0 mL. A 300s-time scan of the emitted fluorescence ($\lambda_{\text{ex}} = 446$ nm, $\lambda_{\text{em}} = 490$ nm) was performed and the intensity values at the plateau were averaged after subtracting the background fluorescence of 1.5 μ M thioflavin T and AChE.

The fluorescence intensities in the presence and in the absence of inhibitor were compared and the percentage of inhibition was calculated by the following expression: $100 - (IF_i/IF_o \times 100)$ where IF_i and IF_o are the fluorescence intensities obtained for $A\beta$ plus AChE in the presence and in the absence of inhibitor, respectively.²⁰⁸

6.3.4. Inhibition of $A\beta_{42}$ self-aggregation

HFIP pretreated $A\beta_{42}$ samples (Bachem AG, Switzerland) were resolubilized with a $\text{CH}_3\text{CN}/0.3$ mM $\text{Na}_2\text{CO}_3/250$ mM NaOH (48.4/48.4/3.2) mixture in order to have a stable stock solution ($[A\beta] = 500$ μ M). Experiments were performed by diluting the peptide stock solution in 10 mM phosphate buffer (pH = 8.0) containing 10 mM NaCl, to a final concentration of 50 μ M in the absence or in the presence of compounds **61-65** at 10 μ M. Samples were then incubated without stirring at 30 $^\circ\text{C}$ for 24 h. To quantify amyloid fibril formation, the thioflavin T fluorescence method was used.^{240,241} After incubation, samples were diluted to a final volume of 2.0 mL with 50 mM glycine-NaOH buffer (pH = 8.5) containing 1.5 μ M thioflavin T. A 300-seconds-time scan of fluorescence intensity was carried out ($\lambda_{\text{ex}} = 446$ nm; $\lambda_{\text{em}} = 490$ nm), and values at plateau were averaged after subtracting the background fluorescence of 1.5 μ M thioflavin T solution.

6.3.5. BACE-1 inhibition: cellular assays procedures

Preparation and culture of neurons

One-day-old fertilized eggs were stored under appropriate conditions until start of breeding. On embryonic day 0 eggs were transferred to the breeding incubator and under turning kept at 37.8 °C and 55 % humidity until embryonic day eight.

All cell culture experiments were carried out under sterile conditions meaning all procedures were performed in a cell culture unit with special cell culture equipment. Items necessary like glassware, forceps or scissors were sterilised prior to the experiment. Stock solutions were purchased already sterile and final suspensions like the culture medium were freshly prepared in the laminar airflow cabinet.

In short, embryos were transferred to a plastic dish, and decapitated. Both hemispheres were removed, collected and cleaned from any loose tissue. Hemispheres were mechanically dissociated.

Administration of test and reference item

For the secretase assay, poly-D-lysine pre-coated 24-well microplates were used with three wells per test items (T.I.) and reference item (R.I.) concentration (n=3). 1.8×10^6 cells were plated per 24 well in a total volume of 2 mL. The cell culture medium consisted of DMEM with 4.5 g glucose/L, 5% Nu Serum, 0.01% gentamycin and 2 mM L-glutamine. Cultures were maintained at 37 °C, 95% humidity and 5% CO₂. 48 h after initiation of culture, medium was exchanged with fresh medium containing T.I., R.I., or vehicle in a total volume of 300 µL. DAPT was used as R.I.

DAPT was dissolved in DMSO to a stock concentration of 5 mM and applied on cultured neurons at a final concentration of 200 nM. All T.I. were dissolved in DMSO. 24 h after treatment, cell culture supernatants were taken off, snap frozen and stored at -80 °C prior to A β ₃₈, A β ₄₀, and A β ₄₂ measurement.

Viability assay

In parallel, test items were evaluated for their effect on cell viability of primary chicken telencephalon neurons in 96-well plates. 3×10^5 cells were plated per 96 well in a total volume of 160 µL. Cultures were maintained at 37 °C, 95% humidity and 5% CO₂. 48 h after initiation of culture, medium was exchanged with fresh medium containing T.I., R.I., or vehicle in a total volume of 60 µL. After 24 h of treatment, viability was determined by using the MTT reduction assay.

Evaluation

Determination of A β species

In cell supernatants, A β ₃₈, A β ₄₀, and A β ₄₂ levels were determined with a commercially available A β -Triplex kit from Mesoscale Discovery, USA. A β levels in cell supernatants were evaluated in comparison to an A β peptide standard as pg per mL.

MTT-Viability Assay

Viability of cultures was determined with the MTT assay using a plate-reader (570 nm). The MTT-assay is a very sensitive assay measuring the mitochondrial dehydrogenase activity in viable cells and is based on the reduction of yellow MTT (3-(4,5-dimethylthiazol-2-yl)-2,5-diphenyl tetrazolium bromide) to dark blue formazan crystals by mitochondrial dehydrogenases (succinate dehydrogenase). Since this reaction is catalysed in living cells only this assay can be used for the quantification of cell viability. For determination of cell viability, MTT solution was added to each well in a final concentration of 0.5 mg/mL. After 2 h the MTT containing medium was aspirated. Cells were lysed with 3% SDS and formazan crystals were dissolved in isopropanol/HCl. To estimate optical density, a plate-reader was used at wavelength 570 nm. Cell viability is expressed in optical density (OD).

Statistics

Descriptive statistical analysis was performed. Data will be represented as mean \pm S.D. or (S.E.M.). To determine statistical significant differences between treatment groups, one-way ANOVA analyses followed by Bonferroni's Multiple Comparison Tests were performed.

6.3.6. CNS penetration: *in vitro* PAMPA-BBB test

Prediction of the brain penetration was evaluated using a parallel artificial membrane permeability assay (PAMPA)¹⁷⁵. Ten commercial drugs, phosphate buffer saline solution at pH 7.4 (PBS), Ethanol and dodecane were purchased from Sigma, Acros organics, Merck, Aldrich and Fluka. The porcine polar brain lipid (PBL) (catalog no. 141101) was from Avanti Polar Lipids. The donor plate was a 96-well filtrate plate (Multiscreen® IP Sterile Plate PDVF membrane, pore size is 0.45 µM, catalog no. MAIPS4510) and the acceptor plate was an indented 96-well plate (Multiscreen®, catalog no. MAMCS9610) both from Millipore. Filter PDVF membrane units (diameter 30 mm, pore size 0.45 µm) from Symta were used to filtered the samples. A 96-well plate UV reader (Thermoscientific, Multiskan spectrum) was used for the UV measurements. Test compounds [(3-5 mg of Caffeine, Enoxacin, Hydrocortisone, Desipramine, Ofloxacin, Piroxicam, Testosterone), (12 mg of Promazine) and 25 mg of Verapamil and Atenolol] were dissolved in EtOH (1000 µL). 100 microlitres of this compound stock solution was taken and 1400 µL of EtOH and 3500 µL of PBS pH 7.4 buffer were added to reach 30% of EtOH concentration in the experiment. These solutions were filtered. The acceptor 96-well microplate was filled with 180 µL of PBS/EtOH (70/30). The donor 96-well plate was coated with 4 µL of porcine brain lipid in dodecane (20 mg mL⁻¹) and after 5 minutes, 180 µL of each compound solution was added. 1-2 mg of every compound to be determined their ability to pass the brain barrier were dissolved in 1500 µL of EtOH and 3500 µL of PBS pH 7.4 buffer, filtered and then added to the donor 96-well plate. Then the donor plate was carefully put on the acceptor plate to form a “sandwich”, which was left undisturbed for 2 h and 30 min at 25 °C. During this time the compounds diffused from the donor plate through the brain lipid membrane into the acceptor plate. After incubation, the donor plate was removed. UV plate reader determined the concentration of compounds and commercial drugs in the acceptor and the donor wells. Every sample was analyzed at three to five wavelengths, in 3 wells and in two independent runs. Results are given as the mean ± S.D. and the average of the two runs is reported. 10 quality control compounds (previously mentioned) of known BBB permeability were included in each experiment to validate the analysis set.

In order to explore the capacity of **27-29** and **31** to penetrate into the brain, we used the PAMPA-BBB method described by Di et al.¹⁷⁵ which employed a brain lipid porcine membrane. The *in vitro* permeabilities (*Pe*) of commercial drugs through lipid membrane extract together with compounds **27-29** and **31** were determined and described in Table 6.5. An assay validation was made comparing the reported permeability values of commercial drugs with the experimental data obtained employing this methodology. A good correlation between experimental-described values was obtained $Pe(\text{exptl}) = 1.0345(\text{bibl}) - 0.584$ ($R^2 = 0.967$) (Figure 6.1). From this equation and

following the pattern established in the literature for BBB permeation prediction^{175,242} we could classify the compounds as CNS+ when they present a permeability $> 3.55 \times 10^{-6} \text{ cm s}^{-1}$ and as CNS+/- when the Pe value is between 3.55×10^{-6} and $2.00 \times 10^{-6} \text{ cm s}^{-1}$.

Based on these results we can consider that compounds **27** and **31** are able to cross the BBB by passive permeation (see Table 6.5). **29** precipitates in the experimental conditions employed so it was not possible to determine the BBB permeability.

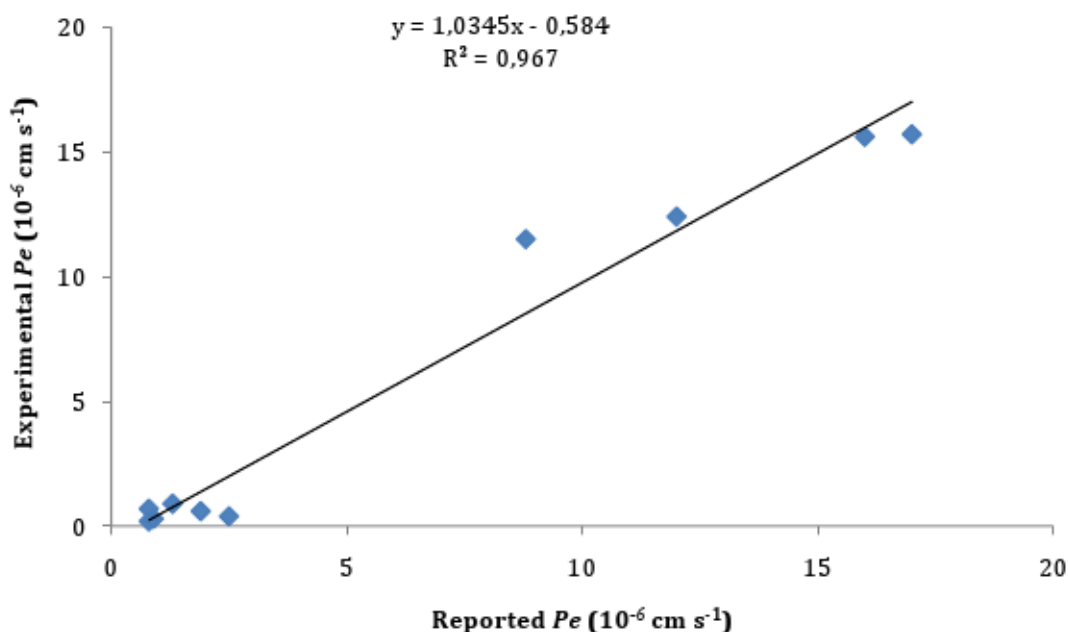


Figure 6.1. Linear correlation between experimental and reported permeability of commercial drugs using the PAMPA-BBB assay.

Table 6.5. Permeability (Pe) in the PAMPA-BBB assay for ten commercial drugs (used in the experiment validation) and the compounds **27-29** and **31** with their predictive penetration in the CNS^a.

Cpds	Bibl. ^b	Pe ($10^{-6} \text{ cm s}^{-1}$) ^c	Prediction ^d
Atenolol	0.8	0.2 ± 0.1	
Caffeine	1.3	0.9 ± 0.2	
Desipramine	12	12.4 ± 1.0	
Enoxacine	0.9	0.3 ± 0.2	
Hydrocortisone	1.9	0.6 ± 0.4	

Ofloxacin	0.8	0.7 ± 0.7	
Piroxicam	2.5	0.4 ± 0.4	
Promazine	8.8	11.5 ± 0.9	
Testosterone	17	15.7 ± 1.2	
Verapamil	16	15.6 ± 1.2	
27		4.0 ± 1.0	CNS+
28		3.2 ± 0.2	CNS+/-
29		n. d. ^e	n. d.
31		4.0 ± 0.7	CNS+

^aPBS/EtOH (70/30) was used as solvent. ^bFrom reference Di et al.¹⁷⁵ ^cValues are mean ± S.D. of two independent experiments. ^dThe compounds were classified¹⁷⁵ as CNS+ when they present a *Pe* value > 3.55 x 10⁻⁶ cm s⁻¹, and as CNS+/- when the *Pe* value is between 3.55 x 10⁻⁶ and 2.00 x 10⁻⁶ cm s⁻¹. ^en. d. = not determined.

Chapter 7

7. Outlook

7.1. 2-Aminoimidazole derivatives as interfering probes in the replication process of prion protein

7.1.1. Overview of Prion diseases (PrDs)

PrDs, also known as transmissible spongiform encephalopathies (TSEs), are a group of invariably fatal disorders, including bovine spongiform encephalopathy (BSE) of cattle, scrapie of sheep, chronic wasting disease (CWD) of deer, moose and elk, Creutzfeldt-Jakob (CJD) and Gerstmann-Sträussler-Scheinker (GSS) diseases of humans.²⁴³ Currently, there is no cure for each one of these PrDs.^{244,245} They are characterized by widespread neurodegeneration; therefore, affected individuals or animals exhibit clinical symptoms of both cognitive and motor dysfunction.

Despite their rare incidence in humans, PrDs have captured very large attention from the scientific community due to the unconventional mechanism of transmission. The typical microscopic features of prion diseases are vacuolation of the neuropil in the grey matter, prominent neuronal loss, exuberant reactive astrogliosis and a variably gradual accumulation of the scrapie form of the prion protein (PrP^{Sc}) in the central nervous system.²⁴⁵ According to the “protein-only hypothesis”, in the CNS of the infected host, the normal cellular form of prion protein (PrP^C) is converted into an abnormal insoluble amyloidogenic isoform (PrP^{Sc}, also simply named prion.²⁴⁵ The latter acts as a template for PrP^C leading to nascent PrP^{Sc} molecules. The conversion process is associated with conformational changes of secondary structure from α -helices to β -sheets. The term “prion” (a small proteinaceous infectious particle that is resistant to inactivation by most procedures that modify nucleic acids)²⁴⁶ was proposed by Stanley B. Prusiner to distinguish the infectious pathogen that causes prion diseases from viruses and viroids. The infection principle consists purely of protein and is capable of replicating and transmitting infections without the need for informational nucleic acids.²⁴⁶ Numerous experiments have provided evidence that PrP^C is a key player in prion replication as well as in prion-induced neurodegeneration.²⁴⁷ PrP^C expression is categorically

required for neurodegeneration in host neurons, because the presence of PrP^{Sc} alone does not cause disease.²⁴⁸ Mice lacking the prion gene are resistant to the infection.^{249,250}

The conversion PrP^C to the PrP^{Sc} form by protein-protein interaction is a characteristic feature of the diseases. PrP^C is one of amyloidogenic proteins, which are associated with a variety of conformational diseases. Indeed, PrDs show many pathologic features analogous to other neurodegenerative disorders similarly characterized by the presence of abnormal protein accumulation in the nervous system leading to a selective neuronal death, such as AD (extra-cellular A β -composed senile plaques and NFTs consisting in intra-cellular deposition of hyper-phosphorilated τ), Parkinson's disease (Lewy bodies formed by α -synuclein), Huntington disease (huntingtin protein aggregates). As it should be pointed out that the commonness in aggregation of these amyloidogenic proteins, despite their differences in sequence, in all conformational diseases might suggest that PrP^{Sc} blockers are also effective to prevent other fibril formation. Hence, studying the antiprion compounds may help to define a common pharmacophore for other amyloidoses.

7.1.2. Introduction

PrDs are neurodegenerative and infectious disorders that affect both human and animals, and not current drugs are available yet. Although reliable proof-of-principle was demonstrated in a variety of experimental models, and several classes of small molecules have been identified, the mode-of-action and targets for most of the antiprion molecules remain largely unexplored. Indeed, structurally diverse chemical antiprion compounds, covering a broad range of the chemical space, have been discovered so far by screening approaches.²⁵¹

Based on these considerations, it emerges that the rational design of antiprion compounds is still a big challenge. The lack of validated molecular targets forces medicinal chemists to undertake a cellular phenotypic approach. However, a favorable point that could further motivate rational drug discovery in PrDs, is that the lessons we can learn from their investigation with small molecules might have an impact on other conformational diseases characterized by a similar pathological aggregation and accumulation of misfolded proteins.

To this end, it is particularly relevant to note that PrP^C was recently identified as a mediator of A β -oligomer-induced synaptic dysfunction, and hence PrP^C-specific compounds might have therapeutic potential for AD.¹³ In addition, several neuropathological and genetic links between AD and PrD have been recently proposed. For example, some cases of coexistent CJD and AD have been reported. The Met–Val129 polymorphism in human PrP^C is a risk factor for early-onset AD, and a systematic meta-analysis of AD genetic association studies revealed that the gene encoding PrP^C is a potential AD susceptibility gene.²⁵² Moreover, there are similarities in the post-translational processing, sequence and copper-binding properties of PrP^C and APP or the A β peptide.^{14,253} Recent experimental evidences have shown that PrP^C inhibits BACE-1-mediated cleavage of APP and the subsequent formation of A β suggesting that PrP^C may be a key protective player against AD.^{12,254} As a result of these findings, it is emerging as alternative and suitable strategy the idea to have common therapeutic approaches for these two distinct neurodegenerative disorders.^{13,253}

In light of this, we considered reasonable to perform a preliminary screening of selected 2-aminoimidazoles (reported in Strategy 1) to verify their potential antiprion activity. This was supported by the following reasons: i) they are synthetically readily accessible and amenable to compounds library generation; ii) some of these 2-aminoimidazoles have been shown to cross the BBB; iii) they have been extensively explored in medicinal chemistry and analogous chemical classes (i. e. 2-aminothiazoles, 2-aminobenzothiazoles and 2-thioimidazoles)²⁵⁵⁻²⁵⁷ have been reported as antiprion compounds. Therefore, it seemed conceivable that 2-aminoimidazoles could

serve as a template for a diverse array of pharmacophores toward the identification of novel chemical class for the treatment of prion diseases.

Here, we present some preliminary results on 2-aminoimidazole derivatives, which resulted able to inhibit PrP^{Sc} aggregation at a micromolar range with a low concomitant cytotoxicity.

7.1.3. Preliminary results

A cell-screening assay was used to test antiprion activity across of the selected 2-aminoimidazoles. Their ability to reduce PrP^{Sc} concentrations in scrapie-infected mouse hypothalamus (ScGT1) cells was determined from Western blot densitometry of the proteinase K (PK)-resistant PrP^{Sc}. The compounds were initially screened at 10 μ M, and their ability to reduce PrP^{Sc} levels after exposure for five days was evaluated by comparison with the untreated control. The effects of tested compounds on ScGT1 cells viability were determined (see Table 7.1). For compounds **26**, **28-30** and **31**, the EC₅₀ values, which represent the effective concentrations for half-maximal inhibition, were also calculated (see Table 7.1). Two well-documented antiprion agents, imipramine and quinacrine, were investigated as positive controls and their EC₅₀ values of 6.2 \pm 0.4 and 0.4 \pm 0.1 μ m were obtained, respectively.

Firstly, the cytotoxic effects of compounds **25-31** were determined by calcein-AM assay in the ScGT1 cell line. As reported in Figure 7.1, the treatment of ScGT1 cells with test compounds (1 μ M) did not lead to any significant change in cell viability, with the exception of **25** and **27**, where the cell viability was lower than 40 and 60% respectively, and which resulted detrimental for the cells at the concentration of 10 μ M (see Figure 7.1).

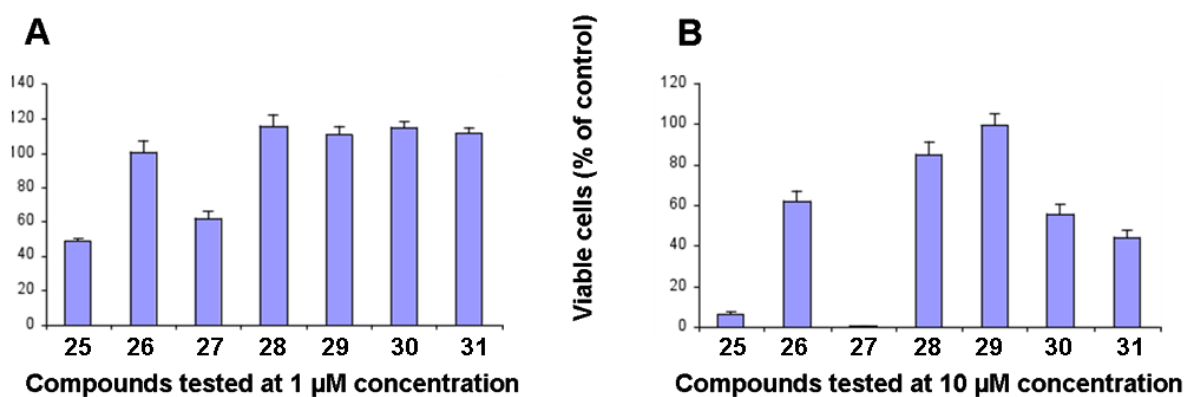
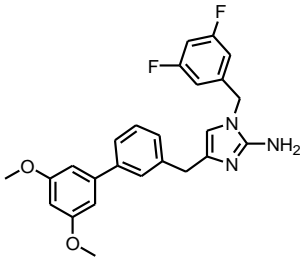
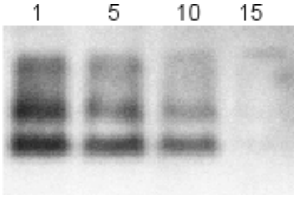
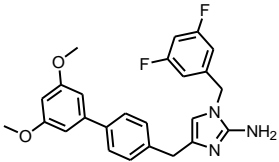
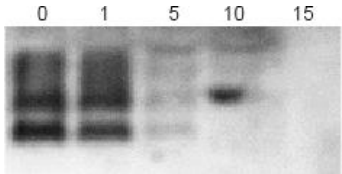
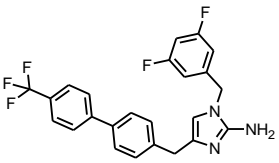
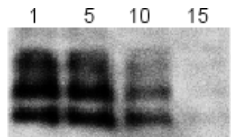
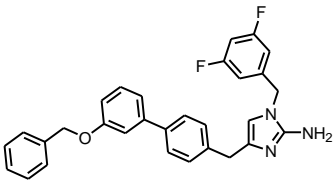
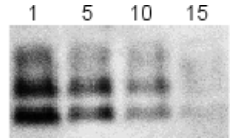
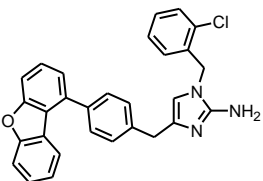
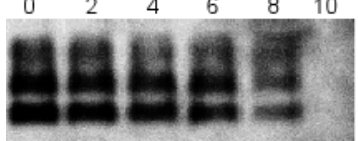


Figure 7.1. Cytotoxic effects of **25-31** determined at two different concentrations (at 1 and 10 μ M as shown in panel A and B, respectively) by calcein-AM assay in the ScGT1 cell line

Therefore, **25** and **27** were not screened for prion replication, whereas other compounds were assayed at different concentrations ranging from 1 to 15 μ M. All the tested 2-aminoimidazoles displayed activity at micromolar range (see EC₅₀ values reported in Table 7.1).

Table 7.1. Cell viability and inhibition of PrP^{Sc} accumulation in ScGT1 cells grown by compounds **26**, **28-30** and **31**.^a

Cpds	Chemical Structure	EC ₅₀ (μ M) ^b	Viable Cells (%) ^c	Western Blot (concentrations μ M)
26		7.8	78.8 \pm 3.5	
28		5.2	92.5 \pm 5.1	
29		8.5	93.9 \pm 3.7	
30		8.0	65.8 \pm 4.4	
31		6.1	70.3 \pm 2.9	

[a] Values given are the mean of three experiments. [b] The concentration of test compound required to reduce the PrP^{Sc} level in cells to 50% versus untreated cells (EC₅₀). [c] Cell viability at the EC₅₀ concentration was determined by calcein-AM cytotoxicity assay and expressed as an average percentage of viable cells versus untreated control cells.

Notably, compounds **28** and **29**, compared with their EC₅₀ values, showed a considerably low cytotoxicity. In addition, as previously reported in the Strategy 1, **28** displayed a relative capability to cross *in vitro* the BBB as assessed by PAMPA test.

In light of these preliminary results and the chemical accessibility, to elucidate the potential mode-of-action of derivatives **28** and **29**, further investigations are in progress in an attempt to better address the future optimization by systematic SAR studies of more potent and novel 2-aminoimidazoles derivatives as potential antiprion drugs.

Bibliography

1. Melnikova, I. Therapies for Alzheimer's disease. *Nat Rev Drug Discov* 2007, 6, 341-342.
2. Karran, E.; Mercken, M.; Strooper, B. D. The amyloid cascade hypothesis for Alzheimer's disease: an appraisal for the development of therapeutics. *Nat Rev Drug Discov* 2011, 10, 698-712.
3. Hardy, J.; Selkoe, D. J. The Amyloid Hypothesis of Alzheimer's Disease: Progress and Problems on the Road to Therapeutics. *Science* 2002, 297, 353-356.
4. Haass, C.; Selkoe, D. J. Soluble protein oligomers in neurodegeneration: lessons from the Alzheimer's amyloid [beta]-peptide. *Nat Rev Mol Cell Biol* 2007, 8, 101-112.
5. Kelleher, R. J.; Shen, J. γ -Secretase and Human Disease. *Science* 2010, 330, 1055-1056.
6. Holloway, M. K.; Hunt, P.; McGaughey, G. B. Structure and modeling in the design of β - and γ -secretase inhibitors. *Drug Dev Res* 2009, 70, 70-93.
7. Haniu, M.; Denis, P.; Young, Y.; Mendiaz, E. A.; Fuller, J.; Hui, J. O.; Bennett, B. D.; Kahn, S.; Ross, S.; Burgess, T.; Katta, V.; Rogers, G.; Vassar, R.; Citron, M. Characterization of Alzheimer's beta-Secretase Protein BACE. A pepsin family member with unusual properties. *J Biol Chem* 2000, 275, 21099-21106.
8. Stockley, J.; O'Neill, C. Understanding BACE1: essential protease for amyloid- β production in Alzheimer's disease. *Cell Mol Life Sci* 2008, 65, 3265-3289.
9. Cascella, M.; Micheletti, C.; Rothlisberger, U.; Carloni, P. Evolutionarily Conserved Functional Mechanics across Pepsin-like and Retroviral Aspartic Proteases. *JACS* 2005, 127, 3734-3742.
10. Ghosh, A. K.; Gemma, S.; Tang, J. β -Secretase as a Therapeutic Target for Alzheimer's Disease. *Neurotherapeutics* 2008, 5, 399-408.
11. Silvestri, R. Boom in the development of non-peptidic β -secretase (BACE1) inhibitors for the treatment of Alzheimer's disease. *Med Res Rev* 2009, 29, 295-338.
12. Griffiths, H. H.; Whitehouse, I. J.; Baybutt, H.; Brown, D.; Kellett, K. A. B.; Jackson, C. D.; Turner, A. J.; Piccardo, P.; Manson, J. C.; Hooper, N. M. Prion protein interacts with bace1 and differentially regulates its activity towards wild type and swedish mutant amyloid precursor protein. *J Biol Chem* 2011, Epub ahead of print.
13. Lauren, J.; Gimbel, D. A.; Nygaard, H. B.; Gilbert, J. W.; Strittmatter, S. M. Cellular prion protein mediates impairment of synaptic plasticity by amyloid-[bgr] oligomers. *Nature* 2009, 457, 1128-1132.
14. Barnham, K. J.; Cappai, R.; Beyreuther, K.; Masters, C. L.; Hill, A. F. Delineating common molecular mechanisms in Alzheimer's and prion diseases. *Trends Biochem Sci* 2006, 31, 465-472.
15. Zhang, H. Y. Same causes, same cures. *Biochem Biophys Res Commun* 2006, 351, 578-581.
16. Cruts, M.; vanBroeckhoven, C. Molecular genetics of Alzheimer's disease. *Ann Med* 1998, 30, 560-565.
17. Rovelet-Lecrux, A.; Hannequin, D.; Raux, G.; Meur, N. L.; Laquerriere, A.; Vital, A.; Dumanchin, C.; Feuillet, S.; Brice, A.; Vercelletto, M.; Dubas, F.; Frebourg, T.; Campion, D. APP locus duplication causes autosomal dominant early-onset Alzheimer disease with cerebral amyloid angiopathy. *Nat Genet* 2006, 38, 24-26.
18. Corder, E. H.; Saunders, A. M.; Strittmatter, W. J.; Schmechel, D. E.; Gaskell, P. C.; Small, G. W.; Roses, A. D.; Haines, J. L.; Pericak-Vance, M. A. Gene dose of apolipoprotein E type 4 allele and the risk of Alzheimer's disease in late onset families. *Science* 1993, 261, 921-923.

19. Stelzmann, R. A.; Norman Schnitzlein, H.; Reed Murtagh, F. An english translation of alzheimer's 1907 paper, "über eine eigenartige erkankung der hirnrinde". *Clinical Anat* 1995, 8, 429-431.
20. Bartus, R. T.; Dean, R. L.; Beer, B.; Lippa, A. S. The cholinergic hypothesis of geriatric memory dysfunction. *Science* 1982, 217, 408-414.
21. Kennedy, G. J.; Golde, T. E.; Tariot, P. N.; Cummings, J. L. Amyloid-based interventions in Alzheimer's disease. *CNS Spectrum* 2007, 12, A1-A14.
22. Esler, W. P.; Wolfe, M. S. A Portrait of Alzheimer Secretases--New Features and Familiar Faces. *Science* 2001, 293, 1449-1454.
23. Portelius, E.; Andreasson, U.; Ringman, J.; Buerger, K.; Daborg, J.; Buchhave, P.; Hansson, O.; Harmsen, A.; Gustavsson, M.; Hanse, E.; Galasko, D.; Hampel, H.; Blennow, K.; Zetterberg, H. Distinct cerebrospinal fluid amyloid beta peptide signatures in sporadic and PSEN1 A431E-associated familial Alzheimer's disease. *Mol Neurodegener* 2010, 5.
24. Tanzi, R. E.; Bertram, L. Twenty Years of the Alzheimer s Disease Amyloid Hypothesis: A Genetic Perspective. *Cell* 2005, 120, 545-555.
25. Lustbader, J. W.; Cirilli, M.; Lin, C.; Xu, H. W.; Takuma, K.; Wang, N.; Caspersen, C.; Chen, X.; Pollak, S.; Chaney, M.; Trinchese, F.; Liu, S.; Gunn-Moore, F.; Lue, L.-F.; Walker, D. G.; Kuppasamy, P.; Zewier, Z. L.; Arancio, O.; Stern, D.; Yan, S. S.; Wu, H. ABAD Directly Links AÅY to Mitochondrial Toxicity in Alzheimer's Disease. *Science* 2004, 304, 448-452.
26. Caricasole, A.; Copani, A.; Caruso, A.; Caraci, F.; Iacovelli, L.; Sortino, M. A.; Terstappen, G. C.; Nicoletti, F. The Wnt pathway, cell-cycle activation and [beta]-amyloid: novel therapeutic strategies in Alzheimer's disease? *Trends Pharmacol Sci* 2003, 24, 233-238.
27. Xie, L.; Helmerhorst, E.; Taddei, K.; Plewright, B.; van Bronswijk, W.; Martins, R. Alzheimer's β -Amyloid Peptides Compete for Insulin Binding to the Insulin Receptor. *J Neurosci* 2002, 22, RC221.
28. Kagan, B. L.; Hirakura, Y.; Azimov, R.; Azimova, R.; Lin, M. C. The channel hypothesis of Alzheimer's disease: current status. *Peptides* 2002, 23, 1311-1315.
29. Tamagno, E.; Parola, M.; Guglielmotto, M.; Santoro, G.; Bardini, P.; Marra, L.; Tabaton, M.; Danni, O. Multiple signaling events in amyloid [beta]-induced, oxidative stress-dependent neuronal apoptosis. *Free Radical Biol Med* 2003, 35, 45-58.
30. Bamberger, M. E.; Landreth, G. E. Microglial interaction with β -amyloid: Implications for the pathogenesis of Alzheimer's disease. *Micros Res Techn* 2001, 54, 59-70.
31. Devi, L.; Prabhu, B. M.; Galati, D. F.; Avadhani, N. G.; Anandatheerthavarada, H. K. Accumulation of Amyloid Precursor Protein in the Mitochondrial Import Channels of Human Alzheimer's Disease Brain Is Associated with Mitochondrial Dysfunction. *J Neurosci* 2006, 26, 9057-9068.
32. Lin, M. T.; Beal, M. F. Alzheimer's APP mangles mitochondria. *Nat Med* 2006, 12, 1241-1243.
33. Wang, J.-Z.; Grundke-Iqbal, I.; Iqbal, K. Kinases and phosphatases and tau sites involved in Alzheimer neurofibrillary degeneration. *Eur J Neurosci* 2007, 25, 59-68.
34. Blennow, K.; de Leon, M. J.; Zetterberg, H. Alzheimer's disease. *Lancet* 2006, 368, 387-403.
35. Sultana, R.; Perluigi, M.; Butterfield, D. A. Protein Oxidation and Lipid Peroxidation in Brain of Subjects with Alzheimer's Disease: Insights into Mechanism of Neurodegeneration from Redox Proteomics. *Antioxid Redox Signaling* 2006, 8, 2021-2037.

36. Liu, Q.; Xie, F.; Rolston, R.; Moreira, P. I.; Nunomura, A.; Zhu, X.; Smith, M. A.; Perry, G. Prevention and treatment of Alzheimer disease and aging: antioxidants. *Min Rev Med Chem* 2007, 7, 171-180.
37. Brewer, G. J. Iron and Copper Toxicity in Diseases of Aging, Particularly Atherosclerosis and Alzheimer's Disease. *Exp. Biol. Med.* 2007, 232, 323-335.
38. El Khoury, J.; Toft, M.; Hickman, S. E.; Means, T. K.; Terada, K.; Geula, C.; Luster, A. D. Ccr2 deficiency impairs microglial accumulation and accelerates progression of Alzheimer-like disease. *Nat Med* 2007, 13, 432-438.
39. Piehl, F. Inflammation and neurodegeneration. *Future Neurol* 2006, 1, 97-105.
40. Fambrough, D.; Pan, D.; Rubin, G. M.; Goodman, C. S. The cell surface metalloprotease/disintegrin Kuzbanian is required for axonal extension in *Drosophila*. *PNAS* 1996, 93, 13233-13238.
41. Rooke, J.; Pan, D.; Xu, T.; Rubin, G. M. KUZ, a Conserved Metalloprotease-Disintegrin Protein with Two Roles in *Drosophila* Neurogenesis. *Science* 1996, 273, 1227-1231.
42. Thathiah, A.; De Strooper, B. The role of G protein-coupled receptors in the pathology of Alzheimer's disease. *Nat Rev Neurosci* 2011, 12, 73-87.
43. Postina, R. A closer look at alpha-secretase. *Curr Alzheimer Res* 2008, 5, 179-186.
44. Bandyopadhyay, S.; Goldstein, L. E.; Lahiri, D. K.; Rogers, J. T. Role of the APP non-amyloidogenic signalling pathway and targeting alpha-secretase as an alternative drug target for treatment of Alzheimer's disease. *Curr Med Chem* 2007, 14, 2848-2864.
45. Vassar, R.; Bennett, B. D.; Babu-Khan, S.; Kahn, S.; Mendiaz, E. A.; Denis, P.; Teplow, D. B.; Ross, S.; Amarante, P.; Loeloff, R.; Luo, Y.; Fisher, S.; Fuller, J.; Edenson, S.; Lile, J.; Jarosinski, M. A.; Biere, A. L.; Curran, E.; Burgess, T.; Louis, J.-C.; Collins, F.; Treanor, J.; Rogers, G.; Citron, M. β -Secretase Cleavage of Alzheimer's Amyloid Precursor Protein by the Transmembrane Aspartic Protease BACE. *Science* 1999, 286, 735-741.
46. Vassar, R. [beta]-Secretase (BACE) as a drug target for alzheimer's disease. *Adv Drug Deliv Rev* 2002, 54, 1589-1602.
47. Citron, M. [beta]-Secretase inhibition for the treatment of Alzheimer's disease - promise and challenge. *Trends Pharmacol Sci* 2004, 25, 92-97.
48. Luo, Y.; Bolon, B.; Kahn, S.; Bennett, B. D.; Babu-Khan, S.; Denis, P.; Fan, W.; Kha, H.; Zhang, J.; Gong, Y.; Martin, L.; Louis, J.-C.; Yan, Q.; Richards, W. G.; Citron, M.; Vassar, R. Mice deficient in BACE1, the Alzheimer's [beta]-secretase, have normal phenotype and abolished [beta]-amyloid generation. *Nat Neurosci* 2001, 4, 231-232.
49. Weggen, S.; Eriksen, J. L.; Das, P.; Sagi, S. A.; Wang, R.; Pietrzik, C. U.; Findlay, K. A.; Smith, T. E.; Murphy, M. P.; Bulter, T.; Kang, D. E.; Marquez-Sterling, N.; Golde, T. E.; Koo, E. H. A subset of NSAIDs lower amyloidogenic A[beta]42 independently of cyclooxygenase activity. *Nature* 2001, 414, 212-216.
50. Walsh, D. M.; Selkoe, D. J. A β Oligomers – a decade of discovery. *J Neurochem* 2007, 101, 1172-1184.
51. Gervais, F.; Paquette, J.; Morissette, C.; Krzykowski, P.; Yu, M.; Azzi, M.; Lacombe, D.; Kong, X.; Aman, A.; Laurin, J.; Szarek, W. A.; Tremblay, P. Targeting soluble A β peptide with Tramiprosate for the treatment of brain amyloidosis. *Neurobiol aging* 2007, 28, 537-547.
52. Aisen, P. A.; Mehran, M.; Poole, R.; Lavoie, I.; Gervais, F.; Briand, R.; Garceau, D. O1-05-06 Clinical data on AlzhemedTM after 12 months of treatment in patients with mild to moderate Alzheimer's disease. *Neurobiol aging* 2004, 25, S20.

53. McLaurin, J.; Kierstead, M. E.; Brown, M. E.; Hawkes, C. A.; Lambermon, M. H. L.; Phinney, A. L.; Darabie, A. A.; Cousins, J. E.; French, J. E.; Lan, M. F.; Chen, F.; Wong, S. S. N.; Mount, H. T. J.; Fraser, P. E.; Westaway, D.; George-Hyslop, P. S. Cyclohexanehexol inhibitors of A[β] aggregation prevent and reverse Alzheimer phenotype in a mouse model. *Nat Med* 2006, 12, 801-808.
54. Frederickson, C. J.; Koh, J.-Y.; Bush, A. I. The neurobiology of zinc in health and disease. *Nat Rev Neurosci* 2005, 6, 449-462.
55. Cherny, R. A.; Atwood, C. S.; Xilinas, M. E.; Gray, D. N.; Jones, W. D.; McLean, C. A.; Barnham, K. J.; Volitakis, I.; Fraser, F. W.; Kim, Y.-S.; Huang, X.; Goldstein, L. E.; Moir, R. D.; Lim, J. T.; Beyreuther, K.; Zheng, H.; Tanzi, R. E.; Masters, C. L.; Bush, A. I. Treatment with a Copper-Zinc Chelator Markedly and Rapidly Inhibits β -Amyloid Accumulation in Alzheimer's Disease Transgenic Mice. *Neuron* 2001, 30, 665-676.
56. Lannfelt, L.; Blennow, K.; Zetterberg, H.; Batsman, S.; Ames, D.; Harrison, J.; Masters, C. L.; Targum, S.; Bush, A. I.; Murdoch, R.; Wilson, J.; Ritchie, C. W. Safety, efficacy, and biomarker findings of PBT2 in targeting A β as a modifying therapy for Alzheimer's disease: a phase IIa, double-blind, randomised, placebo-controlled trial. *Lancet Neurol* 2008, 7, 779-786.
57. Eckman, E. A.; Eckman, C. B. A β -degrading enzymes: modulators of Alzheimer's disease pathogenesis and targets for therapeutic intervention. *Biochem Soc Trans* 2005, 33, 1101-1105.
58. Jacobsen, J. S.; Comery, T. A.; Martone, R. L.; Elokdah, H.; Crandall, D. L.; Oganessian, A.; Aschmies, S.; Kirksey, Y.; Gonzales, C.; Xu, J.; Zhou, H.; Atchison, K.; Wagner, E.; Zaleska, M. M.; Das, I.; Arias, R. L.; Bard, J.; Riddell, D.; Gardell, S. J.; Abou-Gharbia, M.; Robichaud, A.; Magolda, R.; Vlasuk, G. P.; Bjornsson, T.; Reinhart, P. H.; Pangalos, M. N. Enhanced clearance of A β in brain by sustaining the plasmin proteolysis cascade. *PNAS* 2008, 105, 8754-8759.
59. Deane, R.; Wu, Z.; Zlokovic, B. V. RAGE (Yin) Versus LRP (Yang) Balance Regulates Alzheimer Amyloid β -Peptide Clearance Through Transport Across the Blood-Brain Barrier. *Stroke* 2004, 35, 2628-2631.
60. Dodel, R.; Hampel, H.; Depboylu, C.; Lin, S.; Gao, F.; Schock, S.; Jäckel, S.; Wei, X.; Buerger, K.; Höft, C.; Hemmer, B.; Möller, H.-J.; Farlow, M.; Oertel, W. H.; Sommer, N.; Du, Y. Human antibodies against amyloid β peptide: A potential treatment for Alzheimer's disease. *Ann Neurol* 2002, 52, 253-256.
61. Schenk, D.; Barbour, R.; Dunn, W.; Gordon, G.; Grajeda, H.; Guido, T.; Hu, K.; Huang, J.; Johnson-Wood, K.; Khan, K.; Kholodenko, D.; Lee, M.; Liao, Z.; Lieberburg, I.; Motter, R.; Mutter, L.; Soriano, F.; Shopp, G.; Vasquez, N.; Vandeventer, C.; Walker, S.; Wogulis, M.; Yednock, T.; Games, D.; Seubert, P. Immunization with amyloid- β attenuates Alzheimer-disease-like pathology in the PDAPP mouse. *Nature* 1999, 400, 173-177.
62. Morgan, D.; Diamond, D. M.; Gottschall, P. E.; Ugen, K. E.; Dickey, C.; Hardy, J.; Duff, K.; Jantzen, P.; DiCarlo, G.; Wilcock, D.; Connor, K.; Hatcher, J.; Hope, C.; Gordon, M.; Arendash, G. W. A[β] peptide vaccination prevents memory loss in an animal model of Alzheimer's disease. *Nature* 2000, 408, 982-985.
63. Janus, C.; Pearson, J.; McLaurin, J.; Mathews, P. M.; Jiang, Y.; Schmidt, S. D.; Chishti, M. A.; Horne, P.; Heslin, D.; French, J.; Mount, H. T. J.; Nixon, R. A.; Mercken, M.; Bergeron, C.; Fraser, P. E.; St George-Hyslop, P.; Westaway, D. A[β] peptide immunization reduces behavioural impairment and plaques in a model of Alzheimer's disease. *Nature* 2000, 408, 979-982.
64. Hrcic, R.; Wall, J.; Wolfenbarger, D. A.; Murphy, C. L.; Schell, M.; Weiss, D. T.; Solomon, A. Antibody-Mediated Resolution of Light Chain-Associated Amyloid Deposits. *Am J Pathol* 2000, 157, 1239-1246.
65. Bard, F.; Cannon, C.; Barbour, R.; Burke, R.-L.; Games, D.; Grajeda, H.; Guido, T.; Hu, K.; Huang, J.; Johnson-Wood, K.; Khan, K.; Kholodenko, D.; Lee, M.; Lieberburg, I.; Motter, R.; Nguyen, M.; Soriano, F.;

- Vasquez, N.; Weiss, K.; Welch, B.; Seubert, P.; Schenk, D.; Yednock, T. Peripherally administered antibodies against amyloid [beta]-peptide enter the central nervous system and reduce pathology in a mouse model of Alzheimer disease. *Nat Med* 2000, 6, 916-919.
66. Frenkel, D.; Katz, O.; Solomon, B. Immunization against Alzheimer's β -amyloid plaques via EFRH phage administration. *PNAS* 2000, 97, 11455-11459.
 67. Thal, D. R.; Holzer, M.; Rüb, U.; Waldmann, G.; Günzel, S.; Zedlick, D.; Schober, R. Alzheimer-Related [tau]-Pathology in the Perforant Path Target Zone and in the Hippocampal Stratum Oriens and Radiatum Correlates with Onset and Degree of Dementia. *Exp Neurol* 2000, 163, 98-110.
 68. Bulic, B.; Pickhardt, M.; Schmidt, B.; Mandelkow, E.-M.; Waldmann, H.; Mandelkow, E. Development of Tau Aggregation Inhibitors for Alzheimer's Disease. *Angew Chem Int Ed* 2009, 48, 1740-1752.
 69. McGeer, P. L.; McGeer, E. G. NSAIDs and Alzheimer disease: Epidemiological, animal model and clinical studies. *Neurobiol Aging* 2007, 28, 639-647.
 70. Heneka, M. T.; Landreth, G. E. PPARs in the brain. *Biochim Biophys Acta* 2007, 1771, 1031-1045.
 71. Wyss-Coray, T. Inflammation in Alzheimer disease: driving force, bystander or beneficial response? *Nat Med* 2006, 12, 1005-1015.
 72. Mahley, R. W. Apolipoprotein E: cholesterol transport protein with expanding role in cell biology. *Science* 1988, 240, 622-630.
 73. Bertram, L.; Tanzi, R. E. Thirty years of Alzheimer's disease genetics: the implications of systematic meta-analyses. *Nat Rev Neurosci* 2008, 9, 768-778.
 74. Mahley, R. W.; Weisgraber, K. H.; Huang, Y. Apolipoprotein E4: A causative factor and therapeutic target in neuropathology, including Alzheimer's disease. *PNAS* 2006, 103, 5644-5651.
 75. Fagan, A. M.; Watson, M.; Parsadanian, M.; Bales, K. R.; Paul, S. M.; Holtzman, D. M. Human and Murine ApoE Markedly Alters A[beta] Metabolism before and after Plaque Formation in a Mouse Model of Alzheimer's Disease. *Neurobiol Dis* 2002, 9, 305-318.
 76. Cao, G.; Bales, K. R.; DeMattos, R. B.; Paul, S. M. Liver X receptor- mediated gene regulation and cholesterol homeostasis in brain: relevance to Alzheimer's disease therapeutics. *Curr Alzheimer Res* 2007, 4, 179-184.
 77. Mullan, M.; Houlden, H.; Windelspecht, M.; Fidani, L.; Lombardi, C.; Diaz, P.; Rossor, M.; Crook, R.; Hardy, J.; Duff, K.; Crawford, F. A locus for familial early-onset Alzheimer's disease on the long arm of chromosome 14, proximal to the [alpha]1-antichymotrypsin gene. *Nat Genet* 1992, 2, 340-342.
 78. Haass, C.; Lemere, C. A.; Capell, A.; Citron, M.; Seubert, P.; Schenk, D.; Lannfelt, L.; Selkoe, D. J. The Swedish mutation causes early-onset Alzheimer's disease by [beta]-secretase cleavage within the secretory pathway. *Nat Med* 1995, 1, 1291-1296.
 79. Sinha, S.; Anderson, J. P.; Barbour, R.; Basi, G. S.; Caccavello, R.; Davis, D.; Doan, M.; Dovey, H. F.; Frigon, N.; Hong, J.; Jacobson-Croak, K.; Jewett, N.; Keim, P.; Knops, J.; Lieberburg, I.; Power, M.; Tan, H.; Tatsuno, G.; Tung, J.; Schenk, D.; Seubert, P.; Suomensaaari, S. M.; Wang, S.; Walker, D.; Zhao, J.; McConlogue, L.; John, V. Purification and cloning of amyloid precursor protein [beta]-secretase from human brain. *Nature* 1999, 402, 537-540.
 80. Yan, R.; Bienkowski, M. J.; Shuck, M. E.; Miao, H.; Tory, M. C.; Pauley, A. M.; Brashler, J. R.; Stratman, N. C.; Mathews, W. R.; Buhl, A. E.; Carter, D. B.; Tomasselli, A. G.; Parodi, L. A.; Heinrikson, R. L.; Gurney, M. E. Membrane-anchored aspartyl protease with Alzheimer's disease [beta]-secretase activity. *Nature* 1999, 402, 533-537.

81. Hussain, I.; Powell, D.; Howlett, D. R.; Tew, D. G.; Meek, T. D.; Chapman, C.; Gloger, I. S.; Murphy, K. E.; Southan, C. D.; Ryan, D. M.; Smith, T. S.; Simmons, D. L.; Walsh, F. S.; Dingwall, C.; Christie, G. Identification of a Novel Aspartic Protease (Asp 2) as [beta]-Secretase. *Mol Cell Neurosci* 1999, 14, 419-427.
82. Lin, X.; Koelsch, G.; Wu, S.; Downs, D.; Dashti, A.; Tang, J. Human aspartic protease memapsin 2 cleaves the β -secretase site of β -amyloid precursor protein. *PNAS* 2000, 97, 1456-1460.
83. Saunders, A. J.; Kim, T.-W.; Tanzi, R. E. BACE Maps to Chromosome 11 and a BACE Homolog, BACE2, Reside in the Obligate Down Syndrome Region of Chromosome 21. *Science* 1999, 286, 1255.
84. Bennett, B. D.; Babu-Khan, S.; Loeloff, R.; Louis, J.-C.; Curran, E.; Citron, M.; Vassar, R. Expression Analysis of BACE2 in Brain and Peripheral Tissues. *J Biol Chem* 2000, 275, 20647-20651.
85. Gruninger-Leitch, F.; Schlatter, D.; Kung, E.; Nelbock, P.; Dobeli, H. Substrate and Inhibitor Profile of BACE (beta -Secretase) and Comparison with Other Mammalian Aspartic Proteases. *J Biol Chem* 2002, 277, 4687-4693.
86. Haass, C.; Hung, A. Y.; Schlossmacher, M. G.; Oltersdorf, T.; Teplow, D. B.; Selkoe, D. J. Normal Cellular Processing of the β -Amyloid Precursor Protein Results in the Secretion of the Amyloid β Peptide and Related Molecules. *Ann N Y Acad Sci* 1993, 695, 109-116.
87. Koo, E. H.; Squazzo, S. L. Evidence that production and release of amyloid beta-protein involves the endocytic pathway. *J Biol Chem* 1994, 269, 17386-17389.
88. Roberds, S. L.; Anderson, J.; Basi, G.; Bienkowski, M. J.; Branstetter, D. G.; Chen, K. S.; Freedman, S.; Frigon, N. L.; Games, D.; Hu, K.; Johnson-Wood, K.; Kappenman, K. E.; Kawabe, T. T.; Kola, I.; Kuehn, R.; Lee, M.; Liu, W.; Motter, R.; Nichols, N. F.; Power, M.; Robertson, D. W.; Schenk, D.; Schoor, M.; Shopp, G. M.; Shuck, M. E.; Sinha, S.; Svensson, K. A.; Tatsuno, G.; Tintrup, H.; Wijsman, J.; Wright, S.; McConlogue, L. BACE knockout mice are healthy despite lacking the primary β -secretase activity in brain: implications for Alzheimer's disease therapeutics. *Hum Mol Genet* 2001, 10, 1317-1324.
89. Cai, H.; Wang, Y.; McCarthy, D.; Wen, H.; Borchelt, D. R.; Price, D. L.; Wong, P. C. BACE1 is the major [beta]-secretase for generation of A[beta] peptides by neurons. *Nat Neurosci* 2001, 4, 233-234.
90. Fischer, F.; Molinari, M.; Bodendorf, U.; Paganetti, P. The disulphide bonds in the catalytic domain of BACE are critical but not essential for amyloid precursor protein processing activity. *J Neurochem* 2002, 80, 1079-1088.
91. Shi, J.; Zhang, S.; Tang, M.; Liu, X.; Li, T.; Wang, Y.; Han, H.; Guo, Y.; Hao, Y.; Zheng, K.; Kong, X.; Su, Z.; Tong, Y.; Ma, C. The 1239G/C polymorphism in exon 5 of BACE1 gene may be associated with sporadic Alzheimer's disease in Chinese Hans. *Am J Med Genet B Neuropsychiatr Genet* 2004, 124B, 54-57.
92. Capell, A.; Steiner, H.; Willem, M.; Kaiser, H.; Meyer, C.; Walter, J.; Lammich, S.; Multhaup, G.; Haass, C. Maturation and Pro-peptide Cleavage of β -Secretase. *J Biol Chem* 2000, 275, 30849-30854.
93. Benjannet, S.; Elagoz, A.; Wickham, L.; Mamarbachi, M.; Munzer, J. S.; Basak, A.; Lazure, C.; Cromlish, J. A.; Sisodia, S.; Checler, F.; Chrétien, M.; Seidah, N. G. Post-translational Processing of β -Secretase (β -Amyloid-converting Enzyme) and Its Ectodomain Shedding. *J Biol Chem* 2001, 276, 10879-10887.
94. Charlwood, J.; Dingwall, C.; Matico, R.; Hussain, I.; Johanson, K.; Moore, S.; Powell, D. J.; Skehel, J. M.; Ratcliffe, S.; Clarke, B.; Trill, J.; Sweitzer, S.; Camilleri, P. Characterization of the Glycosylation Profiles of Alzheimer's β -Secretase Protein Asp-2 Expressed in a Variety of Cell Lines. *J Biol Chem* 2001, 276, 16739-16748.

95. Huse, J. T.; Pijak, D. S.; Leslie, G. J.; Lee, V. M. Y.; Doms, R. W. Maturation and Endosomal Targeting of β -Site Amyloid Precursor Protein-cleaving Enzyme. *J Biol Chem* 2000, 275, 33729-33737.
96. Patel, S.; Vuillard, L.; Cleasby, A.; Murray, C. W.; Yon, J. Apo and Inhibitor Complex Structures of BACE ([beta]-secretase). *J Mol Biol* 2004, 343, 407-416.
97. Hong, L.; Tang, J. Flap Position of Free Memapsin 2 (β -Secretase), a Model for Flap Opening in Aspartic Protease Catalysis. *Biochemistry* 2004, 43, 4689-4695.
98. Hong, L.; Turner, R. T.; Koelsch, G.; Shin, D.; Ghosh, A. K.; Tang, J. Crystal Structure of Memapsin 2 (beta-Secretase) in Complex with an Inhibitor OM00-3. *Biochemistry* 2002, 41, 10963-10967.
99. Turner, R. T.; Hong, L.; Koelsch, G.; Ghosh, A. K.; Tang, J. Structural Locations and Functional Roles of New Subsites S5, S6, and S7 in Memapsin 2 (β -Secretase). *Biochemistry* 2005, 44, 105-112.
100. Hong, L.; Koelsch, G.; Lin, X.; Wu, S.; Terzyan, S.; Ghosh, A. K.; Zhang, X. C.; Tang, J. Structure of the Protease Domain of Memapsin 2 (beta-Secretase) Complexed with Inhibitor. *Science* 2000, 290, 150-153.
101. Ostermann, N.; Eder, J.; Eidhoff, U.; Zink, F.; Hassiepen, U.; Worpenberg, S.; Maibaum, J.; Simic, O.; Hommel, U.; Gerhartz, B. Crystal Structure of Human BACE2 in Complex with a Hydroxyethylamine Transition-state Inhibitor. *J Mol Biol* 2006, 355, 249-261.
102. Turner, R. T.; Koelsch, G.; Hong, L.; Castenheira, P.; Ghosh, A.; Tang, J. Subsite Specificity of Memapsin 2 (β -Secretase): Implications for Inhibitor Design. *Biochemistry* 2001, 40, 10001-10006.
103. Gorfe, A. A.; Cafflish, A. Functional Plasticity in the Substrate Binding Site of β -Secretase. *Structure* 2005, 13, 1487-1498.
104. Fujinaga, M.; Chernai, M. M.; Mosimann, S. C.; James, M. N. G.; Tarasova, N. I. Crystal structure of human pepsin and its complex with pepstatin. *Protein Sci* 1995, 4, 960-972.
105. Ghosh, A. K.; Kumaragurubaran, N.; Hong, L.; Koelsch, G.; Tang, J. Memapsin 2 (Beta-Secretase) Inhibitors: Drug Development. *Curr Alzheimer Res* 2008, 5, 121-131.
106. Hu, X.; Hicks, C. W.; He, W.; Wong, P.; Macklin, W. B.; Trapp, B. D.; Yan, R. Bace 1 modulates myelination in the central and peripheral nervous system. *Nat Neurosci* 2006, 9, 1520-1525.
107. Willem, M.; Garratt, A. N.; Novak, B.; Citron, M.; Kaufmann, S.; Rittger, A.; DeStrooper, B.; Saftig, P.; Birchmeier, C.; Haass, C. Control of Peripheral Nerve Myelination by the β -Secretase BACE1. *Science* 2006, 314, 664-666.
108. Savonenko, A. V.; Melnikova, T.; Laird, F. M.; Stewart, K. A.; Price, D. L.; Wong, P. C. Alteration of BACE1-dependent NRG1/ErbB4 signaling and schizophrenia-like phenotypes in BACE1-null mice. *PNAS* 2008, 105, 5585-5590.
109. De Strooper, B.; Vassar, R.; Golde, T. The secretases: enzymes with therapeutic potential in Alzheimer disease. *Nat Rev Neurol* 2010, 6, 99-107.
110. De Strooper, B.; Saftig, P.; Craessaerts, K.; Vanderstichele, H.; Guhde, G.; Annaert, W.; Von Figura, K.; Van Leuven, F. Deficiency of presenilin-1 inhibits the normal cleavage of amyloid precursor protein. *Nature* 1998, 391, 387-390.
111. Li, J.; Fici, G. J.; Mao, C.-A.; Myers, R. L.; Shuang, R.; Donoho, G. P.; Pauley, A. M.; Himes, C. S.; Qin, W.; Kola, I.; Merchant, K. M.; Nye, J. S. Positive and Negative Regulation of the γ -Secretase Activity by Nicastrin in a Murine Model. *J Biol Chem* 2003, 278, 33445-33449.
112. Ma, G.; Li, T.; Price, D. L.; Wong, P. C. APH-1a Is the Principal Mammalian APH-1 Isoform Present in β -Secretase Complexes during Embryonic Development. *J Neurosci* 2005, 25, 192-198.

113. Kopan, R.; Turner, D. L. The Notch pathway: democracy and aristocracy in the selection of cell fate. *Curr Opin Neurobiol* 1996, 6, 594-601.
114. Wolfe, M. S. Gamma-secretase: structure, function, and modulation for Alzheimer's disease. *Curr Top Med Chem* 2008, 8, 2-8.
115. Sisodia, S. S.; St George-Hyslop, P. H. [gamma]-Secretase, notch, A[beta] and alzheimer's disease: Where do the presenilins fit in? *Nat Rev Neurosci* 2002, 3, 281-290.
116. Dominguez, D.; Tournoy, J.; Hartmann, D.; Huth, T.; Cryns, K.; Deforce, S.; Serneels, L.; Camacho, I. E.; Marjaux, E.; Craessaerts, K.; Roebroek, A. J. M.; Schwake, M.; D'Hooge, R.; Bach, P.; Kalinke, U.; Moechars, D.; Alzheimer, C.; Reiss, K.; Saftig, P.; De Strooper, B. Phenotypic and Biochemical Analyses of BACE1- and BACE2-deficient Mice. *J Biol Chem* 2005, 280, 30797-30806.
117. Shuto D; Kasai S; Kimura T; Liu P; Hidaka K; Hamada T; Shibakawa S; Hayashi Y; Hattori C; Szabo B; S, I.; Y, K. KMI-008, a novel beta-Secretase inhibitor containing a hydroxymethylcarbonyl isostere as a transition-State mimic: design and synthesis of substrate-based octapeptides. *Bioorg Med Chem Lett* 2003, 13, 4273-4276.
118. Kimura, T.; Shuto, D.; Hamada, Y.; Igawa, N.; Kasai, S.; Liu, P.; Hidaka, K.; Hamada, T.; Hayashi, Y.; Kiso, Y. Design and synthesis of highly active Alzheimer's [beta]-secretase (BACE1) inhibitors, KMI-420 and KMI-429, with enhanced chemical stability. *Bioorg Med Chem Lett* 2005, 15, 211-215.
119. Asai, M.; Hattori, C.; Iwata, N.; Saido, T. C.; Sasagawa, N.; Szabó, B.; Hashimoto, Y.; Maruyama, K.; Tanuma, S.-i.; Kiso, Y.; Ishiura, S. The novel β -secretase inhibitor KMI-429 reduces amyloid β peptide production in amyloid precursor protein transgenic and wild-type mice. *J Neurochem* 2006, 96, 533-540.
120. D.S., W.-P. Animal Models of Alzheimer's Disease: Therapeutic Implications. *J Alzheimers Dis* 2008, 15, 507-521.
121. Hu, J.; Cwi, C. L.; Smiley, D. L.; Timm, D.; Erickson, J. A.; McGee, J. E.; Yang, H.-C.; Mendel, D.; May, P. C.; Shapiro, M.; McCarthy, J. R. Design and synthesis of statine-Containing BACE inhibitors. *Bioorg Med Chem Lett* 2003, 13, 4335-4339.
122. Tung, J. S.; Davis, D. L.; Anderson, J. P.; Walker, D. E.; Mamo, S.; Jewett, N.; Hom, R. K.; Sinha, S.; Thorsett, E. D.; John, V. Design of Substrate-Based Inhibitors of Human β -Secretase. *J Med Chem* 2001, 45, 259-262.
123. Huang Wen-Hai; Sheng Rong ; Yong-Zhou, H. Progress in the Development of Nonpeptidomimetic BACE 1 Inhibitors for Alzheimers Disease. *Curr Med Chem* 2009, 16, 1806-1820.
124. Ghosh, A. K.; Kumaragurubaran, N.; Hong, L.; Kulkarni, S. S.; Xu, X.; Chang, W.; Weerasena, V.; Turner, R.; Koelsch, G.; Bilcer, G.; Tang, J. Design, Synthesis, and X-ray Structure of Potent Memapsin 2 (β -Secretase) Inhibitors with Isophthalamide Derivatives as the P2-P3-Ligands. *J Med Chem* 2007, 50, 2399-2407.
125. Ghosh, A. K.; Kumaragurubaran, N.; Hong, L.; Kulkarni, S.; Xu, X.; Miller, H. B.; Srinivasa Reddy, D.; Weerasena, V.; Turner, R.; Chang, W.; Koelsch, G.; Tang, J. Potent memapsin 2 ([beta]-secretase) inhibitors: Design, synthesis, protein-ligand X-ray structure, and in vivo evaluation. *Bioorg Med Chem Lett* 2008, 18, 1031-1036.
126. Kimura, T.; Hamada, Y.; Stochaj, M.; Ikari, H.; Nagamine, A.; Abdel-Rahman, H.; Igawa, N.; Hidaka, K.; Nguyen, J.-T.; Saito, K.; Hayashi, Y.; Kiso, Y. Design and synthesis of potent [beta]-secretase (BACE1) inhibitors with carboxylic acid bioisosteres. *Bioorg Med Chem Lett* 2006, 16, 2380-2386.

127. Hussain, I.; Hawkins, J.; Harrison, D.; Hille, C.; Wayne, G.; Cutler, L.; Buck, T.; Walter, D.; Demont, E.; Howes, C.; Naylor, A.; Jeffrey, P.; Gonzalez, M. I.; Dingwall, C.; Michel, A.; Redshaw, S.; Davis, J. B. Oral administration of a potent and selective non-peptidic BACE-1 inhibitor decreases β -cleavage of amyloid precursor protein and amyloid- β production in vivo. *J Neurochem* 2007, 100, 802-809.
128. Iserloh, U.; Pan, J.; Stamford, A. W.; Kennedy, M. E.; Zhang, Q.; Zhang, L.; Parker, E. M.; McHugh, N. A.; Favreau, L.; Strickland, C.; Voigt, J. Discovery of an orally efficacious 4-phenoxyproline-based BACE-1 inhibitor. *Bioorg Med Chem Lett* 2008, 18, 418-422.
129. Miyamoto, M.; Matsui, J.; Fukumoto, H.; Tarui, N. Preparation of 2-[2-amino- or 2-(N-heterocyclyl) ethyl]-6-(4-biphenylmethoxy)tetralin derivatives as β -secretase inhibitors. *PCT Int Appl WO2001087293A1* 2001.
130. Cole, D. C.; Manas, E. S.; Stock, J. R.; Condon, J. S.; Jennings, L. D.; Aulabaugh, A.; Chopra, R.; Cowling, R.; Ellingboe, J. W.; Fan, K. Y.; Harrison, B. L.; Hu, Y.; Jacobsen, S.; Jin, G.; Lin, L.; Lovering, F. E.; Malamas, M. S.; Stahl, M. L.; Strand, J.; Sukhdeo, M. N.; Svenson, K.; Turner, M. J.; Wagner, E.; Wu, J.; Zhou, P.; Bard, J. Acylguanidines as Small-Molecule β -Secretase Inhibitors. *J Med Chem* 2006, 49, 6158-6161.
131. Baxter, E. W.; Conway, K. A.; Kennis, L.; Bischoff, F. o.; Mercken, M. H.; De Winter, H. L.; Reynolds, C. H.; Tounge, B. A.; Luo, C.; Scott, M. K.; Huang, Y.; Braeken, M.; Pieters, S. M. A.; Berthelot, D. J. C.; Masure, S.; Bruinzeel, W. D.; Jordan, A. D.; Parker, M. H.; Boyd, R. E.; Qu, J.; Alexander, R. S.; Brenneman, D. E.; Reitz, A. B. 2-Amino-3,4-dihydroquinazolines as Inhibitors of BACE-1 (beta-Site APP Cleaving Enzyme): Use of Structure Based Design to Convert a Micromolar Hit into a Nanomolar Lead. *J Med Chem* 2007, 50, 4261-4264.
132. Geschwindner, S.; Olsson, L.-L.; Albert, J. S.; Deinum, J.; Edwards, P. D.; de Beer, T.; Folmer, R. H. A. Discovery of a Novel Warhead against β -Secretase through Fragment-Based Lead Generation. *J Med Chem* 2007, 50, 5903-5911.
133. Edwards, P. D.; Albert, J. S.; Sylvester, M.; Aharony, D.; Andisik, D.; Callaghan, O.; Campbell, J. B.; Carr, R. A.; Chessari, G.; Congreve, M.; Frederickson, M.; Folmer, R. H. A.; Geschwindner, S.; Koether, G.; Kolmodin, K.; Krumrine, J.; Mauger, R. C.; Murray, C. W.; Olsson, L.-L.; Patel, S.; Spear, N.; Tian, G. Application of Fragment-Based Lead Generation to the Discovery of Novel, Cyclic Amidine beta-Secretase Inhibitors with Nanomolar Potency, Cellular Activity, and High Ligand Efficiency. *J Med Chem* 2007, 50, 5912-5925.
134. Congreve, M.; Aharony, D.; Albert, J.; Callaghan, O.; Campbell, J.; Carr, R. A. E.; Chessari, G.; Cowan, S.; Edwards, P. D.; Frederickson, M.; McMenamin, R.; Murray, C. W.; Patel, S.; Wallis, N. Application of Fragment Screening by X-ray Crystallography to the Discovery of Aminopyridines as Inhibitors of β -Secretase. *J Med Chem* 2007, 50, 1124-1132.
135. Huang, D.; Lüthi, U.; Kolb, P.; Edler, K.; Cecchini, M.; Audetat, S.; Barberis, A.; Caflisch, A. Discovery of Cell-Permeable Non-Peptide Inhibitors of β -Secretase by High-Throughput Docking and Continuum Electrostatics Calculations. *J Med Chem* 2005, 48, 5108-5111.
136. Huang, D.; Lüthi, U.; Kolb, P.; Cecchini, M.; Barberis, A.; Caflisch, A. In Silico Discovery of beta-Secretase Inhibitors. *JACS* 2006, 128, 5436-5443.
137. Godemann, R.; Madden, J.; Krämer, J.; Smith, M.; Fritz, U.; Hestekamp, T.; Barker, J.; Höppner, S.; Hallett, D.; Cesura, A.; Ebnet, A.; Kemp, J. Fragment-Based Discovery of BACE1 Inhibitors Using Functional Assays. *Biochemistry* 2009, 48, 10743-10751.

138. Chang, W.-P.; Downs, D.; Huang, X.-P.; Da, H.; Fung, K.-M.; Tang, J. Amyloid-beta reduction by memapsin 2 (beta-secretase) immunization. *FASEB J* 2007, 21, 3184-3196.
139. Rakover, I.; Arbel, M.; Solomon, B. Immunotherapy against APP beta-secretase cleavage site improves cognitive function and reduces neuroinflammation in Tg2576 mice without a significant effect on brain abeta levels. *Neurodegener Dis* 2007, 4, 392-402.
140. Rajendran, L.; Schneider, A.; Schlechtingen, G.; Weidlich, S.; Ries, J.; Braxmeier, T.; Schwille, P.; Schulz, J. B.; Schroeder, C.; Simons, M.; Jennings, G.; Knölker, H.-J.; Simons, K. Efficient Inhibition of the Alzheimer's Disease β -Secretase by Membrane Targeting. *Science* 2008, 320, 520-523.
141. Bolognesi, M. L.; Matera, R.; Minarini, A.; Rosini, M.; Melchiorre, C. Alzheimer's disease: new approaches to drug discovery. *Curr Opin Chem Biol* 2009, 13, 303-308.
142. Michailov, G. V.; Sereda, M. W.; Brinkmann, B. G.; Fischer, T. M.; Haug, B.; Birchmeier, C.; Role, L.; Lai, C.; Schwab, M. H.; Nave, K.-A. Axonal Neuregulin-1 Regulates Myelin Sheath Thickness. *Science* 2004, 304, 700-703.
143. Nave, K.-A.; Salzer, J. L. Axonal regulation of myelination by neuregulin 1. *Curr Opin Neurobiol* 2006, 16, 492-500.
144. Mei, L.; Xiong, W.-C. Neuregulin 1 in neural development, synaptic plasticity and schizophrenia. *Nat Rev Neurosci* 2008, 9, 437-452.
145. Hu, X.; He, W.; Diaconu, C.; Tang, X.; Kidd, G. J.; Macklin, W. B.; Trapp, B. D.; Yan, R. Genetic deletion of BACE1 in mice affects remyelination of sciatic nerves. *FASEB J* 2008, 22, 2970-2980.
146. Kim, D. Y.; Carey, B. W.; Wang, H.; Ingano, L. A. M.; Binshtok, A. M.; Wertz, M. H.; Pettingell, W. H.; He, P.; Lee, V. M. Y.; Woolf, C. J.; Kovacs, D. M. BACE1 regulates voltage-gated sodium channels and neuronal activity. *Nat Cell Biol* 2007, 9, 755-764.
147. Wong, H.-K.; Sakurai, T.; Oyama, F.; Kaneko, K.; Wada, K.; Miyazaki, H.; Kurosawa, M.; De Strooper, B.; Saftig, P.; Nukina, N. β Subunits of Voltage-gated Sodium Channels Are Novel Substrates of β -Site Amyloid Precursor Protein-cleaving Enzyme (BACE1) and γ -Secretase. *J Biol Chem* 2005, 280, 23009-23017.
148. Catterall, W. A. From Ionic Currents to Molecular Mechanisms: The Structure and Function of Voltage-Gated Sodium Channels. *Neuron* 2000, 26, 13-25.
149. Hu, X.; Zhou, X.; He, W.; Yang, J.; Xiong, W.; Wong, P.; Wilson, C. G.; Yan, R. BACE1 Deficiency Causes Altered Neuronal Activity and Neurodegeneration. *J Neurosci* 2010, 30, 8819-8829.
150. Isom, L. L. Beta subunits: players in neuronal hyperexcitability? *Novartis Found Symp* 2002, 241, 124-138.
151. Luo, X.; Yan, R. Inhibition of BACE1 for therapeutic use in Alzheimer's disease. *Int J Clin Exp Pathol* 2010, 3, 618-628.
152. Jones, G.; Willett, P.; Glen, R. C.; Leach, A. R.; Taylor, R. Development and validation of a genetic algorithm for flexible docking. *J Mol Biol* 1997, 267, 727-748.
153. Morris, G. M.; Huey, R.; Lindstrom, W.; Sanner, M. F.; Belew, R. K.; Goodsell, D. S.; Olson, A. J. AutoDock4 and AutoDockTools4: Automated docking with selective receptor flexibility. *J Comput Chem* 2009, 30, 2785-2791.
154. Morris, G. M.; Goodsell, D. S.; Halliday, R. S.; Huey, R.; Hart, W. E.; Belew, R. K.; Olson, A. J. Automated docking using a Lamarckian genetic algorithm and an empirical binding free energy function. *J Comput Chem* 1998, 19, 1639-1662.

155. Jones, G.; Willett, P.; Glen, R. C. Molecular recognition of receptor sites using a genetic algorithm with a description of desolvation. *J Mol Biol* 1995, 245, 43-53.
156. Schulz-Gasch, T.; Stahl, M. Scoring functions for protein-ligand interactions: a critical perspective. *Drug Discov Today Technol* 2004, 1, 231-239.
157. Solis, F. J.; Wets, R. J. B. Minimization by Random Search Techniques. *MOR* 1981, 6, 19-30.
158. Verdonk, M. L.; Cole, J. C.; Hartshorn, M. J.; Murray, C. W.; Taylor, R. D. Improved protein-ligand docking using GOLD. *Proteins* 2003, 52, 609-623.
159. Eldridge, M. D.; Murray, C. W.; Auton, T. R.; Paolini, G. V.; Mee, R. P. Empirical scoring functions: I. The development of a fast empirical scoring function to estimate the binding affinity of ligands in receptor complexes. *J Comput Aided Mol Des* 1997, 11, 425-445.
160. Bottegoni, G.; Cavalli, A.; Recanatini, M. A Comparative Study on the Application of Hierarchical-Agglomerative Clustering Approaches to Organize Outputs of Reiterated Docking Runs. *J Chem Info Model* 2006, 46, 852-862.
161. Bottegoni, G.; Rocchia, W.; Recanatini, M.; Cavalli, A. ACIAP, Autonomous hierarchical agglomerative Cluster Analysis based protocol to partition conformational datasets. *Bioinformatics* 2006, 22, e58-e65.
162. Kelley, L. A.; Gardner, S. P.; Sutcliffe, M. J. An automated approach for defining core atoms and domains in an ensemble of NMR-derived protein structures. *Protein Eng* 1997, 10, 737-741.
163. Kuntz, I. D. Structure-Based Strategies for Drug Design and Discovery. *Science* 1992, 257, 1078-1082.
164. Kitchen, D. B.; Decornez, H.; Furr, J. R.; Bajorath, J. Docking and scoring in virtual screening for drug discovery: methods and applications. *Nat Rev Drug Discov* 2004, 3, 935-949.
165. Willett, P.; Barnard, J. M.; Downs, G. M. Chemical Similarity Searching. *J Chem Inf Comput Sci* 1998, 38, 983-996.
166. Fobare, W. F.; Solvibile, W. R.; Robichaud, A. J.; Malamas, M. S.; Manas, E.; Turner, J.; Hu, Y.; Wagner, E.; Chopra, R.; Cowling, R.; Jin, G.; Bard, J. Thiophene substituted acylguanidines as BACE1 inhibitors. *Bioorg Med Chem Lett* 2007, 17, 5353-5356.
167. Sullivan, J. D.; Giles, R. L.; Looper, R. E. 2-Aminoimidazoles from Leucetta Sponges: Synthesis and Biology of an Important Pharmacophore. *Curr Bioact Compd* 2009, 5, 39-78.
168. Ermolat'ev, D. S.; Bariwal, J. B.; Steenackers, H. P. L.; De Keersmaecker, S. C. J.; Van der Eycken, E. V. Concise and Diversity-Oriented Route toward Polysubstituted 2-Aminoimidazole Alkaloids and Their Analogues. *Angew Chem Int Ed Engl* 2010, 49, 9465-9468.
169. Ermolat'ev, D. S.; Babaev, E. V.; Van der Eycken, E. V. Efficient One-Pot, Two-Step, Microwave-Assisted Procedure for the Synthesis of Polysubstituted 2-Aminoimidazoles. *Org Lett* 2006, 8, 5781-5784.
170. Camps, P.; Formosa, X.; Galdeano, C.; Muñoz-Torrero, D.; Ramírez, L.; Gómez, E.; Isambert, N.; Lavilla, R.; Badia, A.; Clos, M. V.; Bartolini, M.; Mancini, F.; Andrisano, V.; Arce, M. P.; Rodríguez-Franco, M. I.; Huertas, Ó.; Dafni, T.; Luque, F. J. Pyrano[3,2-c]quinoline-6-chlorotacrine Hybrids as a Novel Family of Acetylcholinesterase- and beta-Amyloid-Directed Anti-Alzheimer Compounds. *J Med Chem* 2009, 52, 5365-5379.
171. Hagmann, W. K. The Many Roles for Fluorine in Medicinal Chemistry. *J Med Chem* 2008, 51, 4359-4369.
172. Stachel, S. J.; Coburn, C. A.; Rush, D.; Jones, K. L. G.; Zhu, H.; Rajapakse, H.; Graham, S. L.; Simon, A.; Katharine Holloway, M.; Allison, T. J.; Munshi, S. K.; Espeseth, A. S.; Zuck, P.; Colussi, D.; Wolfe, A.;

- Pietrak, B. L.; Lai, M.-T.; Vacca, J. P. Discovery of aminoheterocycles as a novel [beta]-secretase inhibitor class: pH dependence on binding activity part 1. *Bioorg Med Chem Lett* 2009, 19, 2977-2980.
173. Hills, I. D.; Katharine Holloway, M.; de León, P.; Nomland, A.; Zhu, H.; Rajapakse, H.; Allison, T. J.; Munshi, S. K.; Colussi, D.; Pietrak, B. L.; Toolan, D.; Haugabook, S. J.; Graham, S. L.; Stachel, S. J. A conformational constraint improves a [beta]-secretase inhibitor but for an unexpected reason. *Bioorg Med Chem Lett* 2009, 19, 4993-4995.
174. Czvitkovich, S.; Duller, S.; Mathiesen, E.; Lorenzoni, K.; Imbimbo, B.; Hutter-Paier, B.; Windisch, M.; Wronski, R. Comparison of Pharmacological Modulation of APP Metabolism in Primary Chicken Telencephalic Neurons and in a Human Neuroglioma Cell Line. *J Mol Neurosci* 2010, 43, 257-267.
175. Di, L.; Kerns, E. H.; Fan, K.; McConnell, O. J.; Carter, G. T. High throughput artificial membrane permeability assay for blood-brain barrier. *Eur J Med Chem* 2003, 38, 223-232.
176. Xu, W.; Chen, G.; Liew, O. W.; Zuo, Z.; Jiang, H.; Zhu, W. Novel non-peptide [beta]-secretase inhibitors derived from structure-based virtual screening and bioassay. *Bioorg Med Chem Lett* 2009, 19, 3188-3192.
177. Fujimoto, T.; Matsushita, Y.; Gouda, H.; Yamaotsu, N.; Hirono, S. In silico multi-filter screening approaches for developing novel [beta]-secretase inhibitors. *Bioorg Med Chem Lett* 2008, 18, 2771-2775.
178. Pardridge, W. M. Alzheimer's disease drug development and the problem of the blood-brain barrier. *Alzheimer's & dementia* 2009, 5, 427-432.
179. Hopkins, A. L.; Groom, C. R.; Alex, A. Ligand efficiency: a useful metric for lead selection. *Drug Discov Today* 2004, 9, 430-431.
180. Hamada, Y.; Ohta, H.; Miyamoto, N.; Sarma, D.; Hamada, T.; Nakanishi, T.; Yamasaki, M.; Yamani, A.; Ishiura, S.; Kiso, Y. Significance of interactions of BACE1-Arg235 with its ligands and design of BACE1 inhibitors with P2 pyridine scaffold. *Bioorg Med Chem Lett* 2009, 19, 2435-2439.
181. Freskos, J. N.; Fobian, Y. M.; Benson, T. E.; Moon, J. B.; Bienkowski, M. J.; Brown, D. L.; Emmons, T. L.; Heintz, R.; Laborde, A.; McDonald, J. J.; Mischke, B. V.; Molyneaux, J. M.; Mullins, P. B.; Bryan Prince, D.; Paddock, D. J.; Tomasselli, A. G.; Winterrowd, G. Design of potent inhibitors of human [beta]-secretase. Part 2. *Bioorg Med Chem Lett* 2007, 17, 78-81.
182. Wang, Y.-S.; Strickland, C.; Voigt, J. H.; Kennedy, M. E.; Beyer, B. M.; Senior, M. M.; Smith, E. M.; Nechuta, T. L.; Madison, V. S.; Czarniecki, M.; McKittrick, B. A.; Stamford, A. W.; Parker, E. M.; Hunter, J. C.; Greenlee, W. J.; Wyss, D. F. Application of Fragment-Based NMR Screening, X-ray Crystallography, Structure-Based Design, and Focused Chemical Library Design to Identify Novel μ M Leads for the Development of nM BACE-1 (β -Site APP Cleaving Enzyme 1) Inhibitors. *J Med Chem* 2010, 53, 942-950.
183. Cavalli, A.; Bolognesi, M. L.; Minarini, A.; Rosini, M.; Tumiatti, V.; Recanatini, M.; Melchiorre, C. Multi-target-Directed Ligands To Combat Neurodegenerative Diseases. *J Med Chem* 2008, 51, 347-372.
184. Decker, M. Recent advances in the development of hybrid molecules/designed multiple compounds with anti-amnesic properties. *Mini Rev Med Chem* 2007, 7, 221-229.
185. Van der Schyf, C. J.; Geldenhuys, W. J.; Youdim, M. B. H. Multifunctional drugs with different CNS targets for neuropsychiatric disorders. *J Neurochem* 2006, 99, 1033-1048.
186. Youdim, M. B. H.; Buccafusco, J. J. Multi-functional drugs for various CNS targets in the treatment of neurodegenerative disorders. *Trends Pharmacol Sci* 2005, 26, 27-35.
187. Zhang, H.-Y. One-compound-multiple-targets strategy to combat Alzheimer's disease. *FEBS Lett* 2005, 579, 5260-5264.

188. Weinreb, O.; Mandel, S.; Bar-Am, O.; Yogev-Falach, M.; Avramovich-Tirosh, Y.; Amit, T.; Youdim, M. B. H. Multifunctional Neuroprotective Derivatives of Rasagiline as Anti-Alzheimer's Disease Drugs. *Neurotherapeutics* 2009, 6, 163-174.
189. Van der Schyf, C. J.; Geldenhuys, W. J.; Youdim, M. B. H. Multifunctional neuroprotective drugs for the treatment of cognitive and movement impairment disorders, including Alzheimer's and Parkinson's diseases. *Drugs Future* 2006, 31, 447-460.
190. Cavalli, A.; Bolognesi, M. L.; Capsoni, S.; Andrisano, V.; Bartolini, M.; Margotti, E.; Cattaneo, A.; Recanatini, M.; Melchiorre, C. A Small Molecule Targeting the Multifactorial Nature of Alzheimer's Disease. *Angew Chem Int Ed Engl* 2007, 46, 3689-3692.
191. Bolognesi, M. L.; Banzi, R.; Bartolini, M.; Cavalli, A.; Tarozzi, A.; Andrisano, V.; Minarini, A.; Rosini, M.; Tumiatti, V.; Bergamini, C.; Fato, R.; Lenaz, G.; Hrelia, P.; Cattaneo, A.; Recanatini, M.; Melchiorre, C. Novel Class of Quinone-Bearing Polyamines as Multi-Target-Directed Ligands To Combat Alzheimer's Disease. *J Med Chem* 2007, 50, 4882-4897.
192. Bolognesi, M.; Cavalli, A.; Melchiorre, C. Memoquin: A multi-target-directed ligand as an innovative therapeutic opportunity for Alzheimer's disease. *Neurotherapeutics* 2009, 6, 152-162.
193. Portoghese, P. S. The role of concepts in structure-activity relationship studies of opioid ligands. *J Med Chem* 1992, 35, 1927-1937.
194. Pang, Y.-P.; Quiram, P.; Jelacic, T.; Hong, F.; Brimijoin, S. Highly Potent, Selective, and Low Cost Bis-tetrahydroaminacrine Inhibitors of Acetylcholinesterase. *J Biol Chem* 1996, 271, 23646-23649.
195. Castro, A. M., A. Peripheral and dual binding site acetylcholinesterase inhibitors: implications in treatment of Alzheimer's disease. *Min Rev Med Chem* 2001, 1, 267-272.
196. Du, D. M.; Carlier, P. R. Development of bivalent acetylcholinesterase inhibitors as potential therapeutic drugs for Alzheimer's disease. *Curr Pharm Des* 2004, 10, 3141-3156.
197. Munoz-Torrero, D.; Camps, P. Dimeric and hybrid anti-Alzheimer drug candidates. *Curr Med Chem* 2006, 13, 399-422.
198. Haviv, H.; Wong, D. M.; Silman, I.; Sussman, J. L. Bivalent ligands derived from Huperzine A as acetylcholinesterase inhibitors. *Curr Top Med Chem* 2007, 7, 375-387.
199. Bolognesi, M. L. M., A.; Rosini, M.; Tumiatti, V.; Melchiorre, C. From dual binding site acetylcholinesterase inhibitors to multi-target-directed ligands (MTDLs): a step forward in the treatment of Alzheimer's disease. *Min Rev Med Chem* 2008, 8, 960-967.
200. Morphy, R.; Kay, C.; Rankovic, Z. From magic bullets to designed multiple ligands. *Drug Discov Today* 2004, 9, 641-651.
201. Bartolini, M.; Andrisano, V. Strategies for the Inhibition of Protein Aggregation in Human Diseases. *ChemBioChem* 2010, 11, 1018-1035.
202. Reinke, A. A.; Gestwicki, J. E. Insight into Amyloid Structure Using Chemical Probes. *Chem Biol Drug Des* 2011, 77, 399-411.
203. Villaverde, M. C.; González-Louro, L.; F., S. The search for drug leads targeted to the beta-secretase: an example of the roles of computer assisted approaches in drug discovery. *Curr Top Med Chem* 2007, 7, 980-990.

204. Capsoni, S.; Andrisano, V.; Bartolini, M.; Bolognesi, M. L.; Cavalli, A.; Margotti, E.; Melchiorre, C.; Recanatini, M.; Cattaneo, A. Memoquin, a novel multifunctional compound for Alzheimer's disease: An update on preclinical studies. *Alzheimer's & Dementia* 2006, 2, S73-S74.
205. Lipinski, C. A.; Lombardo, F.; Dominy, B. W.; Feeney, P. J. Experimental and computational approaches to estimate solubility and permeability in drug discovery and development settings. *Adv Drug Deliv Rev* 2001, 46, 3-26.
206. Bolognesi, M. L.; Bartolini, M.; Mancini, F.; Chiriano, G.; Ceccarini, L.; Rosini, M.; Milelli, A.; Tumiatti, V.; Andrisano, V.; Melchiorre, C. Bis(7)-tacrine Derivatives as Multitarget-Directed Ligands: Focus on Anticholinesterase and Anti-amyloid Activities. *ChemMedChem* 2010, 5, 1215-1220.
207. Kryger, G.; Harel, M.; Giles, K.; Toker, L.; Velan, B.; Lazar, A.; Kronman, C.; Barak, D.; Ariel, N.; Shafferman, A.; Silman, I.; Sussman, J. L. Structures of recombinant native and E202Q mutant human acetylcholinesterase complexed with the snake-venom toxin fasciculin-II. *Acta Crystallogr D Biol Crystallogr* 2000, 56, 1385-1394.
208. Bartolini, M.; Bertucci, C.; Cavrini, V.; Andrisano, V. beta-Amyloid aggregation induced by human acetylcholinesterase: inhibition studies. *Biochem Pharmacol* 2003, 65, 407-416.
209. Bartolini, M.; Bertucci, C.; Bolognesi, M. L.; Cavalli, A.; Melchiorre, C.; Andrisano, V. Insight Into the Kinetic of Amyloid β (1-42) Peptide Self-Aggregation: Elucidation of Inhibitors' Mechanism of Action. *ChemBioChem* 2007, 8, 2152-2161.
210. Reinke, A. A.; Ung, P. M. U.; Quintero, J. J.; Carlson, H. A.; Gestwicki, J. E. Chemical Probes That Selectively Recognize the Earliest A β Oligomers in Complex Mixtures. *JACS* 2010, 132, 17655-17657.
211. Convertino, M.; Pellarin, R.; Catto, M.; Carotti, A.; Cafilisch, A. 9,10-Anthraquinone hinders β -aggregation: How does a small molecule interfere with A β -peptide amyloid fibrillation? *Protein Sci* 2009, 18, 792-800.
212. Scherzer-Attali, R.; Pellarin, R.; Convertino, M.; Frydman-Marom, A.; Egoz-Matia, N.; Peled, S.; Levy-Sakin, M.; Shalev, D. E.; Cafilisch, A.; Gazit, E.; Segal, D. Complete Phenotypic Recovery of an Alzheimer's Disease Model by a Quinone-Tryptophan Hybrid Aggregation Inhibitor. *PLoS ONE* 2010, 5, e11101.
213. Ortega, A.; Rincón, Á.; Jiménez-Aliaga, K. L.; Bermejo-Bescós, P.; Martín-Aragón, S.; Molina, M. T.; Csáky, A. G. Synthesis and evaluation of arylquinones as BACE1 inhibitors, [beta]-amyloid peptide aggregation inhibitors, and destabilizers of preformed [beta]-amyloid fibrils. *Bioorg Med Chem Lett* 2011, 21, 2183-2187.
214. Coburn, C. A.; Stachel, S. J.; Jones, K. G.; Steele, T. G.; Rush, D. M.; DiMuzio, J.; Pietrak, B. L.; Lai, M.-T.; Huang, Q.; Lineberger, J.; Jin, L.; Munshi, S.; Katharine Holloway, M.; Espeseth, A.; Simon, A.; Hazuda, D.; Graham, S. L.; Vacca, J. P. BACE-1 inhibition by a series of [psi][CH2NH] reduced amide isosteres. *Bioorg Med Chem Lett* 2006, 16, 3635-3638.
215. Bolognesi, M. L.; Bartolini, M.; Tarozzi, A.; Morroni, F.; Lizzi, F.; Milelli, A.; Minarini, A.; Rosini, M.; Hrelia, P.; Andrisano, V.; Melchiorre, C. Multitargeted drugs discovery: Balancing anti-amyloid and anticholinesterase capacity in a single chemical entity. *Bioorg Med Chem Lett* 2011, 21, 2655-2658.
216. Morphy, R.; Rankovic, Z. Fragments, network biology and designing multiple ligands. *Drug Discov Today* 2007, 12, 156-160.
217. Malamas, M. S.; Erdei, J.; Gunawan, I.; Barnes, K.; Johnson, M.; Hui, Y.; Turner, J.; Hu, Y.; Wagner, E.; Fan, K.; Olland, A.; Bard, J.; Robichaud, A. J. Aminoimidazoles as Potent and Selective Human β -Secretase (BACE1) Inhibitors. *J Med Chem* 2009, 52, 6314-6323.

218. Chiriano, G.; Sartini, A.; Mancini, F.; Andrisano, V.; Bolognesi, M. L.; Roberti, M.; Recanatini, M.; Carloni, P.; Cavalli, A. Sequential Virtual Screening Approach to the Identification of Small Organic Molecules as Potential BACE-1 Inhibitors. *Chem Biol Drug Des* 2011, 77, 268-271.
219. Yi Mok, N.; Chadwick, J.; Kellett, K. A. B.; Hooper, N. M.; Johnson, A. P.; Fishwick, C. W. G. Discovery of novel non-peptide inhibitors of BACE-1 using virtual high-throughput screening. *Bioorg Med Chem Lett* 2009, 19, 6770-6774.
220. Wang, J.; Cieplak, P.; Kollman, P. A. How well does a restrained electrostatic potential (RESP) model perform in calculating conformational energies of organic and biological molecules? *J Comput Chem* 2000, 21, 1049-1074.
221. Frisch, M. J. T., G. W.; Schlegel, H. B.; Scuseria, G. E.; Robb, M. A.; Cheeseman, J. R.; Scalmani, G.; Barone, V.; Mennucci, B.; Petersson, G. A.; Nakatsuji, H.; Caricato, M.; Li, X.; Hratchian, H. P.; Izmaylov, A. F.; Bloino, J.; Zheng, G.; Sonnenberg, J. L.; Hada, M.; Ehara, M.; Toyota, K.; Fukuda, R.; Hasegawa, J.; Ishida, M.; Nakajima, T.; Honda, Y.; Kitao, O.; Nakai, H.; Vreven, T.; Montgomery, Jr., J. A.; Peralta, J. E.; Ogliaro, F.; Bearpark, M.; Heyd, J. J.; Brothers, E.; Kudin, K. N.; Staroverov, V. N.; Kobayashi, R.; Normand, J.; Raghavachari, K.; Rendell, A.; Burant, J. C.; Iyengar, S. S.; Tomasi, J.; Cossi, M.; Rega, N.; Millam, N. J.; Klene, M.; Knox, J. E.; Cross, J. B.; Bakken, V.; Adamo, C.; Jaramillo, J.; Gomperts, R.; Stratmann, R. E.; Yazyev, O.; Austin, A. J.; Cammi, R.; Pomelli, C.; Ochterski, J. W.; Martin, R. L.; Morokuma, K.; Zakrzewski, V. G.; Voth, G. A.; Salvador, P.; Dannenberg, J. J.; Dapprich, S.; Daniels, A. D.; Farkas, Ö.; Foresman, J. B.; Ortiz, J. V.; Cioslowski, J.; Fox, D. J. Gaussian 09, Revision A.1. 2009, Gaussian, Inc., Wallingford CT, 2009.
222. Humphrey W; Dalke A; K, S. VMD: visual molecular dynamics. *J Mol Graph* 1996, 14, 33-38.
223. Phillips, J. C.; Braun, R.; Wang, W.; Gumbart, J.; Tajkhorshid, E.; Villa, E.; Chipot, C.; Skeel, R. D.; Kalé, L.; Schulten, K. Scalable molecular dynamics with NAMD. *J Comput Chem* 2005, 26, 1781-1802.
224. Hornak, V.; Abel, R.; Okur, A.; Strockbine, B.; Roitberg, A.; Simmerling, C. Comparison of multiple Amber force fields and development of improved protein backbone parameters. *Proteins* 2006, 65, 712-725.
225. Mahoney, M. W.; Jorgensen, W. L. A five-site model for liquid water and the reproduction of the density anomaly by rigid, nonpolarizable potential functions *J Chem Phys* 2000, 112, 8910-8922.
226. Wang, J.; Wolf, R. M.; Caldwell, J. W.; Kollman, P. A.; Case, D. A. Development and testing of a general amber force field. *J Comput Chem* 2004, 25, 1157-1174.
227. Ryckaert, J.; Ciccotti, G.; Berendsen, H. J. C. Numerical Integration of the Cartesian Equations of Motion of a System with Constraints: Molecular Dynamics of n-Alkanes. *J Comput Phys* 1977, 23, 327-341.
228. Essmann, U.; Perera, L.; Berkowitz, M. L.; Darden, T.; Lee, H.; Pedersen, L. G. A smooth particle mesh Ewald method. *J Chem Phys* 1995, 103, 8577-8593.
229. Park, H.; Lee, S. Determination of the Active Site Protonation State of β -Secretase from Molecular Dynamics Simulation and Docking Experiment: Implications for Structure-Based Inhibitor Design. *JACS* 2003, 125, 16416-16422.
230. Yang, W.; Lu, W.; Lu, Y.; Zhong, M.; Sun, J.; Thomas, A. E.; Wilkinson, J. M.; Fucini, R. V.; Lam, M.; Randal, M.; Shi, X.-P.; Jacobs, J. W.; McDowell, R. S.; Gordon, E. M.; Ballinger, M. D. Aminoethylenes: A Tetrahedral Intermediate Isostere Yielding Potent Inhibitors of the Aspartyl Protease BACE-1. *J Med Chem* 2006, 49, 839-842.

231. Rajapakse, H. A.; Nantermet, P. G.; Selnick, H. G.; Munshi, S.; McGaughey, G. B.; Lindsley, S. R.; Young, M. B.; Lai, M.-T.; Espeseth, A. S.; Shi, X.-P.; Colussi, D.; Pietrak, B.; Crouthamel, M.-C.; Tugusheva, K.; Huang, Q.; Xu, M.; Simon, A. J.; Kuo, L.; Hazuda, D. J.; Graham, S.; Vacca, J. P. Discovery of Oxadiazoyl Tertiary Carbinamine Inhibitors of β -Secretase (BACE-1). *J Med Chem* 2006, 49, 7270-7273.
232. Bourne, Y.; Taylor, P.; Radic, Z.; Marchot, P. Structural insights into ligand interactions at the acetylcholinesterase peripheral anionic site. *EMBO J* 2003, 22, 1-12.
233. Kryger, G.; Silman, I.; Sussman, J. L. Structure of acetylcholinesterase complexed with E2020 (Aricept): implications for the design of new anti-Alzheimer drugs. *Structure* 1999, 7, 297-307.
234. Halgren, T. A. Merck molecular force field. 1-5. *J Comput Chem* 1996, 17, 490-641.
235. Abagyan, R.; Totrov, M. J. Biased probability Monte Carlo conformational searches and electrostatic calculations for peptides and proteins. *J Mol Biol* 1994, 235, 983-1002.
236. Totrov, M.; Abagyan, R. Flexible protein-ligand docking by global energy optimization in internal coordinates. *Proteins* 1997, Suppl 1, 215-220.
237. Nemethy, G.; Gibson, K. D.; Palmer, K. A.; Yoon, C. N.; Paterlini, G.; Zagari, A.; Rumsey, S.; Scheraga, H. A. Energy parameters in polypeptides. 10. Improved geometrical parameters and nonbonded interactions for use in the ECEPP/3 algorithm, with application to proline-containing peptides. *J Phys Chem* 1992, 96, 6472-6484.
238. Schapira, M.; Abagyan, R.; Totrov, M. Nuclear Hormone Receptor Targeted Virtual Screening. *J Med Chem* 2003, 46, 3045-3059.
239. Ellman, G. L.; Courtney, K. D.; Andres, V., Jr.; Feather-Stone, R. M. A new and rapid colorimetric determination of acetylcholinesterase activity. *Biochem Pharmacol* 1961, 7, 88-95.
240. Naiki, H.; Higuchi, K.; Nakakuki, K.; Takeda, T. Kinetic analysis of amyloid fibril polymerization in vitro. *Lab Invest* 1991, 65, 104-110.
241. LeVine, H., 3rd. Thioflavine T interaction with synthetic Alzheimer's disease beta-amyloid peptides: detection of amyloid aggregation in solution. *Protein Sci* 1993, 2, 404-410.
242. Crivori, P.; Cruciani, G.; Carrupt, P.-A.; Testa, B. Predicting Blood Brain Barrier Permeation from Three-Dimensional Molecular Structure. *J Med Chem* 2000, 43, 2204-2216.
243. Prusiner, S. B.; DeArmond, S. J. Prion Diseases and Neurodegeneration. *Annu Rev Neurosci* 1994, 17, 311-339.
244. Caughey, B.; Baron, G. S. Prions and their partners in crime. *Nature* 2006, 443, 803-810.
245. Prusiner, S. B. Prions. *PNAS* 1998, 95, 13363-13383.
246. Prusiner, S. B. Novel proteinaceous infectious particles cause scrapie. *Science* 1982, 216, 136-144.
247. Aguzzi, A.; Calella, A. M. Prions: Protein Aggregation and Infectious Diseases. *Physiol Rev* 2009, 89, 1105-1152.
248. Büeler, H.; Aguzzi, A.; Sailer, A.; Greiner, R. A.; Autenried, P.; Aguët, M.; Weissmann, C. Mice devoid of PrP are resistant to scrapie. *Cell* 1993, 73, 1339-1347.
249. Brandner, S.; Isenmann, S.; Raeber, A.; Fischer, M.; Sailer, A.; Kobayashi, Y.; Marino, S.; Weissmann, C.; Aguzzi, A. Normal host prion protein necessary for scrapie-induced neurotoxicity. *Nature* 1996, 379, 339-343.
250. Brandner, S.; Raeber, A.; Sailer, A.; Blättler, T.; Fischer, M.; Weissmann, C.; Aguzzi, A. Normal host prion protein (PrPC) is required for scrapie spread within the central nervous system. *PNAS* 1996, 93, 13148-13151.

251. Trevitt, C. R.; Collinge, J. A systematic review of prion therapeutics in experimental models. *Brain* 2006, 129, 2241-2265.
252. Bertram, L.; McQueen, M. B.; Mullin, K.; Blacker, D.; Tanzi, R. E. Systematic meta-analyses of Alzheimer disease genetic association studies: the AlzGene database. *Nat Genet* 2007, 39, 17-23.
253. Hooper, N. M.; Turner, A. J. A new take on prions: preventing Alzheimer's disease. *Trends Biochem Sci* 2008, 33, 151-155.
254. Parkin, E. T.; Watt, N. T.; Hussain, I.; Eckman, E. A.; Eckman, C. B.; Manson, J. C.; Baybutt, H. N.; Turner, A. J.; Hooper, N. M. Cellular prion protein regulates β -secretase cleavage of the Alzheimer's amyloid precursor protein. *PNAS* 2007, 104, 11062-11067.
255. Gallardo-Godoy, A.; Gever, J.; Fife, K. L.; Silber, B. M.; Prusiner, S. B.; Renslo, A. R. 2-Aminothiazoles as Therapeutic Leads for Prion Diseases. *J Med Chem* 2011, 54, 1010-1021.
256. Ghaemmaghami, S.; May, B. C.; Renslo, A. R.; Prusiner, S. B. Discovery of 2-aminothiazoles as potent antiprion compounds. *J Virol* 2010, 84, 3408-3412.
257. Hosokawa-Muto, J.; Kamatari, Y. O.; Nakamura, H. K.; Kuwata, K. Variety of antiprion compounds discovered through an in silico screen based on cellular-form prion protein structure: Correlation between antiprion activity and binding affinity. *Antimicrob Agents Chemother* 2009, 53, 765-771.

List of publications related to the thesis

Synthesis of monomeric derivatives to probe memoquin's bivalent interactions

Bolognesi, M.L.; Chiriano, G.; Bartolini, M.; Mancini, F.; Bottegoni, G.; Maestri, V.; Czvitkovich, S.; Windisch, M.; Cavalli, A.; Minarini, A.; Rosini, M.; Tumiatti, V.; Andrisano, V.; Melchiorre, C.
Manuscript submitted to *J Med Chem* (under final revision).

A small chemical library of 2-aminoimidazole derivatives as BACE-1 inhibitors: structure-based design, synthesis and biological evaluation

Chiriano G., De Simone A, Mancini F, Perez DI, Cavalli A, Bolognesi ML, Legname G, Martinez A, Andrisano V, Carloni P, Roberti M
Manuscript submitted to *Eur J Med Chem* (under final revision).

Sequential virtual screening approach to the identification of small organic molecules as potential BACE-1 inhibitors

Chiriano G., Sartini A, Mancini F, Andrisano V, Bolognesi ML, Roberti M, Recanatini M, Carloni P, Cavalli A
Chem Biol Drug Des
Published: 2011; Volume: 77; Issue: 4; Pages: 268–271.

Acknowledgments

I would like to express my sincere gratefulness to each of my supervisors, Prof. Marinella Roberti, Prof. Maria Laura Bolognesi, Prof. Andrea Cavalli, Prof. Paolo Carloni and Prof. Giuseppe Legname for providing me their guidance and support during my PhD research project.

I would like to acknowledge Prof. Maurizio Recanatini for successful discussion and contribution, and allowing me to work in the QSAR laboratory during my stay in Bologna.

My acknowledgments are due to Prof. Vincenza Andrisano and her co-workers, Dr. Angela De Simone, Dr. Francesca Mancini and Dr. Manuela Bartolini, and to Prof. Ana Martinez and Dr. Daniel I. Perez, for their fruitful collaboration.

I would like to thank Prof. Cristian Micheletti and all the senior members of the Statistical and Biological Sector (SBP), Dr. Alessandro Laio, Dr. Alessandra Magistrato and Dr. Giovanni Bussi, from SISSA for their support. My thankfulness is particularly for my friends, Dr. Salvatore Bongarzone, Dr. Francesco Colizzi, Dr. Fabio Simona, Dr. Rolando Hong, Dr. Manuela Minozzi, Dr. Xevi Biarnes, Ms Pilar Cossio, Mr. Choung Nguyen and Ms Zhaleh Ghaemi Bafghi.

Thanks to all friends from synthetic and computational laboratories of Bologna: Dr. Elena Simoni, Dr. Andrea Milelli, Dr. Federico Falchi, Ms. Elisa Giacomini, Mr. Alessandro Gambuzzi, Ms. Rossella Buonfiglio, Mr. Giampaolo Di Martino, Ms. Federica Prati, Ms. Valentina Maestri. In particular, I would like to thank those people providing me their scientific support, Dr. Matteo Masetti, Dr. Luisa Ceccarini, Mr. Andrea Sartini, Ms. Sabrina Leone and Ms. Roberta Manfroni.

Thanks are due to Dr. Stephan Czvitkovich and Dr. Manfred Windisch from JSW of Graz and Dr. Giovanni Bottegoni from IIT of Genova for their scientific contribution, and Prof. Daniele Simoni (University of Ferrara) for the use of CEM Discover BenchMate reactor.

At the end, but from my heart, thanks to my family and Valentina, always present and ready to show me their love in all moments of my life.